Award Number: W81XWH-12-1-0338

TITLE: Molecular Innovations Toward Theranostics of Aggressive Prostate Cancer

PRINCIPAL INVESTIGATOR: Dr.Eric Simanek, PhD

CONTRACTING ORGANIZATION: Texas Christian University
Fort Worth, TX 76129

REPORT DATE: November 2017

REPORT TYPE: Final

PREPARED FOR: U.S. Army Medical Research and Materiel Command

Fort Detrick, Maryland 21702-5012

REPORT DOCUMENTATION PAGE

Form Approved
OMB No. 0704-0188

1. REPORT DATE	2. REPORT TYPE	3. DATES COVERED
November 2017	Final	1 Sep 2012 - 31 Aug 2017

4. TITLE AND SUBTITLE

Molecular Innovations Toward Theranostics of Aggressive Prostate Cancer

5a. CONTRACT NUMBER

5b. GRANT NUMBER
W81XWH-12-1-0338

5c. PROGRAM ELEMENT NUMBER

6. AUTHOR(S)

Dr.Eric Simanek, PhD

E-Mail: e.simanek@tcu.edu

5d. PROJECT NUMBER

5e. TASK NUMBER

5f. WORK UNIT NUMBER

7. PERFORMING ORGANIZATION NAME(S) AND ADDRESS(ES)

Texas Christian University
2800 South University Avenue
Fort Worth TX 76129

8. PERFORMING ORGANIZATION REPORT NUMBER

9. SPONSORING / MONITORING AGENCY NAME(S) AND ADDRESS(ES)
U.S. Army Medical Research and Materiel Command
Fort Detrick, Maryland 21702-5012

10. SPONSOR/MONITOR'S ACRONYM(S)

11. SPONSOR/MONITOR'S REPORT NUMBER(S)

12. DISTRIBUTION / AVAILABILITY STATEMENT
Approved for Public Release; Distribution Unlimited

13. SUPPLEMENTARY NOTES

14. ABSTRACT

During the project, strategies for the preparation of new globular polymers (dendrimers) were introduced and methods for their rapid synthesis were pioneered. Both achievements address long-standing shortcomings of this field that have hindered translation to the clinic. Structure-activity relationships revealed design criteria for achieving high water solubility necessary for therapeutic application. Methods were surveyed for attaching varied functional groups including the therapeutic (through biolabile or stable linkages) and imaging agent. This work led to the discovery of new hydrazone chemistry that offers broad application in drug/gene delivery. While the initially proposed multivalent therapeutics failed to recapitulate the activity of the lead compound, targeting prostate cancer cells with these constructs is now possible: a 60x increase in selectivity is seen. In aggregate, this opens opportunities for realizing new treatments.

15. SUBJECT TERMS

16. SECURITY CLASSIFICATION OF:			17. LIMITATION OF ABSTRACT	18. NUMBER OF PAGES	19a. NAME OF RESPONSIBLE PERSON
UNCLASSIFIED					USAMRMC
a. REPORT	b. ABSTRACT	c. THIS PAGE			19b. TELEPHONE NUMBER *(include area code)*
U	U	U	UU	77	

Table of Contents

	Page
Introduction……..	**3**
Keywords…….	**3**
Accomplishments……..	**3**
Training.....…….	**12**
Impact.....……	**13**
Changes/Problems……..……	**14**
Participants.....……...……	**14**
Appendices……	**15**

INTRODUCTION

The long term goal of the proposed project was to explore novel theranostics to stifle metastasis of prostate cancer. The sub-award described here focused on the preparation of these labeled, multivalent displays of peptides in an effort that proceeded through five phases.

Phase 1 (Projected 0-6 months): The goal of phase 1 efforts was to prepare dendrimers ranging from generation 3 to 7 with an alkyne group at the core which could be subsequently functionalized with a chelate for diagnostic imaging. The projected time for this initial synthetic effort was 6 month.

Phase 2 (Projected 4-12 months): An additional 6 months was predicted to be required for developing methods for the installation of the chelate using alkyne-azide click chemistry.

Phase 3 (Projected 9-18 months): The third phase aimed to probe the solubility characteristics of the dendrimers by manipulating the surface groups. These activities were hypothesized to be completed by the 18 month mark.

Phase 4 (Projected 12-24 months): Strategies for the design and incorporation of therapeutic peptides into dendrimers were expected to proceed over the next year with submission of candidates to UTSW by the end of year two. The initial candidates were low-valency targets presenting up to 8 therapeutic peptides.

Phase 5 (24-48 months): An iterative strategy for optimizing activity based on leads was the goal of these efforts.

KEYWORDS

theranostic, dendrimer, triazine, peptide, synthesis, linker, microwave synthesis, maleimide, hydrazone, release, imaging, DOTA, chelation

ACCOMPLISHMENTS

The proposed statement of work identified four action items shown in table 1 and a fifth goal of refinement of activity. These goals and the degree of their completion are indicated.

Table 1. Summary of Major Goals

Task	SOW Description	% Done
1	Synthesis and characterization of dendrimers that vary in size from generation 3-7 with a functional alkyne	100%
2	Installation of a chelate group for diagnostic medical imaging[a]	100%
3	Exploration of surface groups to promote desired behavior[b]	100%
4	Therapeutic peptides will be designed and installed	100%
5	Iteration to yield an active target	failed[c]

[a] A change from a "synthetically expensive," novel chelate to an inexpensive and commercially/clinically relevant alternative was undertaken when the synthetic effort required earlier installation of this group than was originally anticipated. The shift was deemed insignificant given the SOW.

[b] Surface groups were initially believed to be the greatest contributor to physicochemical properties, but research showed the the interior groups played a much more dominant role in determining solubility and computational models in related systems reinforced this hypothesis and observation. The shift was deemed insignificant given the SOW.

[c] Multivalent displays failed to reproduce the activity of the monomeric peptide initially reported. A redesigned monomer showed reduced activity and was synthetically more difficult to obtain.

While the long term goal of a multivalent, bioactive theranostic was achieved, a number of major accomplishments can be identified that stemmed from this work. These accomplishments appear in Table 2. The status of dissemination is also indicated.

Table 2. Summary of Major Accomplishments. Tasks from the SOW appear in column 1. "N" identifies a new accomplishment associated with the original SOW.

Task	Accomplishment	Dissemination Status
1	Synthesis of G3-G6 dendrimers with an alkyne core	Published
1	Evaluation of click chemistry and triazine dendrimers	Negative result
1	Rapid, microwave synthesis efforts of dendrimers	Published
N1A	Using intrinsic fluorescence to probe structure	Published
N1B	Gold nanoparticles as a surrogate for dendrimers	Published
2	Synthetic strategies for carrying a chelate through multi-step dendrimer synthesis relying on orthogonal deprotection of acid labile groups	Published
3	Structure-based understanding of dendrimer solubility in water as a function of interior[a] groups	Published
4	Scope and limitations of maleimide-terminated dendrimers for ligand/peptide display	Published
4	Scope and limitations of covalent ligation of peptides bearing cyclic amines to triazine dendrimers	Negative result
4	Investigation of a novel triazinyl hydrazine and hydrazone formation for biolabile displays of ligands	Published
N4	Triazinylhydrazines show selective conjugation to drugs	In progress
4	Scope and limitations of ligation of peptides bearing an aldehyde or ketone group with dendrimers displaying multiple triazinylhydrazines	In progress
N4	Triazinylhydrazines can form pyrazoles that chelate metals	In progress
N5A	Hemolytic study of dendrimers	Published
N5B	Explore cancer cell targeting in vitro and in vivo	In progress

[a] Initially, we proposed modifying surface groups to affect solubility, but found during the course of these studies, that the interior groups were critically important.

The long term goal of delivering biological activity within a multivalent theranostic was not met. However, the list of major accomplishments serve to reinforce the value of triazine dendrimers as candidate platforms for nanomedicines based on increasing ease of

synthesis, an understanding of how interior groups control the solubility properties of these architectures, and the operational space available for ligating groups of interest (here the therapeutic peptide and models) using covalent and biolabile linking groups.

Many of these accomplishments have been published in the scientific literature, and these papers appear in the appendix. The following paragraphs summarize those results that have not been published. The following paragraphs provide details for each task of the SOW.

Task 1: Synthesis and characterization of dendrimers that vary in size from generation 3-7 with a functional alkyne

Dendrimer synthesis relies on iterative, polymer chemistry. The strategy is most efficient when common building blocks are readily available. For this task, three building blocks were prepared (Chart 1.1). These vary by the choice of linking diamine (shown in a colored box). Each macromonomer (**M1**-**M3**) provide two generations of dendrimer for every reaction.

Chart 1.1. Macronomonomers **M1**-**M3** with the linking diamines indicated with color.

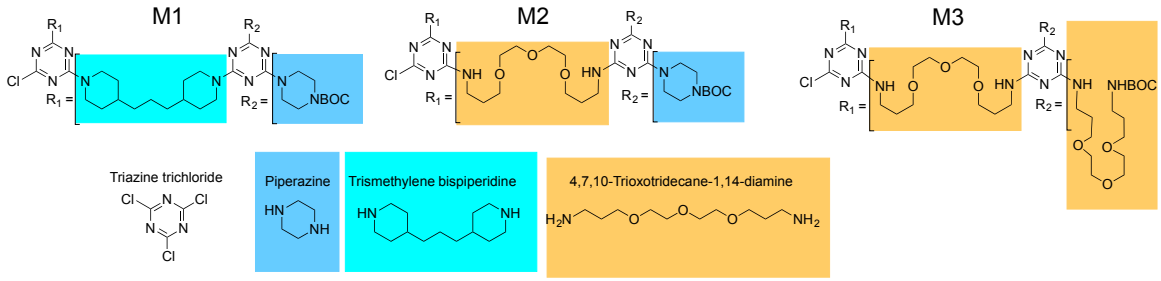

To obtain the desired dendrimers (Chart 1.2, following page), a macromonomer is reacted with propargyl amine to afford the alkyne core. Then, the peripheral BOC-protected amines are unmasked and the resulting material is reacted with macromonomer. The process of deprotection and reaction is iterated until the desired product results. An important lesson emerged from the library of molecules shown in Chart 1.2. Water solubility of a dendrimer with a hydrophobic core (derived from **M1**) could be rescued if **M3** was used on the periphery. Surprisingly, the hydrophilic, cationic character of **M2** was insufficient.

Task 2: Installation of a chelate group for diagnostic medical imaging

The initial SOW called for manipulation of the single alkyne installed at the core of the dendrimer using click chemistry so that any imaging agent might be installed, although we proposed an experimental chelator of copper from co-PI Xiankai Sun's lab as the focus of these efforts. Preliminary model studies of copper-catalyzed click reactions failed to reproduce the levels of conversions reported in the literature, rarely exceeding 25% in unhindered, low-generation dendrimers. Computer simulations that suggested that the linking groups that were required to promote water solubility also were likely to shield this alkyne from reaction. (The more rigid, hydrophobic core of the dendrimer was intended to promote access of the click reagents.)

These failures led to a shift in strategy wherein the imaging group was installed early in the synthesis. To mimic the experimental chelator, a much less expensive, commercially available, conventional DOTA group was used. The goal was to optimizing bioactivity before optimizing the imaging. The strategy required the development of methods that allowed for the deprotection of peripheral BOC-groups on the dendrimer while retaining the protective t-butyl esters of the DOTA group. Conditions were uncovered that worked surprisingly well. The synthetic plan that was adopted is shown in Scheme 2.1.

Task 3: Exploration of surface groups to promote desired behavior

This task was completed given the solubility promoted by the groups discovered in pursuit of Task 1.

Chart 1.2. Targets of macromonomer synthesis.

Compound	Organic Solubility	Aqueous Solubility	Organic Solubility (Protected)
1	Y	N	Y
2	Y	N	Y
3	Y	Low <3mg/mL	Y
4	Y	High 20mg/mL	Y
5	N	N	N
6	N	Very Low <<1mg/mL	Y
7	Y	Low <1mg/mL	Y
8	Y	Very High >50mg/mL	Y

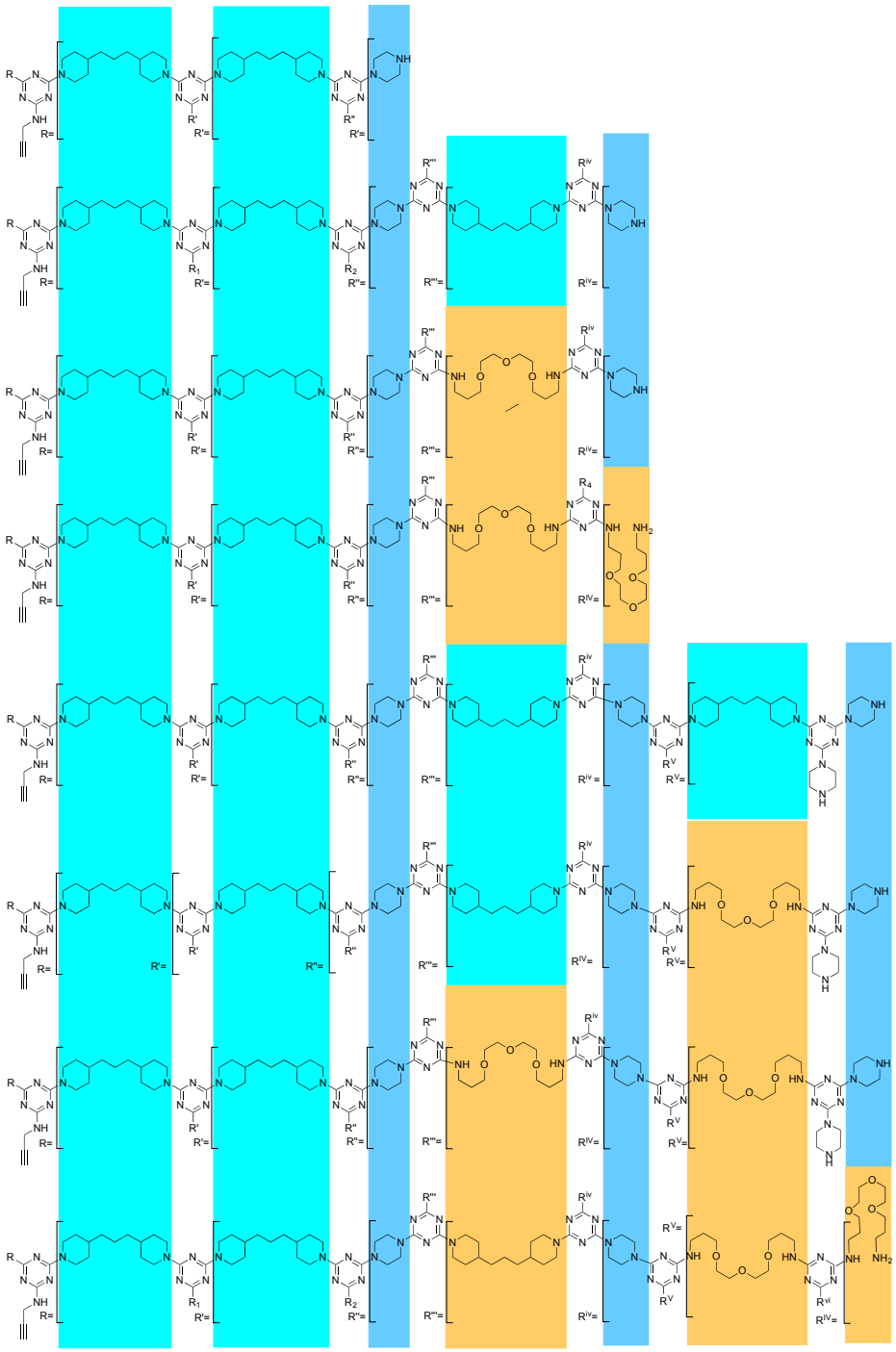

Scheme 2.1. Synthesis of the DOTA-core dendrimer. A G3 dendrimer was also prepared.

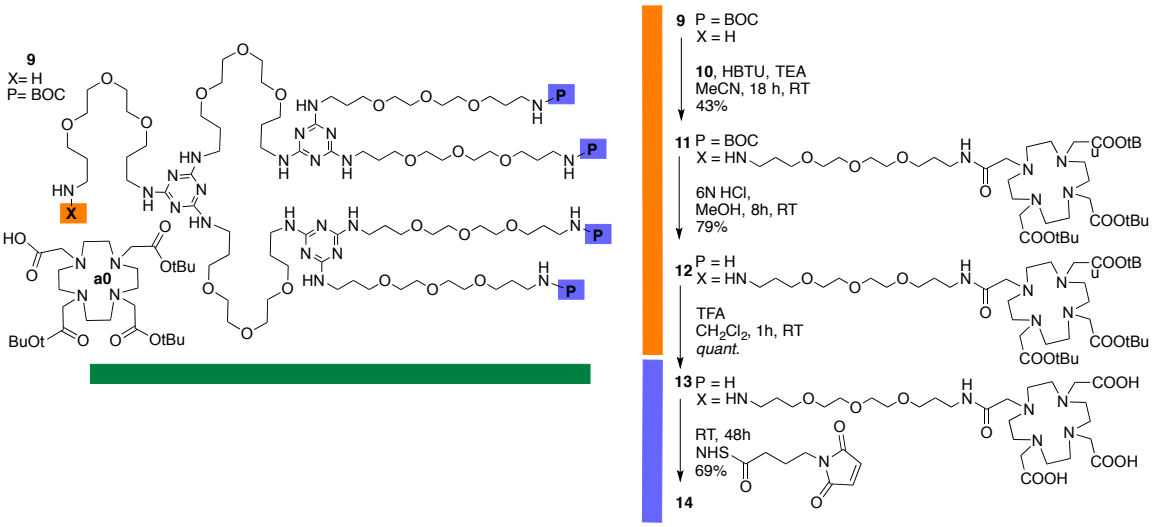

Task 4: Therapeutic peptides will be designed and installed

A solid phase peptide synthesizer was purchased with start-up funds (not grant monies) to further these aims. Therapeutic peptides were prepared and strategies for installation onto the dendrimer target were pursued. Three strategies were examined; 1) non-labile attachment via reactive cyclic amines, 2) non-labile attachment via maleimide chemistry, and 3) biolabile linkage derived from triazinyl hydrazines. Each will be addressed independently.

Strategy 4.1: Non-labile attachment via reactive cyclic amines

The *N*-terminus of peptides offers a site for the installation of non-native amino acids that might bear highly reactive, constrained secondary amines predicted to be reactive with mono- or dichlorotriazines that might appear on the periphery of a dendrimer (Scheme 4.1). From the standpoint of relative reactivity, an *N*-terminal isonipecotic acid would be expected to be more than 20 times more reactive than a primary amine displayed on the N-terminus of a native peptide or lysine sidechain.

Scheme 4.1. Preparation of a peptide functionalized dendrimer bearing dichlorotriazines using peptides terminated in isonipecotic acid.

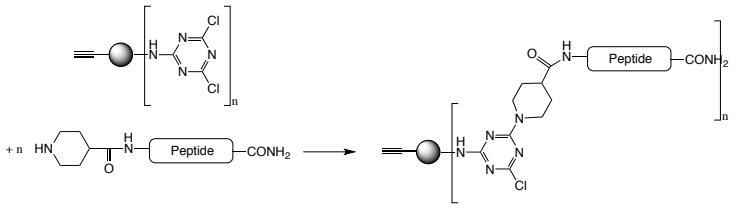

Decreasing ring size from the 6-membered isonipecotic acid to a 5-membered pyrimidine or 4-membered azetidine further increases selectivity in model systems to up over 300-fold over primary amines. During the course of these studies, we have established that these hypotheses bear out for peptides bearing isonipecotic acid and proline, but when an azetidine is incorporated during solid phase synthesis, acid-catalyzed cleavage from the resin destroys the ring. For *N*-terminal installation of an azetidine, a base-labile FMOC-azetidine acid and soluble peptide would required, or an alternative to

the standard Wang solid phase resin. Incorporating this azetidine on a native peptide would prove challenging in the presence of competing lysine sidechains. Azetidine degradation can be avoided in the C-terminus is targeted instead, with aminoazetide. Similarly, aminopyrrolidine and aminopiperazines are now hypothesized to accomplish similar ends. However, the lessons learned from this chemistry are now being considered for use in the creation of new therapeutics, including next-generation cyclic antibiotics based on nisin which, serendipitously, was reported last year to show anticancer activity in rats.

Strategy 4.2: Non-labile attachment via maleimide chemistry

The use of maleimide chemistry developed in the laboratory was explored for the therapeutic peptide of interest. The chemistry relied on synthesizing dendrimers with maleimide groups on the periphery ad reacting them the therapeutic peptide containing an additional N-terminal cysteine (Scheme 4.2). The constructs resulting from this reaction are not ordinarily considered "biolabile", but the perceived ease of access, storage, and hypothesized stability in vivo led us to pursue them briefly. The maleimide dendrimer prepared featured the DOTA group at the core. The constructs derived showed no biological activity.

Scheme 4.2. The chemistry utilized to make tetravalent constructs.

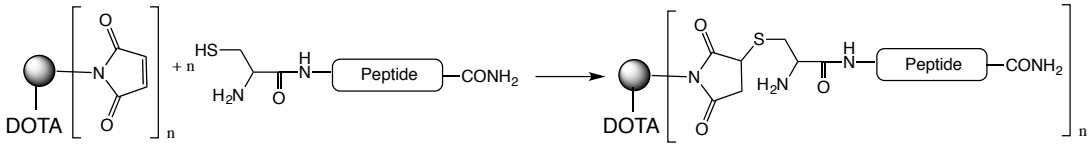

Strategy 4.3: Biolabile linkage derived from triazinyl hydrazines

The lack of activity seen in multivalent constructs that displayed peptides using non-labile covalent bonds led to the exploration of hydrolytically sensitive linkages. The chemistry explored presented an extension of the triazine chemistry of interest. Triazines bearing hydrazine groups were prepared as acylhydrazine equivalents. The work showed that triazinylhydrazine condense with the carbonyl groups of aldehydes and ketones. The intrinsic advantage of using a triazine comes with the potential to rapidly elaborate it to a theranostic with suitable biophysical properties. We reported the stability and kinetics of release of model systems wherein the triazinylhydrazine showed higher stability than the corresponding acylhydrazones at pHs below the pKa of the triazine. Whether this can be exploited for these intents, there is potential applications of these materials for buffering in gene therapy applications. The triazinylhydrazine chemistry that has been reported has been elaborated to prepare dendrimers displaying multiple groups as shown in Chart 4.3. The compound reacts efficiently with simple aldehydes and ketones, and with bioactives including the drug doxorubicin and bruceantin. Peptides bearing an N-terminal p-formylbenzyoic acid group have been explored.

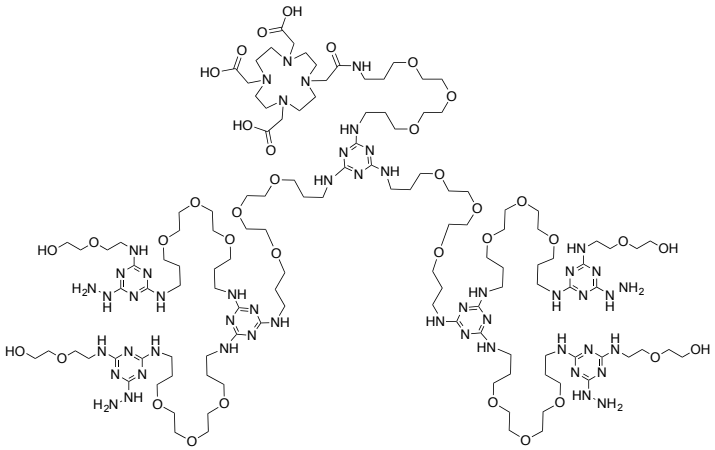

Chart 4.3. The theranostic platform comprising a DOTA imaging chelate and four triazinyl hydrazines.

Task 5: Iteration to yield an active target

Throughout the efforts, the only target that proved to have activity competitive with the lead construct was a monomer that presented a triazine linker between the therapeutic peptide and targeting sequence derived from an arginine-rich sequence. Studies of this peptide are ongoing.

New Task 1A: Using intrinsic fluorescence to probe structure

Function is intimately linked to structure. However, probing structure in these macromolecules presents fundamental challenges to existing technique. For example, the repetitive use of building blocks (the hallmark of polymer chemistry) leads to degeneracy in the NMR spectrum. Mass spectrometry is inherently difficult with macromolecules of these sizes even with deconvolution of multi-charged species. As an alternative, we explored the intrinsic fluorescence of triazines. The absorption and emission spectra are shown in Figure N1.1

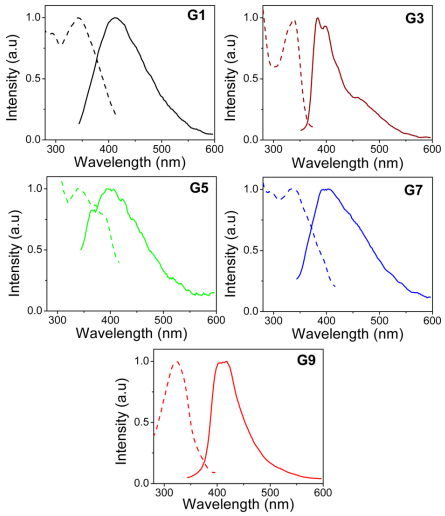

Figure N1.1 The absorption and emission spectra of triazine dendrimers (right) and optical images (below) at 366 nm excitation.

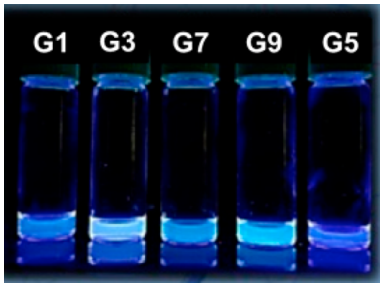

These studies proved important for many reasons. First, they establish a rapid method for evaluating behavior and structure. Second, they reveal that extiniction spectra results from two components that can be separated; the triazine absorption and Rayleigh scattering by the presence of aggregates. The results of these analyses reveals a structural transformation at generation 5 materials. The core of the dendrimers become increasingly compact from generation 1 to generation 5. However, generation 7 and 9 dendrimers present a more extended and porous structure with a less dense core, but denser peripheries. Computational models corroborate these observations and offer an additional method for assessment.

New Task N1B: Au nanoparticles as dendrimer surrogates

The goal of multivalent displays of therapeutic peptides on large dendrimer nanoparticles relies on dendrimer synthesis. While efforts from this grant yielded methods for the facile synthesis of these materials, inorganic nanoparticles might be even more ready attained and provide additional opportunities intrinsic to their structure including opportunities for thermal ablation therapies and microscopic imaging. To this end, a surfactant-free nanoparticle synthesis was developed that yielded dendrimer-coated gold nanoparticles. The synthetic pathways is shown in Scheme N1B.1. These nanoparticles were amenable to chemistries that changed solubility characteristics of the particle. Curiously, G0 and G2 nanoparticles proved more soluble than G1. Relying on computation and the trends revealed in the previous studies, we found that hydration of the interior (and not the surface group) was the determining factor. These simulations are shown in Figure N1B.1 on the following page.

Scheme N1B.1 Dendrons with aniline at the core (G0, G1 and G2) were subjected to diazotization in the presence of gold salts. Upon addition of sodium borohydride, dendrimer coated nanoparticles were produced.

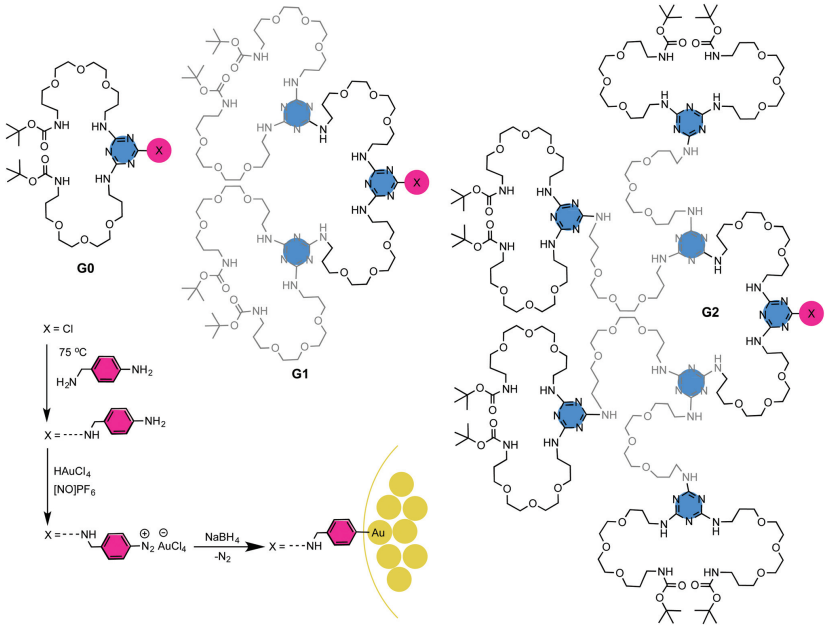

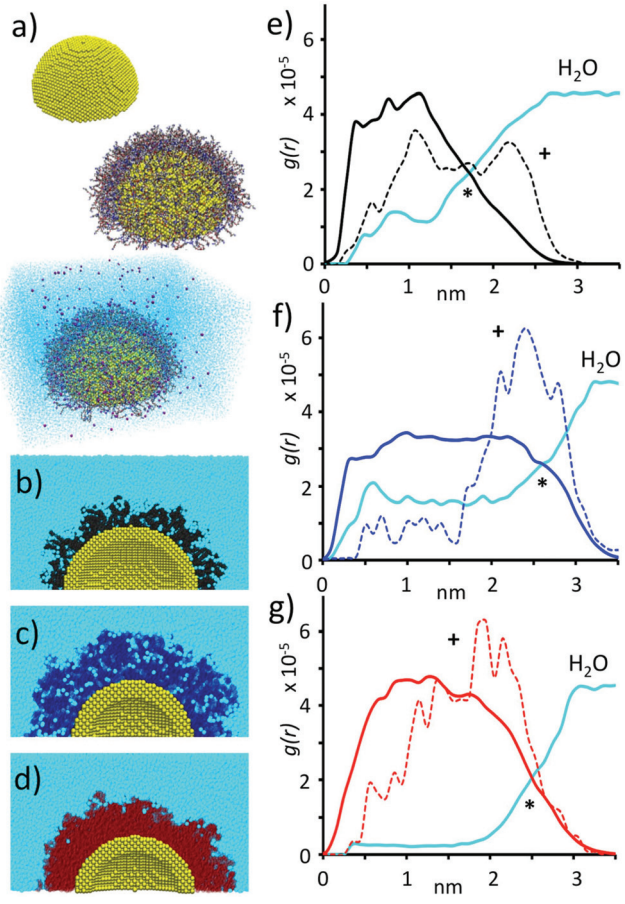

Figure N1B.1. Models of gold nanoparticles functionalized with amine-terminated dendrimers. a) The computational surface and dense grafting starting point. b-d) Edge dissections of nanoparticles derived from G0, G1, and G2 dendrons respectively. e-g) Gyration plots showing the positions of atoms derived from dendrimer (solid), surface charges (dashed) and those from water (blue).

New Task N4: Pyrazole formation and metal chelation

While surveying carbonyl-containing compounds for hydrazone formation, we found that some 1,3-diketones (but not all) form pyrazole rings at room temperature (Scheme N4.1).

Scheme N4.1 Pyrazole formation occurs with some 1,3-ketones (right) instead of the desired hydrazone formation.

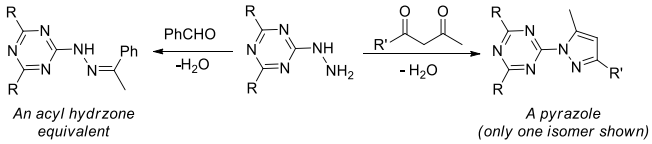

The implications for this behavior are multi-fold. First, because these pyrazoles prove stable to hydrolysis even under very acidic conditions (pH<4), the linkage represents a new facile route to functionalizing dendrimers with bio-stable groups of interest, including therapeutic peptides or other molecules. Second, pyrazole formation can introduce a strongly chelating group that could engender toxicity by scavenging metals. To explore this, a hydroxypyrazole was prepared and evaluated for coordination of ions of zinc, copper and nickel. Spectroscopic analysis and single-crystal x-ray diffraction data like that shown for the nickel complex in Figure N4.1, confirm this behavior. This behavior can be used, potentially, as an orthogonal measure of functionalization efficiency.

Figure N4.1 Nickel chelation (as well as other metals) occurs with triazinylpyrazoles.

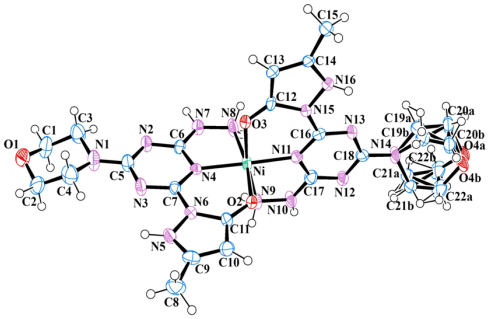

New Task N5A: Hemolytic studies of triazine dendrimers

During the course of these studies, we had an opportunity to evaluate and disclose hemolytic characteristics of triazine dendrimers in collaboration with the Nanotechnology Characterization Laboratory of NCL. Figure N5A.1 shows the varying degrees of platelet aggregation as a function of dendrimer generation. Toxicity (as reflected by aggregation) increases in a concentration dependent manner with small generation 3 dendrimers show little toxicity until high dosing. Direct comparison (Figure N5A.1) of small and large triazine dendrimers to their PAMAM dendrimer equivalents bears out the markedly low toxicity for our platform at small generations(left), but an onset comparable toxicity for larger dendrimers (right).

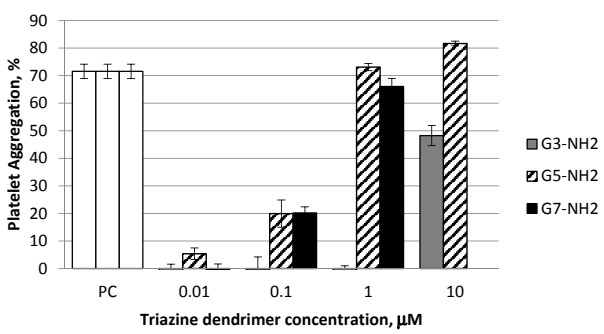

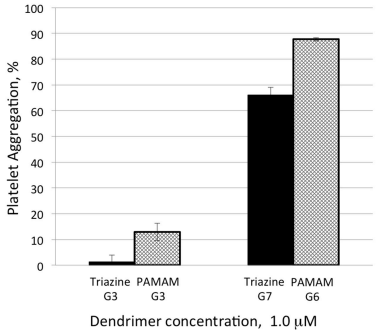

New Task N5B: Targeted theranostics

The failure to recapitulate activity in the constructs led us to explore whether specifically targeting the molecules to prostate cancer cells bearing the prostrate specific membrane antigen (PSMA receptor) might beneficial for these or future studies. Preliminary assessments of the constructs (Chart N5B.1) in vivo show that a 60-fold increase in selectivity is achieved in tumored animals using PSMA(-) prostate cancer cell lines as a control.

Chart N5B.1 The first target with the DUPA ligand (upper left), a therapeutic poly-proline sequence and a chelating group for imaging.

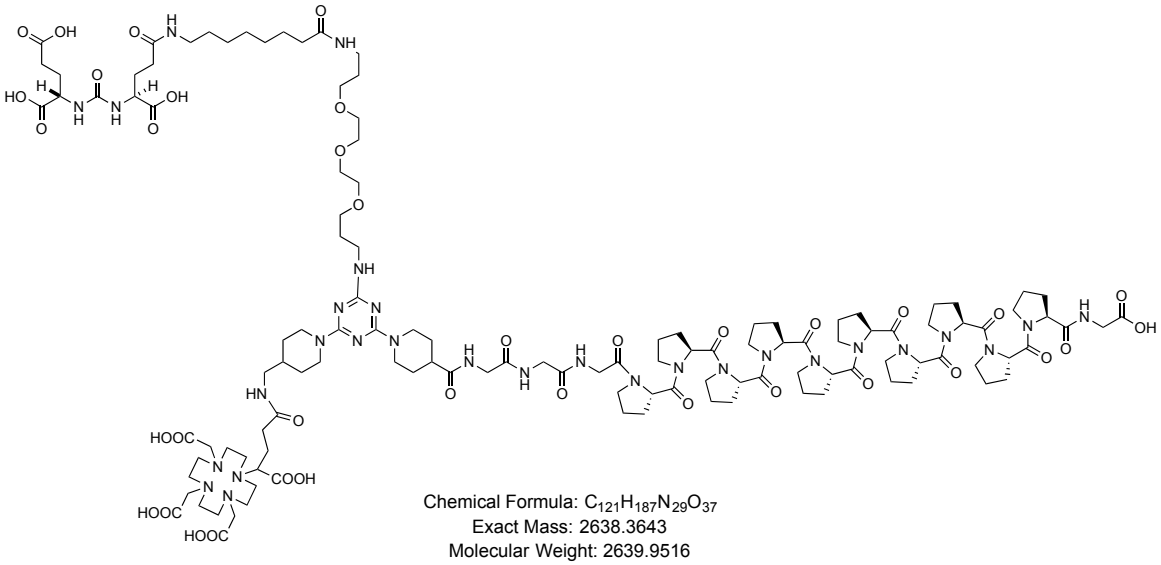

The results are very significant. In aggregate, we now believe that theranostic dendrimers--ones displaying multiple (perhaps more conventional therapeutic groups) and an imaging agent--that is specifically targeted to aggressive prostate cancer cells is now achievable. The increase in selectivity is hypothesized to lead to reduced dosing and meet the expectations for further translational advance.

Training

The project served as a mechanism for professional development for the post-doctoral fellow who executed early efforts, the graduate student who took over as his skill set developed, an international research exchange student who explored elements of these chemistries (specifically, polyproline synthesis and reactivity), and simulatneously catalyzed a cross department collaborative effort. Neither the research exchange student nor departmental collaborators (Professors Janesko, Minter, and more recently Green) derived any financial support from the project, but became engaged in the different elements (computation, hydrazone experimental efforts, and metal coordination, respectively).

Dissemination has centered on the submission and publication of peer-reviewed manuscripts. Six manuscripts have appeared in print and two more will be submitted in the upcoming months. An additional 2-4 that acknowledge this grant are expected in the 2017-2018 period. Table 3 summarizes this activity.

In addition, manuscipts describing 1) the ability of triazinyl-N-methyl-hydrazines to condense with carbonyls to form hydrazones and 2) the biological activity of some hydrazones are expected in the next year. A full account of the last fifteen years worth of exploration is being outlined for *Accounts of Chemical Research.*

Table 3. Products of dissemination currently identifiable. The title, journal and year, and page number for the reprint is provided.

#	Title	Status	Page
1	Influence of linker groups on the solubility of triazine dendrimers	*New J. Chem.* 2015	
2	Accelerated synthesis of large generation triazine dendrimers using microwave assisted reactions: a 24 hour challenge	*Polymer Chem.* 2015	
3	Triazine-Substituted and Acyl Hydrazones: Experiment and Computation Reveal a Stability Inversion at Low pH	*Molec. Pharm.* 2015	
4	Functionalization of a triazine dendrimer presenting four maleimides on the periphery and a DOTA group at the core	*Molecules* 2016	
5	Thermoregulated Coacervation, Metal-encapsulation and Nanoparticle Synthesis in Novel Triazine Dendrimers	*Molecules* 2016	
6	Intrinsic Fluorescence of Triazine Dendrimers Provides a New Approach to Study Dendrimer Structure and Conformational Dynamics	*J. Phys. Chem. C* 2016	
6	Facile synthesis of stable, water soluble, dendron-coated gold nanoparticles	*RSC* 2016	
7	Nanoparticle Effects on Human Platelets *in Vitro*: A Comparison between PAMAM &Triazine Dendrimers	*Molecules* 2016	
8	Chelation of copper, nickel, and zinc with a triazine bearing a hydroxypyrazole group	For *Inorg. Chem.*	NA
9	Functionalization of a triazine dendrimer displaying hydrazine-substituted triazines on the periphery	For *J. Poly. Sci.*	NA

IMPACT

On the discipline. The primary impact on the specific discipline of polymer chemistry, more specifically, dendrimer chemistry, was to conquer remaining challenges including the identification of methods for the rapid synthesis of these materials and strategies for conjugating both diagnostic groups and multiple bioactives.

On other disciplines. The lessons learned make this platform increasingly useful for clinical future clinical relevance. One specific example came to light in mid-2016 when a biotech company (in collaboration with the NIH) identified the triazine chemistry developed here as motivation for pursuing explorations of a platform for gene therapy. Collaborative efforts are commence next month. In another example, the ability of the triazinylhydrazines to coordinate metals suggest a role in combatting cancer and other diseases where oxidative stress can be exploited. Collaboration with Dr. Kayla Green in our department are proceeding. The application of this chemistry to the creation of new bioactives with potential anti-cancer and anti-microbial activity is also expected.

On tech transfer. While no patents have been issued covering this work, the lessons learned can be applied (and are being pursued) in areas where intellectual property is expected to be generated as described above.

On society. While limited now to the department and college, the effort has initiated broad interest in focused research collaboratives including theranostic nanomaterials and antimicrobials. The ability to attract international student researchers to work on these

projects the US has untold implications. The design criteria that have emerged for targeted theranostics will propel the efforts into the future.

CHANGES/PROBLEMS

No substantive changes in delivery of the SOW were encountered that extended beyond what is broadly considered scientific exploration and optimization. We are left with a significant problem outside our foreseeable control: it is unlikely that multivalent displays of a peptide envisioned to interact with the intracellular target of interest is likely to yield advantageous activity that overcomes the burdens of synthesis and characterization associated with its creation. Multivalent displays have shown promise with extracellular receptors. However, this "problem" served to focus synthetic efforts that led to major accomplishments.

PRODUCTS

The products, research papers, were enumerated in Table 3.

PARTICIPANTS

The participants supported financially on this project included:

Dr. Eric Simanek, PI, oversaw the project from conception through completion.

Dr. Changsuk Lee, postdoc, 32 person months, who initiated these efforts with emphasis on the maleimide chemistry and creation of the theranostic platform.

Mr. (now Dr.) Kun Ji, graduate student, 16 person months, who took over the project from Dr. Lee, developed the hydrazone chemistry, and explored their use in dendrimers and with novel bioactives including bruceantin.

Participants that worked on this project, but were *not* supported financially included:

Mr. (now Dr.) Alan Enciso, graduate studentwho developed the rapid synthesis of the dendrimers and explored solubility properties as a function of internal linker, explored alternative interiors including gold nanoparticles, prepared materials for photophysical characterization, and initiated the work on prostate cancer cell targeting.

Mr. Vishal Sharma who is extending the chemistry of the triazinylhydrazines.

Mr. Akop Yepremyan for materials synthesis.

Mr. (now Dr.) Fermin Ramirez-Crescrencio who assisted Mr. Enciso in various aspects of his studies.

Mr. Benjamin Large who assisted Mr. Enciso in various aspects of his studies and prepared model compounds for NMR analysis.

Professor Karol Gryczynski and his photophysics group who explored the intrinsic fluorescence of the materials prepared by Mr. Enciso and Mr. Yepremyan.

Professor Benjamin Janesko who provided computational analyses of the hydrazone chemistry.

Professor Onofrio Annunziata for collecting biophysical characterization data.

Professor David Minter for assisting with spectroscopy and data interpretation.

Professor Kayla Green all of this department who collaborated on metal coordination studies.

NJC

PAPER

Cite this: *New J. Chem.*, 2015, **39**, 1247

Influence of linker groups on the solubility of triazine dendrimers†

Alan E. Enciso,[a] Matteo Garzoni,[b] Giovanni M. Pavan[b] and Eric E. Simanek*[a]

Received (in Montpellier, France) 4th June 2014,
Accepted 14th November 2014

DOI: 10.1039/c4nj00917g

www.rsc.org/njc

Eight triazine dendrimers were prepared to probe the impact of linker choice on water solubility. Three different linkers were assessed including two hydrophobic diamines that show high reactivity, piperazine and trismethylene bispiperidine, as well as a hydrophilic diamine, 4,7,10-trioxotridecane-1,14-diamine, which is less reactive. Dendrimers **1–8** share a common, generation two, hydrophobic core, **1**. Dendrimer **1** is insoluble in water. Of the three generation four dendrimers, **2–4**, that were prepared, **2** is also insoluble in water, but substitution of one or two of the hydrophobic linkers with 4,7,10-trioxotridecane-1,14-diamine yields sparingly soluble **3** and more soluble **4**, respectively. Molecular dynamics simulations of dendrimers **2–4** in water provide additional insight into their shape, hydration and hydrophobicity. Generation six targets, **5–8**, are also sensitive to choice of interior and surface groups. Dendrimer **5** is insoluble in water, but replacing one or two hydrophobic linkers with 4,7,10-trioxotridecane-1,14-diamine yields dendrimers **6** and **7** with modest affect unless the double substitution occurs in tandem at the periphery to yield **8** which shows high solubility in water. The solubility trends suggest that the choice of cationic surface group is critical, and that piperazine groups on the periphery and interior do little to promote solubility of triazine dendrimers in water compared with the hydrophilic amine 4,7,10-trioxotridecane-1,14-diamine.

Introduction

Dendrimers are often considered for applications that require solubility in aqueous solutions including their use as drugs and drug delivery vehicles.[1] Solubility behavior is most commonly attributed to the nature of the surface groups which can be chosen to manipulate the type and density of charge or other solubilizing groups like poly(ethyleneglycol).[2] In addition to the periphery, the interior groups of triazine dendrimers are subject to facile manipulation because the dendrimers comprise triazine branching points and linking diamines.[3] Historically, the selection criteria for the diamine—while influenced by whether a convergent or divergent approach was being adopted—rested on (i) the reactivity of the diamine, (ii) its cost, and (iii) the commercial availability of protected derivatives. Given the wealth of diamines that meet many of these expectations, the choice of diamine incorporated into triazine dendrimers has evolved over time.

Initially, *p*-aminobenzylamine was favored because the difference in the relative reactivity of the individual amines offered an opportunity to execute a convergent syntheses without functional group interconversions or protecting group manipulations.[4] However, reactivity was sluggish in comparison to other choices like 4-aminomethylpiperidine and intermediates containing the former discolored over time.[5] Piperazine became a linker of choice for small dendrimers due to its high reactivity (compared with primary amines) and the commercial availability of a low cost BOC-derivative.[6] Unfortunately, synthesis was limited to generation 3 targets due to solubility limitations attributed to the disc-like shape of the molecules.[7] To preserve the reactivity of constrained diamines and introduce flexibility, trismethylene bispiperdine was explored. The dendrimers that resulted displayed higher solubility than all-piperazine molecules, but access to high generation materials was still limited based on solubility.[8]

More recently, 4,7,10-trioxotridecane-1,14-diamine has been employed (Chart 1). Here, we probe the role of combinations of these different amines on the solubility of the resulting dendrimers. Chart 2 shows the targets in this phenomenological

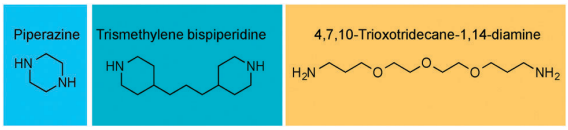

Chart 1 Diamines employed in this study.

[a] *Department of Chemistry, Texas Christian University, Fort Worth, TX 76129, USA. E-mail: e.simanek@tcu.edu*
[b] *Department of Innovative Technologies, University of Applied Science of Southern Switzerland, 6962 Manno, CH, Switzerland*

† Electronic supplementary information (ESI) available: Complete experimental procedures, spectral data, and schemes. Figures associated with computation. See DOI: 10.1039/c4nj00917g

Compound	Organic Solubility	Aqueous Solubility	Organic Solubility (Protected)
1	Y	N	Y
2	Y	N	Y
3	Y	Low 3mg/mL	Y
4	Y	High 20mg/mL	Y
5	N	N	N
6	N	Very Low <<1mg/mL	Y
7	Y	Low 1mg/mL	Y
8	Y	Very High 50mg/mL	Y

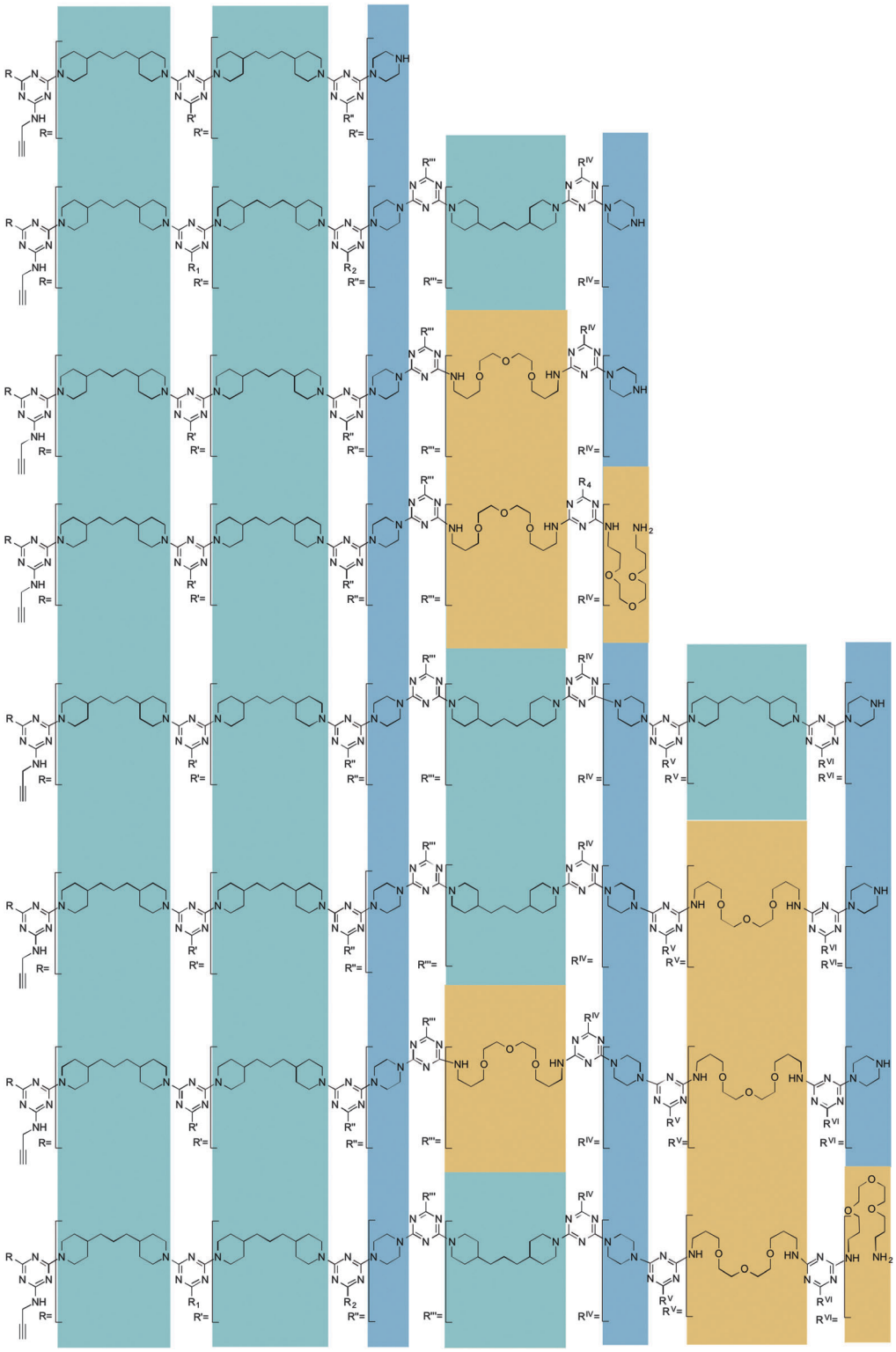

Chart 2 Dendrimers examined in this study. The organic and aqueous solubility data are shown in columns 2 and 3. Column 4 reports the solubility of the BOC-protected precursor in organic solvent.

study. Sharing a common hydrophobic core, triazine dendrimers **1–8** were chosen to anchor our intuition on both (i) the nature of the cationic peripheral group and (ii) the influence of piperazine groups in conveying solubility.

Results and discussion

All targets examined in this study derive from a hydrophobic interior with modest flexibility. This generation 2 dendrimer, **1**, displays 8 piperazine groups on the surface and an alkyne at the core. Dendrimer **1** can be elaborated with macromonomers **9–11** shown in Chart 3 to yield the compounds **2–8.** Specifically, **1** is reacted with **9**, **10**, or **11** to yield BOC-protected derivatives of **2**, **3**, or **4**, respectively. Deprotection with a 1 : 1 mixture of MeOH and conc., HCl yields **2**, **3**, or **4**. Dendrimers **2** and **3** are further reacted with **9**, **10**, or **11** to yield protected **5–8** which are similarly deprotected. Solubility tests were performed by addition of dendrimer to one milliliter of Millipore water (18 MΩ cm). Sonication was used to determine saturation as measured with the naked eye. The solubility observations are reported in Chart 2.

The data anchors our intuition about solubility in three ways. First, substitution of the flexible hydrophilic linker 4,7,10-trioxotridecane-1,14-diamine for hydrophobic trismethylene bispiperidine within the interior of the dendrimer conveys critical, albeit slight water solubility to dendrimers. That is, **2** is insoluble while **3** is sparingly soluble. Similarly, **5** is insoluble while **6** and **7** show increased solubility. Solubility increases from **5** < **6** < **7** as do the number of substitutions of 4,7,10-trioxotridecane-1,14-diamine for trismethylene bispiperidine. Second, the nature of the cationic peripheral group appears to have a profound affect on solubility. That is, replacing the terminal piperazine group with 4,7,10-trioxotridecane-1,14-diamine at the dendrimer surface significantly increases solubility. Dendrimer **4** is much more soluble than either **2** or **3**. Similarly, dendrimer **8** is much more soluble than **5**, **6**, or **7**. Third, the trends are conserved across all generations. Dendrimers **1**, **2** and **5** are all insoluble, and solubility decreases in going from **3** to **6**. This is surprising at some level, as the behavior at the onset of globular structure—predicted here to be at generation 5—might be expected to affect this trend.

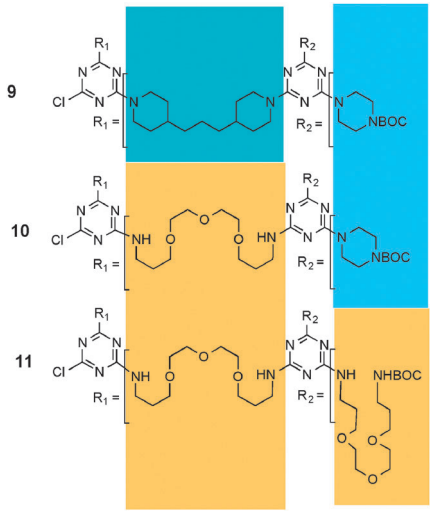

Chart 3 Macromonomers used in the synthesis.

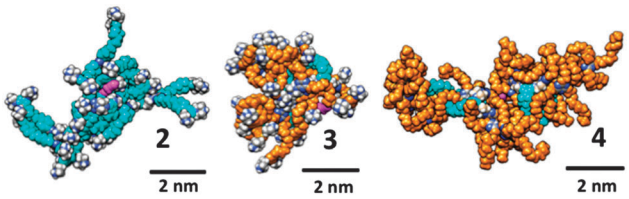

Fig. 1 MD simulation of **2–4** dendrimers in solution. Equilibrated (last) snapshot taken from the MD simulations of **2**, **3** and **4**. Trismethylene bispiperidine and 4,7,10-trioxotridecane-1,14-diamine are colored in cyan and orange respectively. The central residue of the dendrimers is colored in pink. Piperazine and all other groups are colored per-atom (C: grey, N: blue, H: white), water molecules and ions are not shown for clarity.

Computation offers further insight into the role of these linkers in solvation. Molecular models of **2–4** were immersed in a periodic simulation box containing explicit water molecules and 150 mM NaCl and were investigated by means of molecular dynamics (MD) simulations. Equilibrated configurations of **2** and **4** in solution were obtained within 250 ns. Dendrimer **3** required a longer equilibration time, and the MD simulation in this case lasted 400 ns (see ESI†). The equilibrated configurations of **2**, **3** and **4** shown in Fig. 1 reflect the color scheme adopted throughout the manuscript with cyan representing trismethylene bispiperidine and orange representing 4,7,10-trioxotridecane-1,14-diamine.

Computation reveals differences that are consistent with the solubility trend observed. In all cases, the hydrophobic core is sufficiently rigid that complete hydrophobic collapse is precluded. Instead, **2** displays an extended hydrophobic surface that leads us to hypothesize a role in promoting precipitation. For **3** and **4**, the 4,7,10-trioxotridecane-1,14-diamine groups collapse to partially shield hydrophobic domains. This behavior is consistent with previous simulations[9] and typical of the behaviour of PEG chains in water.[10] The shapes of **3** and **4** differ: **3** appears more spherical/globular while **4** adopts an elongated oval shape. Table 1 summarizes computed parameters for **2**, **3** and **4**. At the equilibrium, **3** has smaller radius of gyration (R_g) than **2**. We hypothesize the difference derives from the flexibility differences between 4,7,10-trioxotridecane-1,14-diamine and trismethylene bispiperidine. This difference is reflected in the solvent accessible surface area (SASA): **2** has a

Table 1 Structural features of dendrimers **2–4** obtained from the equilibrated phase MD simulations

Dendrimer	MW (Da)	R_g (Å)	SASA (Å^2)	Density[a] (Da Å^{-3})	H (kcal mol^{-1})
2	10 487	19.2	10 193	0.35	−11 254 ± 26
3	10 646	17.5	9409	0.47	−12 812 ± 35
4	14 940	21.2	13 116	0.37	−15 914 ± 39

[a] Density parameter is calculated by dividing the dendrimer MW for the volume of a sphere with radius R_g.

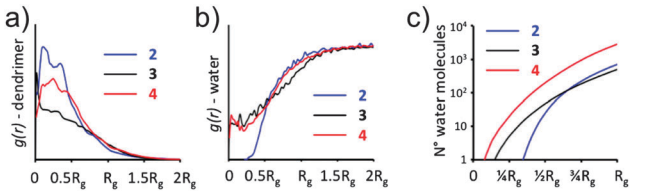

Fig. 2 Radial distribution functions, $g(r)$, obtained from the equilibrated phase MD simulations. The $g(r)$ curves are indicative of the probability to find atoms of the dendrimers (a) and water molecules (b) at given distance from the dendrimer's center of mass (CM). (c) Number of water molecules.

slightly larger SASA than **3** (10 193 A^2 *versus* 9049 A^2, respectively). The SASA of **4** is greater as would be inferred from the depiction, 13 116 A^2 and consistent with the larger R_g of 21.2 Å.

The enthalpy (H) values of the three dendrimers were calculated from the equilibrated phase MD simulations. A relative comparison of H shows that **2** is least stable (relatively) in water. Dendrimers **3** and **4** have more favorable (negative) H values indicating higher relative stability. By comparing calculated H values, we can quantify differences in stability (ΔH) of the dendrimers with respect to **2**. With similar numbers of atoms, **2** and **3** differ in enthalpy with $\Delta H = -1558 \pm 61$ kcal mol^{-1}, indicating that the substitution of trismethylene bispiperidine with 4,7,10-trioxotridecane-1,14-diamine has positive effect on the stability of **3** in water. Consistently, the ΔH of **4** is even more favourable difference with $\Delta H = -4659 \pm 66$ kcal mol^{-1}.

Radial distribution functions $g(r)$ were calculated from the equilibrated phase MD trajectories to probe hydration of **2**, **3** and **4** (Fig. 2). The $g(r)$ curves represent the relative probability to find dendrimer atoms (Fig. 2a) or water molecules (Fig. 2b) at a given distance from the dendrimer's center of mass (CM). Higher $g(r)$ peaks correspond to a high density of atoms and/or restricted migration, while low and broad peaks are indicative of higher molecular flexibility. In all cases, distances from CM are expressed in R_g units to allow comparison between different size dendrimers.

Fig. 2 reveals poorer solvation for **2** compared with **3** and **4**. In fact, the $g(r)$ curves show the dense core of **2** (Fig. 2a, blue) reduces the probability of hydration to 0 at distances lower than $\approx 1/2R_g$ (Fig. 2b). On the other hand, the same results demonstrate that **3** and **4** have a higher levels of core hydration. Fig. 2c plots the number of water molecules present in the interior of the dendrimers. This result corroborates experimental observations of solubility with the solvent penetration of **4** > **3** > **2**.

Conclusions

Solubility remains one of the most significant challenges in the synthesis of triazine dendrimers and limits the generation that these architectures can reach. Here, we show that solubility is impacted substantially by the choice of linking and surface groups across a range of dendrimer sizes. Piperazine, though inexpensive and highly reactive, does little to convey solubility of architectures in water when appearing on either the periphery or interior. This sensitivity to the source of cation is somewhat curious. Flexibility, as offered by trismethylene bispiperidine, improves solubility only slightly while maintaining high reactivity. The emergence of 4,7,10-trioxotridecane-1,14-diamine as a useful building block for dendrimers comes as a surprise: primary amines sacrifice reactivity. Moreover, the introduction of hydrogen bond donors should seemingly promote aggregation, especially in common organic solvents. However, using **11**, the resulting protected dendrimers are soluble in polar organic solvents including chloroform, dichloromethane, DMSO, ethyl acetate, tetrahydrofuran, dioxane, and methanol. These targets are not soluble in ether (which facilitates purification given the solubility of **11** in ether) or hexanes. The deprotected dendrimers containing **11** are soluble in the same subset of organic solvents with the exception of ethyl acetate.

The results obtained here are consistent with our recent success in reaching virus-sized dendrimers of generation 13.[11] There, 4,7,10-trioxotridecane-1,14-diamine was used exclusively as the linking diamine. Surmountable challenges to solubility in water appeared at generation 9, persisted through 11, and were deemed limiting at 13. When 4,7,10-trioxotridecane-1,14-diamine and piperazine linkers are alternated at each generation, dendrimers up to generation 9 were obtained.[12] Generation 11 materials were insoluble in both the protected form (in common organic solvents) and deprotected (in water).

The criteria for diamine choice continue to be refined. While these studies suggest that solubility of an advanced dendrimer might be rescued using macromonomers such as **11**, there appears to be additional room for improvement. Diamines that confer the reactivity of constrained secondary amines like piperazine and trismethylene bispiperidine and retain the advantageous solubility properties of 4,7,10-trioxotridecane-1,14-diamine could prove optimal in our pursuit of the rapid synthesis of large triazine dendrimers. Further experiment and computation will be required to meet these challenges.

Experimental

Molecular dynamics (MD) simulation

The simulation work was conducted using the AMBER 12 software.[13] The molecular models for **2**, **3**, and **4** dendrimers were created and parameterized according to a validated procedure used previously for similar derivatives.[9,14] In particular, **2**, **3**, and **4** dendrimers were parameterized with the "general AMBER force field (GAFF)" (*gaff.dat*).[15] The *parm99* all-atom force field (*leaprc.ff99*)[16] was used to parameterize all the other standard residues present in the simulated molecular systems.

The models of the three dendrimers were placed in a periodic box containing explicit TIP3P water molecules[17] and the necessary number of ions to neutralize the systems and reproduce the experimental ionic strength of 150 mM [NaCl]. Each system underwent initial minimization, and further heating through 50 ps of *NVT* MD simulation to reach the temperature of 300 K. During this second step the solute was maintained as fixed and the solvent was relaxed. Following to this phase, all systems

were equilibrated by running *NPT* MD simulations at the temperature of 300 K and 1 atm of pressure under periodic boundary conditions using a time step of 2 femtoseconds. The Langevin thermostat, and a 8 Å cutoff were used for all equilibration runs. The particle mesh Ewald[18] (PME) approach was adopted to treat the long-range electrostatic effects, and all bonds involving hydrogen atoms were treated by means of the SHAKE algorithm.[19] All MD simulations were carried out using the *pmemd.cuda* module of AMBER 12 working on GTX580 GPU cards. The root mean square deviation (RMSD) and radius of gyration (R_g) data were extracted from the MD trajectories with the *ptraj* module of AMBER 12 and were used to assess the equilibration of each dendrimer (see ESI†). In this respect, while a simulation time of 250 ns was enough for **2** and **4** to reach the equilibrium with good stability, having a sufficiently long equilibrated phase to allow for satisfactory analysis of the MD trajectory (the last 100 ns of MD simulations), a longer simulation time was necessary for **3** (400 ns).

The enthalpy (H) values for **2–4** dendrimers were calculated directly from the equilibrated phase MD trajectories according to the MM-PBSA approach.[20] H is the sum of the total gas-phase *in vacuo* non-bond energy (ΔE_{gas}) of the dendrimers and of a solvation term ($\Delta G_{solv} = \Delta G_{PB} + \Delta G_{NP}$).[21] The polar component of ΔG_{PB} was calculated according to the Poisson–Boltzmann[22] (PB) approach with a numerical solver implemented in the *pbsa* program of AMBER 12.[23] The non-polar contribution to the solvation energy was calculated as $\Delta G_{NP} = \gamma(\text{SASA}) + \beta$, in which $\gamma = 0.00542$ kcal Å^{-2}, $\beta = 0.92$ kcal mol^{-1}, and the solvent-accessible surface area (SASA) was estimated with the MSMS program.[24]

General procedure for deprotection

Compound **1-Boc** (0.417 g, 0.125 mmol) is dissolved in concentrated HCl (3 mL) and methanol (3 mL) and stirred for 15 h at room temperature. After evaporating the reaction mixture under vacuum, the residue is dissolved in dichloromethane, washed with 5 M NaOH (aq), and passed through a phase separator (Whatman). Evaporation of the organic phase yields **1** (0.316 g, quantitative).

General procedure for addition of macromonomer

A solution of **1** (0.160 g, 0.063 mmol), **9** (1.44 g, 1.01 mmol), and diisopropylethylamine (0.19 mL, 1.0 mmol) in 0.6 mL of THF is stirred at 75 °C for 6 days in a pressure relief reaction vial. After evaporation of the reaction mixture, the residue was dissolved in dichloromethane and washed with brine. The organic layer was passed through a phase separator (Whatman), and evaporated under vacuum. The solid was purified by silica gel chromatography (100% dichloromethane to 9 : 1 dichloromethane : methanol). Compound **12** (0.576 g, 67%)—the protected precursor of **5**—was recovered as a white solid.

Acknowledgements

EES thanks the Robert A. Welch Foundation (A-0008) for support and DOD W81XWH-12-1-0338.

Notes and references

1 (*a*) *Dendrimer-Based Drug Delivery Systems: From Theory to Practice*, ed. Y. Chen, Hoboken NJ, 2012, p. 542; (*b*) M. Ciolkowski, M. Rozanek, M. Bryszewska and B. Klajnert, *Biochim. Biophys. Acta*, 2013, **1834**, 1982–1987; (*c*) M. Zhang, R. Guo, M. Keri, I. Banyai, Y. Zheng, M. Cao, X. Cao and X. Shi, *J. Phys. Chem. B*, 2014, **118**, 1696–1706; (*d*) S. J. Guillaudeu, M. E. Fox, Y. M. Haidar, E. E. Dy, F. C. Szoka and J. M. J. Frechèt, *Bioconjugate Chem.*, 2008, **19**, 461–469; (*e*) K. T. Al-Jamal, J. T. W. Wang, N. Rubio, J. Buddle, D. Gathercole, M. Zloh and K. Kostarelos, *ACS Nano*, 2013, **7**, 1905–1917; (*f*) V. Jain, V. Maingi, P. K. Maiti and P. V. Bharatam, *Soft Matter*, 2013, **9**, 6482–6496.

2 (*a*) M. Bucoș, T. Sierra, A. Golemme, R. Termine, J. Barberà, R. Gimènez, J. Serrano, P. Romero and M. Marcos, *Chem. – Eur. J.*, 2014, **20**, 10027–10037; (*b*) J. Lim, B. Turkbey, M. Bernardo, H. Bryant, M. Garzoni, G. M. Pavan, T. Nakajima, P. Choyke, E. Simanek and H. Kobayashi, *Bioconjugate Chem.*, 2012, **23**, 2291–2299; (*c*) S. Patra, B. Kozura, Y.-T. A. Huang, A. Enciso, X. Sun, J.-T. Hsieh, C.-L. Kao, H.-T. Chen and E. Simanek, *Org. Lett.*, 2013, **15**, 3808–3811.

3 (*a*) E. E. Simanek, H. Abdou, S. Lalwani, J. Lim, M. Mintzer, V. J. Venditto and B. Vittur, *Proc. R. Soc. A*, 2010, **466**, 1445–1468; (*b*) M. Adeli, Z. Zarnegar and R. Kabiri, *J. Appl. Polym. Sci.*, 2010, **115**, 9–14.

4 W. Zhang and E. E. Simanek, *Tetrahedron Lett.*, 2001, **42**, 5355–5357.

5 4-AMP still plays a role in current dendrimer syntheses. When drugs are conjugated as dichlorotriazine derivatives, the resulting poly(monochlorotriazine) is readily elaborated to PEG derivatives in a two-step procedure involving (i) reaction with 4-AMP and subsequent acylation of the pendant primary amine.

6 The relative reactivity of different amines with monochlorotriazines has been quantified and ranges from benzylamine with a relative reactivity of 1, through primary amines to constrained secondary amines with azetidine being 320 times more reactive than benzylamine. Piperazine and piperidine have relative reactivity values around 60. See: (*a*) K. Moreno and E. E. Simanek, *Tetrahedron Lett.*, 2008, **49**, 1152–1154; (*b*) M. Steffensen and E. E. Simanek, *Angew. Chem., Int. Ed.*, 2004, **43**, 5178–5180.

7 Dendrimers with piperazine linkers gelated at higher concentrations in organic solvent in comparison to dendrimers with comprising primary amines that can donate hydrogen bonds: W. Zhang, S. O. Gonzalez and E. E. Simanek, *Macromolecules*, 2002, **35**, 9015–9021.

8 M. A. Mintzer, L. M. Perez and E. E. Simanek, *Tetrahedron Lett.*, 2010, **51**, 1631–1634.

9 (*a*) O. M. Merkel, M. Zheng, M. A. Mintzer, G. M. Pavan, D. Librizzi, M. Maly, H. Höffken, A. Danani, E. E. Simanek and T. Kissel, *J. Controlled Release*, 2011, **153**, 23–33; (*b*) O. M. Merkel, M. A. Mintzer, D. Librizzi, O. Samsonova, T. Dicke, B. Sproat, H. Garn, P. J. Barth, E. E. Simanek and T. Kissel, *Mol. Pharmaceutics*, 2010, **7**, 969–983; (*c*) G. M. Pavan,

M. A. Mintzer, E. E. Simanek, O. M. Merkel, T. Kissel and A. Danani, *Biomacromolecules*, 2010, **11**, 721–730.

10 (*a*) G. M. Pavan, A. Barducci, L. Albertazzi and M. Parrinello, *Soft Matter*, 2013, **9**, 2593–2597; (*b*) M. Garzoni, K. Okuro, N. Ishii, T. Aida and G. M. Pavan, *ACS Nano*, 2014, **8**, 904–914; (*c*) A. O. Kasimova, G. M. Pavan, A. Danani, K. Mondon, A. Cristiani, L. Scapozza, R. Gurny and M. Moeller, *J. Phys. Chem. B*, 2012, **116**, 4338–4345.

11 J. Lim, M. Kostiainen, J. Maly, V. C. P. da Costa, O. Annunziata, G. M. Pavan and E. E. Simanek, *J. Am. Chem. Soc.*, 2013, **135**, 4660–4663.

12 J. Lim, G. M. Pavan, O. Annunziata and E. E. Simanek, *J. Am. Chem. Soc.*, 2012, **134**, 1942–1945.

13 D. A. Case, T. A. Darden, T. E. Cheatham III, C. L. Simmerling, J. Wang, R. E. Duke, R. Luo, R. C. Walker, W. Zhang, K. M. Merz, B. Roberts, S. Hayik, A. Roitberg, G. Seabra, J. Swails, A. W. Goetz, I. Kolossvary, K. F. Wong, F. Paesani, J. Vanicek, R. M. Wolf, J. Liu, X. Wu, S. Brozell, T. Steinbrecher, H. Gohlke, Q. Cai, X. Ye, J. Wang, M.-J. Hsieh, G. Cui, D. R. Roe, D. H. Mathews, M. G. Seetin, R. Salomon-Ferrer, C. Sangui, V. Babin, T. Luchko, S. Gusarov, A. Kovalenko and P. A. Kollman, *AMBER 12*, University of California, San Francisco, 2012.

14 (*a*) E. E. Simanek, A. E. Enciso and G. M. Pavan, *Expert Opin. Drug Discovery*, 2013, **8**, 1057–1069; (*b*) J. Lim, S.-T. Lo, S. Hill, G. M. Pavan, X. Sun and E. E. Simanek, *Mol. Pharmaceutics*, 2012, **9**, 404–412.

15 J. Wang, R. M. Wolf, J. W. Caldwell, P. A. Kollman and D. A. Case, *J. Comput. Chem.*, 2004, **25**, 1157–1174.

16 T. E. Cheatham, P. Cieplak and P. A. Kollman, *J. Biomol. Struct. Dyn.*, 1999, **16**, 845–862.

17 W. L. Jorgensen, J. Chandrasekhar, J. D. Madura, R. W. Impey and M. L. Klein, *J. Chem. Phys.*, 1983, **79**, 926–935.

18 T. Darden, D. York and L. Pedersen, *J. Chem. Phys.*, 1993, **98**, 10089–10092.

19 V. Krautler, W. F. van Gunsteren and P. H. Hunenberger, *J. Comput. Chem.*, 2001, **22**, 501–508.

20 (*a*) P. A. Kollman, I. Massova, C. Reyes, B. Kuhn, S. H. Huo, L. Chong, M. Lee, T. Lee, Y. Duan and W. Wang, *et al.*, *Acc. Chem. Res.*, 2000, **33**, 889–897; (*b*) J. Srinivasan, T. E. Cheatham, P. Cieplak, P. A. Kollman and D. A. Case, *J. Am. Chem. Soc.*, 1998, **120**, 9401–9409.

21 B. Jayaram, D. Sprous and D. L. Beveridge, *J. Phys. Chem.*, 1998, **102**, 9571–9576.

22 D. Sitkoff, K. A. Sharp and B. Honig, *J. Phys. Chem.*, 1994, **98**, 1978–1988.

23 R. Luo, L. David and M. K. Gilson, *J. Comput. Chem.*, 2002, **23**, 1244–1253.

24 M. F. Sanner, A. J. Olson and J. C. Spehner, *Biopolymers*, 1996, **38**, 305–320.

Polymer Chemistry

PAPER

Accelerated synthesis of large generation triazine dendrimers using microwave assisted reactions: a 24 hour challenge†

A. E. Enciso,[a] F. Ramirez-Crescencio,[b] M. Zeiser,[a] R. Redón[b] and E. E. Simanek*[a]

Cite this: *Polym. Chem.*, 2015, **6**, 5219

Received 10th June 2015,
Accepted 11th June 2015

DOI: 10.1039/c5py00899a

www.rsc.org/polymers

The expedited synthesis of odd generation triazine dendrimers up to generation 9 can be executed in high yields using microwave irradiation. The efforts commence from commercially-available and inexpensive materials. Execution is facilitated by automated chromatography.

Introduction

Unlike linear polymers that are available in one step through polymerization of monomer(s), the synthesis of dendrimers relies on multiple steps. While burdensome in terms of both scale and time, strategies to reduce these tolls continue to be advanced.[1] In 2010, Hawker and Malkoch reported the synthesis of a generation 6 dendrimer in less than a day exploiting thiol–ene reactivity and click chemistry.[2] Two different, orthogonal monomers were employed. One monomer presented one thiol and two azides. The other presented two alkenes and an alkyne. The iterative synthesis produced highly monodisperse materials at low generations (PDI $\leq$ 1.03) and the onset of low polydispersity at generations 5 and 6. The only drawback to the strategy rested in the preparation of the monomers which entailed six overnight reactions and four chromatographic purifications. More recently, Malkoch *et al.* achieved a generation 6 dendrimer derived from bismethylolpropionic acid in less than a day (including the synthesis of starting materials) using the reactivity of carbonyldiimidazole and CsF as a catalyst.[3]

These efforts punctuate a long standing challenge to the community—the rapid and facile synthesis of dendrimers. To this end, many different approaches have been pursued.[4] In most of the cases, hypermonomers are employed that exploit the simplicity of Michael additions,[5] acid–amine conjugations,[6] thiol–ene photoadditions[7] and click chemistry.[8] The "onion peel" dendrimers described by Roy *et al.* provide a noteworthy example.[9] Our own efforts in accelerating the synthesis of triazine dendrimers using microwave irradiation have inspired us to take on this "24 hour challenge" to synthesis. We have shown that microwave irradiation substantially decrease times of reaction in low generation dendrimers synthesized by convergent route.[10] In light of this success and motivated by the long standing interest of performing an easy and fast synthesis, we decide to extend this chemistry to large generation triazine dendrimers using a divergent approach. We have shown that triazine dendrimers may have potential applications in many areas based on the ability to create versatile structures including areas in gene and drug delivery as well as materials science.[11]

Results and discussion

The synthesis strategy employed here to reach generation 9 dendrimers utilizes a macromonomer, **3**, that affords two generations per iterative reaction cycle (Scheme 1).[12] This macromonomer comprises hydrophilic linkers based on 4,7,10-trioxa-1,13-tridecanediamine and BOC-piperazine groups. Previous studies have established that piperazine and other constrained secondary amines provide the necessary reactivity for substitution of a monochlorotriazine.[13] All three building blocks employed; BOC-piperazine, cyanuric chloride, and 4,7,10-trioxa-1,13-tridecanediamine are commercially available and used as received. Cost analysis based on yields and solvent

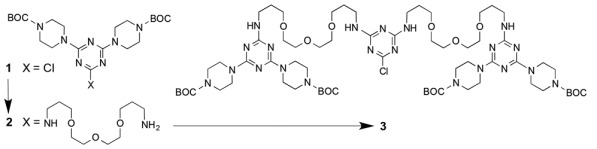

Scheme 1 Synthesis of macromonomer **3** from **1** and **2**. See text for details.

[a]*Department of Chemistry, Texas Christian University, Fort Worth, TX 76129, USA. E-mail: e.simanek@tcu.edu*

[b]*Departamento de Tecnociencias, Universidad Nacional Autónoma de México, Centro de Ciencias Aplicadas y Desarrollo Tecnológico, Universidad Nacional Autónoma de México, Cd. Universitaria A.P. 70-186, C.P. 04510, Coyoacán, México D. F., México*

† Electronic supplementary information (ESI) available: Spectral data and assignments. See DOI: 10.1039/c5py00899a

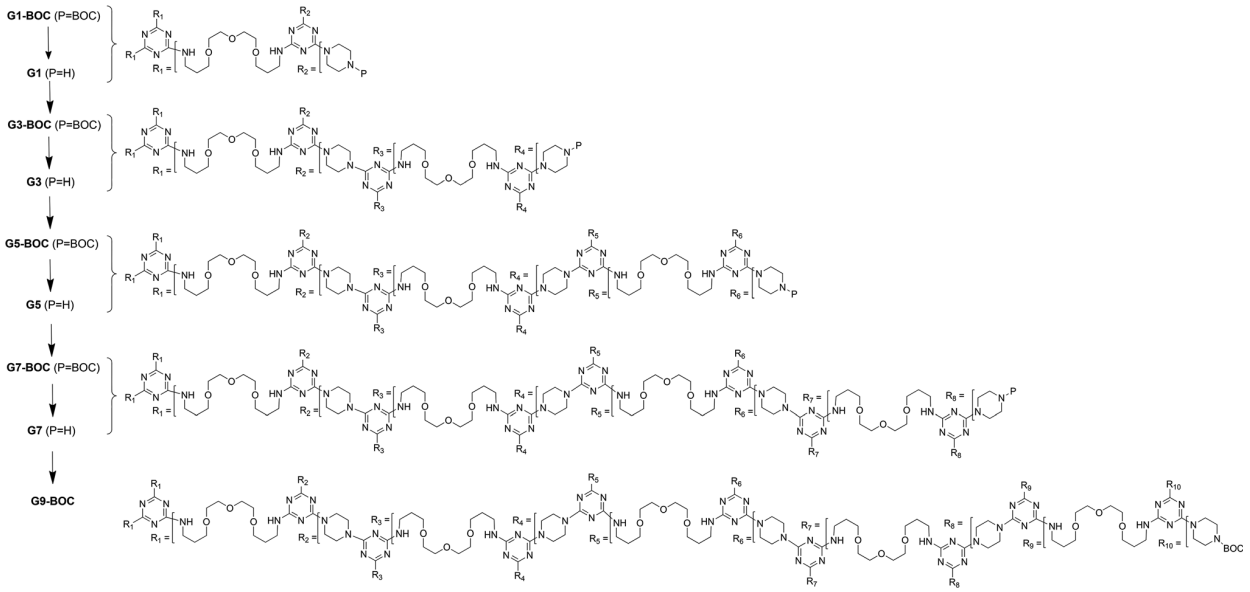

Chart 1 Dendrimers prepared in this study.

consumption for both synthesis and purification lead to a cost of $280 per g of generation 9 dendrimer at the modest scales employed here. Macromonomer **3** is readily prepared in three steps in 50 minutes of total reaction time (Scheme 1). Specifically, cyanuric chloride was disubstituted with BOC-piperazine in tetrahydrofuran (THF) using diisopropylethylamine (DIPEA) as a base with an irradiation time of 10 minutes at 60 °C. The product, **1**, is recovered by precipitation. Next, monochlorotriazine **1** is reacted with an excess of 4,7,10-trioxa-1,13-tridecanediamine in dioxane at 95 °C for 30 minutes using cesium carbonate as a base. Following chromatography, amine **2**, was reacted with cyanuric chloride in THF at 60 °C for 10 minutes with DIPEA as a base to yield **3**. Macromonomer **3** was purified by chromatography. The overall yield for this three-step procedure is 55%.

Chart 1 shows the structures of the dendrimers prepared in this study. These materials are named by the generation number "*x*" as **G*x***. Intermediates carrying BOC protecting groups are identified as **G*x*-BOC**. The synthesis is divergent and rests on the availability of large amounts of macronomer **3**. To prepare the generation one dendrimer, **G1**, macromonomer **3** is reacted with additional **2**. The primary amine of **2** reacts much more sluggishly with monochlorotriazines than piperazine groups. Accordingly, in presence of an excess of **2** in dioxane with cesium carbonate as a base, the reaction requires 95 °C for 2.5 hours. The result, **G1-BOC** is obtained at 60% yield after chromatography.

Deprotection to yield **G1** in dioxane/HCl requires only 6 minutes at 60 °C in the microwave. The product is obtained quantitatively and used without further purification.

The remaining steps of the synthesis follow this iterative process of addition of **3** and acid-catalyzed deprotection.

Cmpd	Rxn Time	Yield (%)	Cume (%)	Iso.	Isolation Time	Ends	MW (Da)
1	10 min	82	82	Prec	1 hr	NA	484
2	30 min	70	57	Chrm	2 hr	NA	667
3	10 min	95	55	Chrm	1 hr	NA	1446
G1-BOC	2.5 h	60	33	Chrm	1 hr	6	2077
G1	6 min	Quant.	33	Extr	30 min	6	1477
G3-BOC	4 h	82	27	Chrm.	1 hr	24	9936
G3	6 min	Quant.	27	Extr	30 min	24	7535
G5-BOC	4 h	75	20	Prec	1 hr	96	41K
G5	6 min	Quant.	20	Extr	30 min	96	32K
G7-BOC	6 h	85	17	Prec	1 hr	384	167K
G7	6 min	90	15	Extr	30 min	384	128K
G9-BOC	6 h	80	12	Prec	1 hr	1536	670K

Chart 2 Targets, reaction times, yields for individual reactions and the cumulative process (cume) over the entire sequence, isolation procedure (precipitation, chromatography, or extraction), isolation time and theoretical characteristics of the products.

All addition reactions are executed at 95 °C under microwave irradiation. All deprotection reactions are executed similarly, but at 60 °C. Beyond **G1**, the solvent system used for addition of **3** is dioxane : methanol : water at 2 : 1 : 0.1 Deprotections are carried out in 2 : 1 dioxane : conc. HCl. Chart 2 summarizes the individual yields, cumulative yields, and other attributes of the target molecules. The time for addition of **3** increases as the dendrimer generation increases. However, this increase is offset by the ease of purification: **3** and product dendrimer show markedly different solubility in ether with trace methanol.

Throughout the course of the synthesis, the intermediates and targets can be characterized by ^{1}H and ^{13}C NMR spectroscopy and mass spectrometry. ^{1}H NMR spectra show characteristic loss of BOC groups on deprotection, and appearance of substituted piperazine groups at δ 2.81–2.87. Mass spectrometry shows isotopic resolution and lines for materials

up to **G5-BOC**. Defects for **G5** and **G5-BOC** can be seen by ESI-MS. Larger dendrimers show a broad peak that can be attributed to incomplete reaction. Using GPC analysis, PDI values were possible to calculate for **G1-BOC**, **G3-BOC**, **G5-BOC**, and **G7-BOC** (1.05, 1.09, 1.11 and 1.18). When **G5** dendrimer was resubjected to reaction conditions with additional **3**, the PDI value did not decrease, remaining 1.11. No PDI could be obtained for **G9-BOC**.

While reaction times for synthesis of dendrimers up to **G9** might suggest that effort can be executed in under a day, purification does increase the burden. To simplify purification we use an automated flash chromatography unit that allows a total purification time of approximately 5 h for gram scale reactions for the four steps indicated. Precipitations can be performed repeatedly to incrementally increase yields as well.

Experimental

Compound 1

1-Boc-piperazine (11.14 g, 60 mmol) was added to a solution of cyanuric chloride (5.02 g, 27 mmol) in THF (200 mL). Afterwards DIPEA (19 mL, 0.109 mol) was added dropwise. The solution was stirred for 2 minutes in order to allow reagents to mix. Then, the solution was separated in multiple vessels and irradiated in the microwave while stirring for 10 minutes at 60 °C using dynamic mode. The crude product was purified by precipitations hexanes/EtOAc to give **1** (10.83 g, 82%) as a white solid. ^{1}H NMR (400 MHz, $CDCl_3$) δ 3.74 (br, 8H, NCH_2CH_2NBoc), 3.44 (br, 8H, NCH_2CH_2NBoc), 1.45 (s, 18H, $C(CH_3)_3$); ^{13}C NMR (100 MHz, $CDCl_3$) δ 169.6, 164.4 (C_3N_3), 156.5 (CO), 80.1 ($C(CH_3)_3$), 43.2 (NCH_2CH_2N), 28.3 ($C(CH_3)_3$); MS (ESI-TOF) calcd for $C_{21}H_{34}ClN_7O_4$ 483.2361, found 484.3702 $(M + H)^+$.

Compound 2

A solution of **1** (3 g, 6 mmol) with 4,7,10-trioxa-1,13-tridecanediamine (13.65 mL, 62 mmol) and Cs_2CO_3 (4 g, 12 mmol) in 40 mL of 1,4 dioxane was stirred for 2 minutes. Then, the solution was separated in multiple vessels and irradiated in the microwave while stirring for 30 minutes at 95 °C and then evaporated under vacuum. The residue was dissolved in dichloromethane, washed with brine solution and dried over $MgSO_4$, filtered, and evaporated under vacuum. The solvent system (in column volumes) used was the following: 5CV (100% DCM), 5CV (95 : 5 = DCM : MeOH), 5CV (90 : 10 = DCM : MeOH), 5CV (85 : 15 = DCM : MeOH), 5CV (80 : 20 = DCM : MeOH) to give **2** (3.26 g, 79%) as a white solid. ^{1}H NMR (400 MHz, $CDCl_3$) δ 3.73 (br, 8H, NCH_2CH_2NBoc), 3.67–3.57 (m, 12H, $CH_2OCH_2CH_2OCH_2CH_2OCH_2$), 3.44 (br, 10H, $NHCH_2CH_2CH_2O$, NCH_2CH_2NBoc), 2.81 (t, 2H, $OCH_2CH_2CH_2NH_2$), 1.84 (m, 2H, $OCH_2CH_2CH_2NH$), 1.76 (m, 2H, $OCH_2CH_2CH_2NH_2$), 1.47 (s, 18H, $C(CH_3)_3$); ^{13}C NMR (100 MHz, $CDCl_3$) δ 166.3, 165.2 (C_3N_3), 154.8 (CO), 79.8 ($C(CH_3)_3$), 70.5 (OCH_2CH_2O), 70.2 (OCH_2CH_2O), 70.1 (OCH_2CH_2O), 69.5 (two lines, $NHCH_2CH_2CH_2O$, $OCH_2CH_2CH_2NH_2$), 43.8 (piperazine), 39.4 ($NHCH_2CH_2CH_2O$), 38.2 ($OCH_2CH_2CH_2NH_2$), 32.6 ($OCH_2CH_2CH_2NH_2$), 29.6 ($NHCH_2CH_2CH_2O$), 28.6 ($C(CH_3)_3$); MS (ESI-TOF) calcd for $C_{31}H_{57}N_9O_7$ 667.4381, found 668.5915 $(M + H)^+$.

Compound 3 (macromonomer)

Compound **2** (3.26 g, 4.8 mmol) was added to a solution of cyanuric chloride (0.411 g, 2.2 mmol) in THF (20 mL). Afterwards DIPEA (3.2 mL, 18 mmol) was added dropwise, and the solution was sonicated for 2 minutes in order to allow reagents to mix. Then, the solution was irradiated in the microwave while stirring for 10 minutes at 60 °C using dynamic mode. The solvent system (in column volumes) used was the following: 5 CV (100% DCM), 5 CV (95 : 5 = DCM : MeOH), 5CV (90 : 10 = DCM : MeOH), 5CV (85 : 15 = DCM : MeOH), 5 CV (80 : 20 = DCM : MeOH) to give **3** (3.07 g, 95%) as a white solid. ^{1}H NMR (400 MHz, $CDCl_3$) δ 3.73 (br, 16H, NCH_2CH_2NBoc), 3.69–3.57 (m, 24H, $CH_2OCH_2CH_2OCH_2CH_2OCH_2$), 3.44 (br, 24H, C_3N_3–$NHCH_2CH_2CH_2O$, NCH_2CH_2NBoc), 1.86 (m, 8H, $OCH_2CH_2CH_2NH$), 1.48 (s, 36H, $C(CH_3)_3$); ^{13}C NMR (100 MHz, $CDCl_3$) δ 166.3 (C_3N_3), 165.7 (C_3N_3), 165.2 (C_3N_3), 154.8 (CO), 79.8 ($C(CH_3)_3$), 70.6 (OCH_2CH_2O), 70.3 (OCH_2CH_2O), 69.4 ($NHCH_2CH_2CH_2O$), 42.9 (piperazine), 38.9 ($NHCH_2CH_2CH_2O$), 38.3 ($NHCH_2CH_2CH_2O$), 29.6 ($NHCH_2CH_2CH_2O$), 28.8 ($NHCH_2CH_2CH_2O$), 28.4 ($C(CH_3)_3$); MS (ESI-TOF) calcd for $C_{65}H_{112}ClN_{21}O_{14}$ 1445.8386, found 1447.1735 $(M + H)^+$.

Compound 4 (G1-Boc)

A solution of **3** (0.743 g, 0.5 mmol) with **2** (1.042 g, 2 mmol) and Cs_2CO_3 (1.066 g, 3 mmol) in 5 mL of 1,4 dioxane and 0.5 mL MeOH was stirred for 2 minutes. Then, the solution was irradiated in the microwave while stirring for 2 hours 30 minutes at 95 °C using dynamic mode and then evaporated under vacuum. The residue was dissolved in dichloromethane, washed with brine solution and dried over $MgSO_4$, filtered, and evaporated under vacuum. The crude was purified by automated chromatography. The solvent system (in column volumes) used was the following: 20CV (100% DCM), 5CV (90 : 10 = DCM : MeOH) to give **4** (0.709 g, 66%) as a white solid. ^{1}H NMR (400 MHz, $CDCl_3$) δ 3.71 (br, 24H, NCH_2CH_2NBoc), 3.64–3.52 (m, 36H, $CH_2OCH_2CH_2OCH_2$-CH_2OCH_2) 3.43 (br, 36H, C_3N_3–$NHCH_2CH_2CH_2O$, $BocNCH_2$-CH_2N), 1.83 (m, 12H, $OCH_2CH_2CH_2NH$), 1.46 (s, 54H, $C(CH_3)_3$); ^{13}C NMR (100 MHz, $CDCl_3$) δ 166.3, 165.26 (C_3N_3), 154.8 (CO), 79.8 ($C(CH_3)_3$), 70.6 (OCH_2CH_2O), 70.2 (two lines, OCH_2CH_2O), 69.2 (two lines, $NHCH_2CH_2CH_2O$), 42.9 (piperazine), 38.2 ($NHCH_2CH_2CH_2O$), 38.1 ($NHCH_2CH_2CH_2O$), 29.6 ($NHCH_2CH_2CH_2O$), 28.4 ($C(CH_3)_3$); MS (ESI-TOF) calcd for $C_{96}H_{168}N_{30}O_{21}$ 2077.3000, found 2079.6681 $(M + H)^+$.

Compound 5 (G1 deprotected)

A solution of **4** (0.800 g, 0.385 mmol) in concentrated HCl (3 mL) and 1,4 dioxane (6 mL) was stirred for 1 min at room temperature and then was irradiated in the microwave while stirring for two periods of 3 minutes at 60 °C using dynamic mode and then evaporated with air. The residue was dissolved

in dichloromethane, washed with 5 M NaOH (aq.), dried over $MgSO_4$, filtered, and evaporated under vacuum to give **5** (0.571 g, quantitative) as a white solid. ^{1}H NMR (400 MHz, $CDCl_3$) δ 3.69 (br, 24H, NC**H**$_2$CH$_2$NH), 3.64–3.51 (m, 36H, C**H**$_2$OC**H**$_2$C**H**$_2$OC**H**$_2$C**H**$_2$OC**H**$_2$) 3.40 (br, 12H, C_3N_3–NHC**H**$_2$-CH$_2$CH$_2$O), 2.83 (br, 24H, HNC**H**$_2$CH$_2$N), 1.82 (m, 12H, OCH$_2$C**H**$_2$CH$_2$NH); ^{13}C NMR (100 MHz, $CDCl_3$) δ 166.3, 165.2 (**C**$_3$N$_3$), 70.6 (O**C**H$_2$CH$_2$O), 70.2 (two lines, OCH$_2$**C**H$_2$O), 69.3 (NHCH$_2$CH$_2$**C**H$_2$O), 69.2 (NHCH$_2$CH$_2$**C**H$_2$O), 46.0 (NCH$_2$**C**H$_2$NH), 44.2 (N**C**H$_2$CH$_2$NH), 38.2 (NH**C**H$_2$CH$_2$CH$_2$O), 38.1 (NH**C**H$_2$CH$_2$CH$_2$O), 29.6 (NHCH$_2$**C**H$_2$CH$_2$O); MS (ESI-TOF) calcd for $C_{66}H_{120}N_{30}O_9$ 1476.9855, found 1478.2639 $(M + H)^+$.

Compound 6 (G3-Boc)

A solution of **3** (2.35 g, 1.624 mmol) with **5** (0.200 g, 0.135 mmol) and DIPEA (0.42 mL, 2.44 mmol) in 4 mL of 1,4 dioxane and 0.5 mL MeOH was stirred for 2 minutes. Then, the solution was irradiated in the microwave while stirring for 4 hours at 95 °C using dynamic mode and then evaporated under vacuum. The residue was dissolved in dichloromethane, washed with brine solution and dried over $MgSO_4$, filtered, and evaporated under vacuum. The crude was purified by automated chromatography. The solvent system (in column volumes) used was the following: 5CV (99 : 1 = EtoAc : MeOH), 5CV (98 : 2 = EtoAc : MeOH), 5CV (100% DCM) to give **6** (1.1 g, 82%) as a white solid. ^{1}H NMR (400 MHz, $CDCl_3$) δ 3.72 (br, 144H, NC**H**$_2$CH$_2$NBoc, NCH$_2$**C**H$_2$N), 3.66–3.53 (m, 180H, C**H**$_2$OC**H**$_2$C**H**$_2$OC**H**$_2$C**H**$_2$OC**H**$_2$), 3.45 (br, 156H, C_3N_3–NHC**H**$_2$-CH$_2$CH$_2$O, BocNC**H**$_2$CH$_2$N), 1.86 (m, 60H, OCH$_2$C**H**$_2$CH$_2$NH), 1.47 (s, 216H, C(C**H**$_3$)$_3$); ^{13}C NMR (100 MHz, $CDCl_3$) δ 166.3, 165.26 (**C**$_3$N$_3$), 154.8 (**C**O), 79.8 (**C**(CH$_3$)$_3$), 70.6 (O**C**H$_2$CH$_2$O), 70.2 (two lines, OCH$_2$**C**H$_2$O), 69.3 (two lines, NHCH$_2$CH$_2$-**C**H$_2$O), 42.9 (piperazine), 38.2 (NH**C**H$_2$CH$_2$CH$_2$O), 38.1 (NH**C**H$_2$CH$_2$CH$_2$O), 29.6 (NHCH$_2$**C**H$_2$CH$_2$O), 28.4 (C(**C**H$_3$)$_3$); MS (ESI-TOF) calcd for $C_{456}H_{786}N_{156}O_{93}$ 9936.16, found 9944.5803 $(M + H)^+$.

Compound 7 (G3 deprotected)

A solution of **6** (0.650 g, 65.4 μmol) in concentrated HCl (3 mL) and dioxane (6 mL) was stirred for 1 min at room temperature and then was irradiated in the microwave while stirring for two periods of 3 minutes at 60 °C using dynamic mode and then evaporated with air. The residue was dissolved in dichloromethane, washed with 5 M NaOH (aq.), dried over $MgSO_4$, filtered, and evaporated under vacuum to give **7** (0.493 g, quantitative) as a white solid. ^{1}H NMR (400 MHz, $CDCl_3$) δ 3.72 (br, 144H, NC**H**$_2$CH$_2$NH, NC**H**$_2$C**H**$_2$N), 3.67–3.53 (m, 180H, C**H**$_2$OC**H**$_2$C**H**$_2$OC**H**$_2$C**H**$_2$OC**H**$_2$), 3.47 (br, 60H, C_3N_3–NHC**H**$_2$CH$_2$CH$_2$O), 2.87 (br, 96H, HNC**H**$_2$CH$_2$N), 1.85 (m, 60H, OCH$_2$C**H**$_2$CH$_2$NH); ^{13}C NMR (100 MHz, $CDCl_3$) δ 166.3, 165.2 (**C**$_3$N$_3$), 70.6 (O**C**H$_2$CH$_2$O), 70.2 (O**C**H$_2$CH$_2$O), 69.3 (two lines, NHCH$_2$CH$_2$**C**H$_2$O), 46.0 (NCH$_2$CH$_2$NH), 44.2 (N**C**H$_2$CH$_2$NH), 43.0 (NCH$_2$**C**H$_2$N), 38.1 (NH**C**H$_2$CH$_2$CH$_2$O), 29.6 (NHCH$_2$**C**H$_2$-CH$_2$O); MS (ESI-TOF) calcd for $C_{336}H_{594}N_{156}O_{45}$ 7534.90, found 7541.6290 $(M + H)^+$.

Compound 8 (G5-Boc)

A solution of **3** (1.84 g, 1.274 mmol) with **7** (0.200 g, 26.53 μmol) and DIPEA (0.33 mL, 1.9 mmol) in 6 mL of 1,4 dioxane, 0.5 mL MeOH and 0.5 mL H_2O was stirred for 2 minutes. Then, the solution was irradiated in the microwave while stirring for 4 hours at 95 °C using dynamic mode and then evaporated under vacuum. The residue was dissolved in dichloromethane, washed with brine solution and dried over $MgSO_4$, filtered, and evaporated under vacuum. The crude was purified by several washes with a solution of 98 : 2 = EtoEt : MeOH to give **8** (0.76 g, 75%) as a white solid. ^{1}H NMR (400 MHz, $CDCl_3$) δ 3.73 (br, 624H, NC**H**$_2$CH$_2$NBoc, NCH$_2$**C**H$_2$N), 3.67–3.53 (m, 756H, C**H**$_2$OC**H**$_2$C**H**$_2$OC**H**$_2$-C**H**$_2$OC**H**$_2$), 3.44 (br, 636H, C_3N_3–NHC**H**$_2$CH$_2$CH$_2$O, BocNC**H**$_2$CH$_2$N), 1.85 (m, 252H, OCH$_2$C**H**$_2$CH$_2$NH), 1.48 (s, 864H, C(C**H**$_3$)$_3$); ^{13}C NMR (100 MHz, $CDCl_3$) δ 166.3, 165.2, 165.1 (**C**$_3$N$_3$), 154.8 (**C**O), 79.8 (**C**(CH$_3$)$_3$), 70.6 (O**C**H$_2$CH$_2$O), 70.2 (two lines, OCH$_2$**C**H$_2$O), 69.3 (two lines, NHCH$_2$CH$_2$-**C**H$_2$O), 42.9 (piperazine), 38.2 (NH**C**H$_2$CH$_2$CH$_2$O), 38.1 (NH**C**H$_2$CH$_2$CH$_2$O), 29.6 (two lines, NHCH$_2$**C**H$_2$CH$_2$O), 28.4 (C(**C**H$_3$)$_3$); MS (ESI-TOF) calcd for $C_{1896}H_{3258}N_{660}O_{381}$ 41371.59, found 41404.7224 $(M + H)^+$.

Compound 9 (G5 deprotected)

A solution of **8** (0.400 g, 9.67 μmol) in concentrated HCl (2 mL) and dioxane (4 mL) was stirred for 1 min at room temperature and then was irradiated in the microwave while stirring for three periods of 3 minutes at 60 °C using dynamic mode and then evaporated with air. The residue was dissolved in dichloromethane, washed with 5 M NaOH (aq.), dried over $MgSO_4$, filtered, and evaporated under vacuum to give **9** (0.307 g, quantitative) as a white solid. ^{1}H NMR (400 MHz, $CDCl_3$) δ 3.68 (br, 624H, NC**H**$_2$CH$_2$NH, NC**H**$_2$C**H**$_2$N), 3.62–3.49 (br m, 756H, C**H**$_2$OC**H**$_2$C**H**$_2$OC**H**$_2$C**H**$_2$OC**H**$_2$), 3.40 (br, 252H, C_3N_3–NHC**H**$_2$CH$_2$CH$_2$O), 2.81 (br m, 384H, HNC**H**$_2$CH$_2$N), 1.80 (m, 252H, OCH$_2$C**H**$_2$CH$_2$NH); ^{13}C NMR (100 MHz, $CDCl_3$) δ 166.3, 165.2 (**C**$_3$N$_3$), 70.6 (O**C**H$_2$CH$_2$O), 70.2 (O**C**H$_2$CH$_2$O), 69.3 (NHCH$_2$CH$_2$**C**H$_2$O), 69.2 (NHCH$_2$CH$_2$**C**H$_2$O), 46.0 (NCH$_2$**C**H$_2$NH), 44.2 (N**C**H$_2$CH$_2$NH), 43.0 (NCH$_2$**C**H$_2$N), 38.1 (NH**C**H$_2$CH$_2$CH$_2$O), 29.6 (NHCH$_2$**C**H$_2$CH$_2$O); MS (ESI-TOF) calcd for $C_{1416}H_{2490}N_{660}O_{189}$ 31766.55, found 31792.1374 $(M + H)^+$.

Compound 10 (G7-Boc)

A solution of **3** (1.75 g, 1.2 mmol) with **9** (0.200 g, 6.3 μmol) and DIPEA (0.33 mL, 1.91 mmol) in 7 mL of 1,4 dioxane, 1 mL MeOH and 0.5 mL H_2O was stirred for 2 minutes. Then, the solution was irradiated in the microwave while stirring for 6 hours at 95 °C using dynamic mode and then evaporated under vacuum. The residue was dissolved in dichloromethane, washed with brine solution and dried over $MgSO_4$, filtered, and evaporated under vacuum. The crude was purified by several washes with a solution of 97 : 3 = EtoEt : MeOH to give **10** (0.850 g, 81%) as a white solid. ^{1}H NMR (400 MHz, $CDCl_3$) δ 3.73 (br, 2544H, NC**H**$_2$CH$_2$NBoc, NCH$_2$CH$_2$N),

3.65–3.52 (m, 3060H, C**H**$_2$OC**H**$_2$C**H**$_2$OC**H**$_2$C**H**$_2$OC**H**$_2$), 3.43 (br, 2556H, C_3N_3–NHC**H**$_2$CH$_2$CH$_2$O, BocNC**H**$_2$CH$_2$N), 1.84 (m, 1020H, OCH$_2$C**H**$_2$CH$_2$NH), 1.48 (s, 3456H, C(C**H**$_3$)$_3$); ^{13}C NMR (100 MHz, $CDCl_3$) δ 166.3, 165.2 (**C**$_3$N$_3$), 154.8 (**C**O), 79.8 (**C**(CH$_3$)$_3$), 70.6 (O**C**H$_2$**C**H$_2$O), 70.2 (two lines, O**C**H$_2$**C**H$_2$O), 69.3 (NHCH$_2$CH$_2$**C**H$_2$O), 69.2 (NHCH$_2$CH$_2$**C**H$_2$O), 42.9 (piperazine), 38.2 (NH**C**H$_2$CH$_2$CH$_2$O), 29.6 (NHCH$_2$**C**H$_2$CH$_2$O), 28.4 (C(**C**H$_3$)$_3$); MS (ESI-TOF) calcd for $C_{7656}H_{13146}N_{2676}O_{1533}$ 167113.30, not found.

Compound 11 (G7 deprotected)

A solution of **10** (0.390 g, 2.3 μmol) in concentrated HCl (2.5 mL) and dioxane (5 mL) was stirred for 1 min at room temperature and then was irradiated in the microwave while stirring for three periods of 3 minutes at 60 °C using dynamic mode and then evaporated with air. The residue was dissolved in dichloromethane, washed with 5 M NaOH (aq.), dried over $MgSO_4$, filtered, and evaporated under vacuum to give **9** (0.270 g, 90%) as a white solid. ^{1}H NMR (400 MHz, $CDCl_3$) δ 3.71 (br, 2544H, NC**H**$_2$CH$_2$NH, NC**H**$_2$C**H**$_2$N), 3.64–3.51 (br m, 3060H, C**H**$_2$OC**H**$_2$C**H**$_2$OC**H**$_2$C**H**$_2$OC**H**$_2$), 3.44 (br, 1020H, C_3N_3–NHC**H**$_2$CH$_2$CH$_2$O), 2.84 (br, 1536H, HNC**H**$_2$CH$_2$N), 1.83 (m, 1020H, OCH$_2$C**H**$_2$CH$_2$NH); ^{13}C NMR (100 MHz, $CDCl_3$) δ 166.3, 165.2 (**C**$_3$N$_3$), 70.6 (O**C**H$_2$**C**H$_2$O), 70.2 (O**C**H$_2$**C**H$_2$O), 69.3 (NHCH$_2$CH$_2$**C**H$_2$O), 69.2 (NHCH$_2$CH$_2$**C**H$_2$O), 46.0 (NCH$_2$**C**H$_2$-NH), 44.2 (N**C**H$_2$CH$_2$NH), 43.0 (NC**H**$_2$CH$_2$N), 38.1 (NH**C**H$_2$CH$_2$CH$_2$O), 29.7 (NHCH$_2$**C**H$_2$CH$_2$O); MS (MALDI-TOF) calcd for $C_{5736}H_{10074}N_{2676}O_{765}$ 128693.17, not found.

Compound 12 (G9-Boc)

A solution of **3** (0.430 g, 0.30 mmol) with **11** (0.050 g, 0.39 μmol) and DIPEA (0.08 mL, 0.45 mmol) in 3 mL of 1,4 dioxane, 1 mL MeOH and 0.5 mL H_2O was stirred for 2 minutes. Then, the solution was irradiated in the microwave while stirring for 6 hours at 95 °C using dynamic mode and then evaporated under vacuum. The residue was dissolved in dichloromethane, washed with brine solution and dried over $MgSO_4$, filtered, and evaporated under vacuum. The crude was purified by several washes with MeOH to give **10** (0.209 g, 80%) as a white wax.^{1}H NMR (400 MHz, $CDCl_3$) δ 3.71 (br, 10224H, NC**H**$_2$CH$_2$NBoc, NC**H**$_2$C**H**$_2$N), 3.63–3.52 (br m, 12276H, C**H**$_2$OC**H**$_2$C**H**$_2$OC**H**$_2$C**H**$_2$OC**H**$_2$), 3.41 (br, 10236H, C_3N_3–NHC**H**$_2$CH$_2$CH$_2$O, BocNC**H**$_2$CH$_2$N), 1.80 (m, 4092H, OCH$_2$C**H**$_2$CH$_2$NH), 1.46 (s, 13824H, C(C**H**$_3$)$_3$); ^{13}C NMR (100 MHz, $CDCl_3$) δ 166.2, 165.2 (**C**$_3$N$_3$), 154.7 (**C**O), 79.8 (**C**(CH$_3$)$_3$), 70.6 (O**C**H$_2$**C**H$_2$O), 70.2 (O**C**H$_2$**C**H$_2$O), 69.3 (NHCH$_2$CH$_2$**C**H$_2$O), 42.9 (piperazine), 38.2 (NH**C**H$_2$CH$_2$CH$_2$O), 29.6 (NHCH$_2$**C**H$_2$CH$_2$O), 28.4 (C(**C**H$_3$)$_3$); MS (MALDI-TOF) calcd for $C_{30696}H_{52698}N_{10740}O_{6141}$ 670080.15, not found.

Conclusions

Advancing dendrimers to applications requires readily available materials. While low generation triazine dendrimers have been readily available for some time,[14] the efficient preparation of moderate and higher generation dendrimers has been elusive until now. Triazines now join the architectures advanced by Hawker, Malkoch, and Roy as rapidly assessable at high generations.

Acknowledgements

We thank the Robert A. Welch Foundation (A-0008) and DOD (W81XWH-12-1-0338) for support. FRC and RR thank CONACyT for a fellowship (227152-332714) and funding (167356). RR also thanks PAPIIT for support (IN117514).

Notes and references

1 (*a*) A.-M. Caminade, C.-O. Turrin, R. Laurent, A. Ouali and B. Delavaux-Nicot, *Dendrimers: towards Catalytic, Material and Biomedical Uses*, Wiley, United Kingdom, 1st edn, 2011; (*b*) S. Campagna, P. Ceroni and F. Puntoriero, *Designing Dendrimers*, Wiley, New Jersey, 1st edn, 2012; (*c*) R. J. Young and P. A. Lovell, *Introduction to Polymers*, Taylor & Francis Group, Florida, 3rd edn, 2011; (*d*) C. Bouillon, A. Tintaru, V. Monnier, L. Charles, G. Quelever and L. Peng, *J. Org. Chem.*, 2010, **75**, 8685–8688.

2 P. Antoni, M. J. Robb, L. Campos, M. Montanez, A. Hult, E. Malmstrom, M. Malkoch and C. J. Hawker, *Macromolecules*, 2010, **43**, 6625.

3 S. Garcia-Gallego, D. Hult, J. V. Olsson and M. Malkoch, *Angew. Chem., Int. Ed.*, 2015, **54**, 2416.

4 M. V. Walter and M. Malkoch, *Chem. Soc. Rev.*, 2012, **13**, 4593.

5 (*a*) M. Xinpeng, Z. Zhou, E. Jin, Q. Sun, B. Zhang, J. Tang and Y. Shen, *Macromolecules*, 2013, **46**, 37; (*b*) S. Chatani, M. Podgorski, C. Wang and C. N. Bowman, *Macromolecules*, 2014, **47**, 4894.

6 Y. Ito, T. Higashihara and M. Ueda, *Macromolecules*, 2012, **45**, 4175.

7 (*a*) N. Kottari, Y. M. Chabre, T. C. Shiao, R. Rej and R. Roy, *Chem. Commun.*, 2014, **50**, 1983; (*b*) A. R. Jennings and D. Y. Son, *Chem. Commun.*, 2013, **49**, 3467.

8 (*a*) M. Arseneault, I. Levesque and J.-F. Morin, *Macromolecules*, 2012, **45**, 3687; (*b*) V. Haridas, Y. K. Sharma, S. Sahu, R. P. Verma, S. Sadanandan and B. G. Kacheswar, *Tetrahedron*, 2011, **67**, 1873.

9 (*a*) R. Sharma, N. Kottari, Y. M. Chabre, L. Abbassi, T. C. Shiao and R. Roy, *Chem. Commun.*, 2014, **50**, 13300; (*b*) R. Sharma, K. Naresh, Y. M. Chabre, R. Rej, N. Saadeh and R. Roy, *Polym. Chem.*, 2014, **5**, 4321.

10 A. E. Enciso, Z. M. Abid and E. E. Simanek, *Polym. Chem.*, 2014, **5**, 4635.

11 (*a*) J. Lim, B. Turkbey, M. Bernardo, L. H. Bryant, Jr., M. Garzoni, G. M. Pavan, T. Nakajima, P. L. Choyke, E. E. Simanek and H. Kobayashi, *Bioconjugate Chem.*, 2012, **23**, 2291–2299; (*b*) C. S. Lee, S.-T. Lo, J. Lim, V. C. P. da Costa, S. Ramezani, O. K. Oz, G. M. Pavan, O. Annunziata,

X. Sun and E. E. Simanek, *Mol. Pharmaceutics*, 2013, **10**, 4452–4461; (*c*) O. M. Merkel, M. A. Mintzer, D. Librizzi, O. Samsonova, T. Dicke, B. Sproat, H. Garn, P. J. Barth, E. E. Simanek and T. Kissel, *Mol. Pharmaceutics*, 2010, **7**, 969–983; (*d*) S. Yoo, S. Yeu, R. L. Sherman, D. E. Shantz, E. E. Simanek and D. A. Ford, *J. Membrane Sci.*, 2009, **334**, 16–22.

12 J. Lim, G. M. Pavan, O. Annunziata and E. E. Simanek, *J. Am. Chem. Soc.*, 2012, **134**, 1942.

13 (*a*) K. X. Moreno and E. E. Simanek, *Tetrahedron Lett.*, 2008, **49**, 1152; (*b*) M. B. Steffensen and E. E. Simanek, *Org. Lett.*, 2003, **5**, 2359–2361.

14 A. Chouai and E. E. Simanek, *J. Org. Chem.*, 2008, **73**, 2357.

molecular pharmaceutics

Article

pubs.acs.org/molecularpharmaceutics

Triazine-Substituted and Acyl Hydrazones: Experiment and Computation Reveal a Stability Inversion at Low pH

Kun Ji, Changsuk Lee, Benjamin G. Janesko,* and Eric E. Simanek*

Department of Chemistry, Texas Christian University, Fort Worth, Texas 76129, United States

Supporting Information

ABSTRACT: Condensation of a hydrazine-substituted *s*-triazine with an aldehyde or ketone yields an equivalent to the widely used, acid-labile acyl hydrazone. Hydrolysis of these hydrazones using a formaldehyde trap as monitored using HPLC reveals that triazine-substituted hydrazones are more labile than acetyl hydrazones at pH >5. The reactivity trends mirror that of the corresponding acetyl hydrazones, with hydrolysis rates increasing along the series (aromatic aldehyde < aromatic ketone < aliphatic ketone). Computational and experimental studies indicate a reversal in stability around the triazine pK_a (pH ∼5). Protonation of the triazine moiety retards acid-catalyzed hydrolysis of triazinyl hydrazones in comparison to acetyl hydrazone analogues. This behavior supports mechanistic interpretations suggesting that resistance to protonation of the hydrazone N1 is the critical factor in affecting the reaction rate.

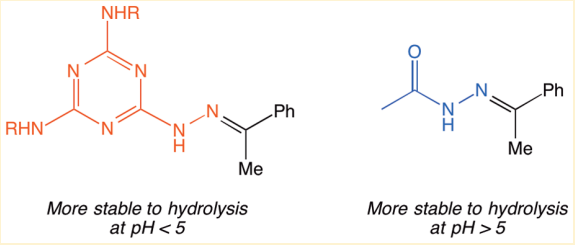

KEYWORDS: *triazine, hydrazine, hydrazone, pH labile, release, computation*

Labile bonds in general, and hydrazones in particular, find diverse roles in chemistry ranging from materials to medical sciences. Hydrazones have been employed in the creation of dynamic combinatorial libraries[1] and as reagents and auxiliaries in organic synthesis.[2] Fragrant aldehydes and ketones have been incorporated into materials as pro-perfumes using hydrazone chemistry.[3] Hydrazones can be bioactive in their own right,[4] including uses as antitrypanasomals[5] and tools for molecular biology.[6] The lability of hydrazones in acid inspires the application of these groups as linkers in drug conjugates. Calicheamicin is conjugated to an oxidized antibody through an acyl hydrazone in Mylotarg.[7] Conjugates of other drugs have been reported, including doxorubicin.[8] Hydrazones have been used as the basis for switches, sensors, and other materials.[9] While the literature is replete with examples of aliphatic, acyl, and aromatic hydrazine derivatives of triazines and the resulting hydrazones, the mechanism of hydrazone hydrolysis is unreported.[10]

Our longstanding interest in triazine chemistry[11] led us to examine whether hydrazine derivatives of triazines—so-called triazinyl hydrazines—might mirror acyl hydrazines in hydrazone formation and hydrolysis. A priori, it was unclear whether such hydrazones would be more or less stable than the acyl analogues. To start, a four-step synthesis of triazinyl hydrazine **1** (Scheme 1) was adopted. The aminoethoxyethanol substituents were included to enhance the water solubility. The moderate reactivity of BOC-$NHNH_2$ (BOC = *tert*-butoxycarbonyl) led to its installation on a dichlorotriazine intermediate that could be subsequently elaborated to give **1** as shown. In contrast, the reaction of cyanuric chloride with BOC-$NHNH_2$ led to a mixture of products, including the desired monoaddition product, the diaddition product, and other impurities that were not identified.[12] Similarly, the elevated temperatures required for installation of BOC-$NHNH_2$ (or hydrazine) on a suitably derivatized monochlorotriazine led to the desired compound but also to additional impurities identified in HPLC chromatograms. Our interest in applying poly(dichlorotriazines) as intermediates in dendrimer synthesis or on other scaffolds makes this seemingly laborious synthesis generally applicable, if not desirable.[13]

Scheme 1. Synthesis of Triazinylhydrazine 1[a]

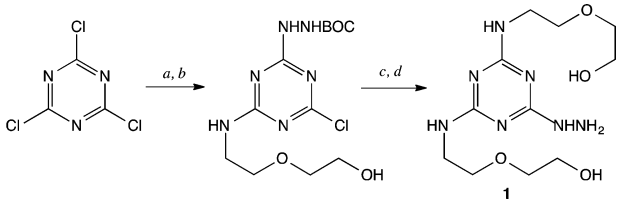

[a]Reagents and conditions: (*a*) Aminoethoxyethanol, THF, DIPEA, −15 to 0 °C, 1 h. (*b*) BOC-$NHNH_2$, THF, DIPEA, RT, 12 h. (*c*) Aminoethoxyethanol, dioxane, DIPEA, 80 °C, 12 h. (*d*) 4 M HCl/MeOH, 12 h.

We examined a suite of five aldehydes and ketones (**a**–**e**; Chart 1). We denote the hydrazone formed by the condensation of **1** and **a** as **1-a** and the corresponding acetyl

Received: March 12, 2015
Revised: June 1, 2015
Accepted: June 15, 2015
Published: June 15, 2015

DOI: 10.1021/acs.molpharmaceut.5b00205
Mol. Pharmaceutics 2015, 12, 2924−2927

Chart 1. Aldehydes and Ketones Used in This Study

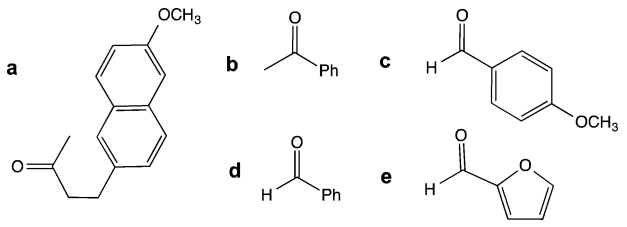

hydrazone as **Ac-a**. The alphabetical ordering of these compounds reflects their measured stabilities toward hydrolysis (vide infra).

Condensation of **1** or acetyl hydrazine, $AcNHNH_2$, to form the corresponding hydrazone was accomplished readily by mixing with a 3-fold excess of **a**–**e** and 0.5 equiv of acetic acid at room temperature in ethanol overnight followed by chromatographic purification. Structures were validated by ^1H and ^{13}C NMR spectroscopy as well as mass spectrometry. Each of the compounds showed a single peak in its HPLC chromatogram with a unique retention time. Hydrolysis rates were measured in a mixed solvent system to account for the varying hydrophobicity of these molecules. Briefly, 50 mM stock solutions of **1-a** through **1-e** were prepared in methanol (**Ac-a** through **Ac-e** were prepared in THF) and diluted to 10 mM with disodium phosphate/citric acid buffers to reach pH 5.2, 6.8, and 8.0. Hydrolysis was monitored in the presence of a 10-fold excess of formaldehyde as a trap[14] using HPLC (see the Supporting Information). Hydrolysis was pronounced at pH 5.2. Figure 1 shows the data derived from HPLC traces. Comparatively, acyl hydrazones are more stable than their triazinyl hydrazone counterparts. The stability increases with hydrazones **a** < **b** < **c** < **d** < **e**.

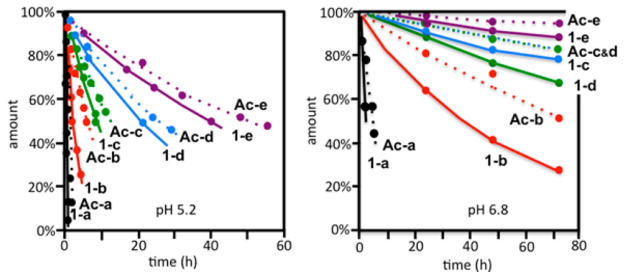

Figure 1. Hydrolysis profiles at pH 5.2 (left) and 6.8 (right).

At pH 6.8, similar trends were observed over 72 h, as shown in Figure 1, with most showing less than 20% hydrolysis over this period. At pH 8.0, neglible hydrolysis was observed over 72 h: only **1-a** and **Ac-a** showed measurable hydrolysis rates (0.0006 and 0.0001 min^{-1}, respectively). First-order reaction rate constants and half-lives are shown in Table 1.

The accepted mechanism for hydrazone hydrolysis starts with protonation of nitrogen N1 to yield **I** (Scheme 2).[15] Addition of a molecule of water yields carbinolamine intermediate **II**. Proton migration to give **III** leads to C–N bond cleavage to complete the hydrolysis. Subject to historical and contemporary inquiry,[14−17] this mechanism is consistent with catalysis observed in acid. Three different interpretations have been invoked to rationalize differences in the rates of hydrolyses of different hydrazones (and oximes and imines). These include a thermodynamic argument based on ground-state stabilities,[16] resonance stabilization arguments focusing on the reduction of electrophilicity of C1,[17] and stabilities derived from resistance to protonation of N1, which was recently invoked by Kalia and Raines[14] to explain the relative stabilities of hydrazones and oximes.

Scheme 2. Mechanism of Hydrolysis (R = Acetyl or Triazinyl)

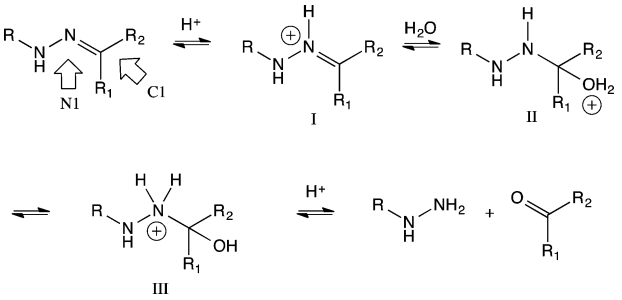

Table 1 includes density functional theory (DFT) calculations[18−20] of proton affinities (ΔE_{prot}) of N1 of the hydrazone. These values are assigned relative to **Ac-b**. Positive values correspond to stable proton binding. The calculations used the B3LYP exchange–correlation functional,[18] the 6-31+G(d,p) basis set,[19] and the SMD continuum model for aqueous solvent[20] as implemented in the Gaussian 09 suite of programs.[21] Other computational details and energies and geometries of all species are reported in the Supporting Information. The measured rates of hydrolysis for **Ac-a** through

Table 1. First-Order Reaction Constants and Half-Lives and DFT-Computed N1 Proton Affinities ΔE_{prot} Relative to Ac-b[a]

	pH 4.0		pH 5.2		pH 6.8		
compd	k (10^{-3} min^{-1})	$t_{1/2}$ (min)	k (10^{-3} min^{-1})	$t_{1/2}$ (min)	k (10^{-3} min^{-1})	$t_{1/2}$ (min)	ΔE_{prot} (kcal/mol)[a]
1-a	–	–	39	18	4.7	150	4.4 (−5.0)
Ac-a	–	–	20	34	2.6	270	1.7
1-b	8.0	87	5.2	130	0.3	2310	2.3 (−4.3)
Ac-b	30	23	1.9	370	0.1	6900	0.0
1-c	1.9	360	1.3	530	0.09	–	1.0 (−4.1)
Ac-c	8.6	81	0.5	1400	0.04	–	−0.7
1-d	1.8	390	0.9	770	0.059	–	−1.3 (−4.2)
Ac-d	2.9	240	0.4	1700	0.046	–	−3.0
1-e	0.7	990	0.3	2300	0.014	–	−0.1 (−4.4)
Ac-e	3.1	224	0.2	3500	0.027	–	−1.9

[a]Changes in ΔE_{prot} upon triazine protonation are given in parentheses.

DOI: 10.1021/acs.molpharmaceut.5b00205
Mol. Pharmaceutics 2015, 12, 2924–2927

Ac-e correlate with the computed N1 proton affinities, consistent with the work of Kalia and Raines.[14] For example, ketone-derived **Ac-a** has a shorter half-life and larger proton affinity than **Ac-b**, while aldehyde-derived **Ac-c**, **Ac-d**, and **Ac-e** have longer half-lives and smaller (more negative) proton affinities than **Ac-b**. **Ac-c** has a larger proton affinity and shorter half-life than **Ac-d**, consistent with an increase in the proton affinity due to resonance electron donation from the *p*-methoxy group to N1.

Table 1 also shows that the triazinyl hydrazones **1-a** through **1-e** all have shorter half-lives at pH 5 and larger N1 proton affinities than the corresponding acetyl hydrazones. Computation clearly supports an interpretation that resistance of N1 to protonation is the key predictor of the stability of hydrazones toward hydrolysis. Consistent with this analysis, computational models of simple imines (H_2NMe) and oximes (H_2NOMe) derived from **b** (PhMeC═NMe and PhMeC═NOMe) gave a large computed N1 proton affinity (relative to **Ac-b**) of 14.9 kcal/mol for the rapidly hydrolyzed imine and a small proton affinity of −1.5 kcal/mol for the stable oxime.[14]

Triazinyl hydrazones, unlike acyl hyrazones, imines, and oximes, offer additional basic sites on the triazine. Kalia and Raines noted that protonation of N1 is disfavored across a range of pH because the pK_a of N1 is <0.7. Accordingly, activated species will exist at very low concentrations in the pH range of interest. The pK_a of protonated triazines is ∼5,[22] and thus, protonated triazines must be considered at low pH. Triazine protonation should promote hydrolysis by increasing the electrophilicity of C1 through induction, but counterproductively, should increase the resistance of N1 to protonation (Scheme 3), the perceived critical event in hydrolysis.

Scheme 3. Triazine Protonation (pK_a ≈ 5) Could Increase the Electrophilicity of C1 through Induction (Increasing the Hydrolysis Rate) or Increase the Resistance to N1 Protonation (Decreasing the Hydrolysis Rate)

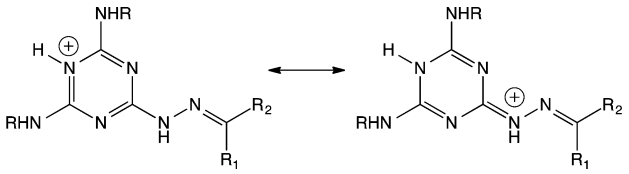

Computation bears out this prediction. Table 1 shows that para protonation of the triazine in **1-a** through **1-e** reduces the predicted N1 proton affinity by 4−5 kcal/mol. Ortho protonation of **1-d** reduces the predicted N1 proton affinity by 6−10 kcal/mol, partially as a result of steric clashes between the *o*-N−H and N1−H protons. We note that ortho protonation could conceivably accelerate hydrolysis that proceeds without N1 protonation by increasing the electrophilicity of C1. Test calculations suggested that this is a small effect. The reaction of C1 of molecule **1-d** with hydroxide is made 45 kcal/mol more favorable by N1 protonation but only 11 kcal/mol more favorable by ortho protonation.

To explore this effect, we measured the rates of hydrolysis of **1-b** and **Ac-b** at pH 4. Indeed, an inversion in stability was observed, with **Ac-b** hydrolyzing more rapidly than **1-b** (Figure 2). Specifically, at pH 4, the rate constants (in units of 10^{-3} min^{-1}) for **1-b**, **Ac-b**, **1-c**, and **Ac-c** are 8.4, 2.7, 1.9, and 0.9,

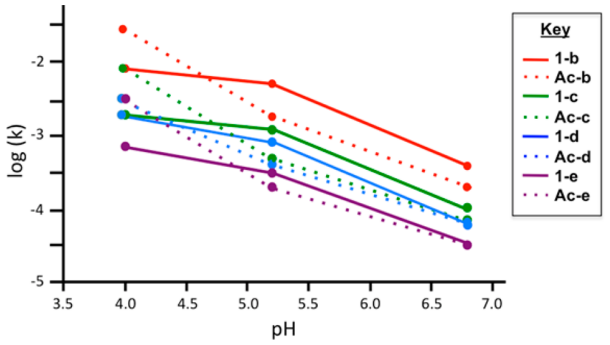

Figure 2. Hydrolysis profiles at pH 4 in the presence of a 10-fold molar excess of formaldehyde.

respectively, and the half-lives (in min) for **1-b**, **Ac-b**, **1-c**, and **Ac-c** are 83, 25, 364, and 81, respectively.

In summary, the data presented here support the Kalia/Raines mechanism for hydrolysis. This "resistance to protonation" hypothesis is further supported by the inversion of stability seen in triazinyl and acetyl hydrazones at low pH. This inversion in stability occurs at a pH that is biologically relevant—that associated with the cellular uptake and the endosome. Whether it can be exploited advantageously for the delivery of drugs or other agents remains to be seen.

■ ASSOCIATED CONTENT

Supporting Information

Synthetic details; characterization data, including spectra and kinetic studies; and a text file containing computational details and computed structures and energies. The Supporting Information is available free of charge on the ACS Publications website at DOI: 10.1021/acs.molpharmaceut.5b00205.

■ AUTHOR INFORMATION

Corresponding Authors

*E-mail: b.janesko@tcu.edu.
*E-mail: E.simanek@tcu.edu.

Notes

The authors declare no competing financial interest.

■ ACKNOWLEDGMENTS

We thank the Robert A. Welch Foundation (A-0008) and the DOD (W81XWH-12-1-0338) for support.

■ DEDICATION

E.E.S. dedicates this manuscript to the memory of Professor John L. Hogg, decorated and tireless educator of Texas A&M University who showed a proclivity for protons and hydrolysis reactions.[23]

■ REFERENCES

(1) (a) Corbett, P. T.; Leclaire, J.; Vial, L.; West, K. R.; Wietor, J.-L.; Sanders, J. K. M.; Otto, S. Dynamic Combinatorial Chemistry. *Chem. Rev.* **2006**, *106*, 3652−3711. (b) Li, J.; Nowak, P.; Otto, S. Dynamic Combinatorial Libraries: From Exploring Molecular Recognition to Systems Chemistry. *J. Am. Chem. Soc.* **2013**, *135*, 9222−9239. (c) Lehn, J.-M.; Ramström, O. Drug discovery by dynamic combinatorial libraries. *Nat. Rev. Drug Discovery* **2002**, *1*, 26−36. (d) Dirksen, A.; Dirksen, S.; Hackeng, T. M.; Dawson, P. E. Implications for Dynamic Covalent Chemistry. *J. Am. Chem. Soc.* **2006**, *128*, 15602−15603.

DOI: 10.1021/acs.molpharmaceut.5b00205
Mol. Pharmaceutics 2015, 12, 2924−2927

(2) Lazny, R.; Nodzewska, A. *N,N*-Dialkylhydrazones in Organic Synthesis. From Simple *N,N*-Dimethylhydrazones to Supported Chiral Auxiliaries. *Chem. Rev.* **2010**, *110*, 1386−1434.
(3) Levrand, B.; Fieber, W.; Lehn, J.-M.; Herrmann, A. Controlled release of volatile aldehydes and ketones from dynamic mixtures generated by reversible hydrazone formation. *Helv. Chim. Acta* **2007**, *90*, 2281−2314.
(4) Rollas, S.; Kucukguzel, S. G. Biological activities of hydrazone derivatives. *Molecules* **2007**, *12*, 1910−1939.
(5) Baliani, A.; Bueno, G. J.; Stewart, M. L.; Yardley, V.; Brun, R.; Barrett, M. P.; Gilbert, I. H. Design and Synthesis of a Series of Melamine-Based Nitroheterocycles with Activity against Trypanosomatid Parasites. *J. Med. Chem.* **2005**, *48*, 5570−5579.
(6) For an example using carbonyl cyanide 3-chlorophenylhydrazone, see: Webber, M. A.; Coldham, N. G. Measuring the activity of active efflux in Gram-negative bacteria. *Methods Mol. Biol.* **2010**, *642*, 173−180.
(7) Hamann, P. R.; Hinman, L. M.; Beyer, C. F.; Lindh, D.; Upeslacis, J.; Flowers, D. A.; Bernstein, I. An Anti-CD33 Antibody−Calicheamicin Conjugate for Treatment of Acute Myeloid Leukemia. Choice of Linker. *Bioconjugate Chem.* **2002**, *13*, 40−46.
(8) (a) Zhang, X.; Achazi, K.; Steinhilber, D.; Kratz, F.; Dernedde, J.; Haag, R. A facile approach for dual-responsive prodrug nanogels based on dendritic polyglycerols with minimal leaching. *J. Controlled Release* **2014**, *174*, 209−216. (b) Kruger, H. R.; Schutz, I.; Justies, A.; Licha, K.; Welker, P.; Haucke, V.; Calderon, M. Imaging of doxorubicin release from theranostic macromolecular prodrugs via fluorescence resonance energy transfer. *J. Controlled Release* **2014**, *194*, 189−196.
(9) (a) Su, X.; Aprahamian, I. Hydrazone-based switches, metallo-assemblies and sensors. *Chem. Soc. Rev.* **2014**, *43*, 1963−1981. (b) McKinnon, D. D.; Domaille, D. W.; Cha, J. N.; Anseth, K. N. Bis-Aliphatic Hydrazone-Linked Hydrogels Form Most Rapidly at Physiological pH: Identifying the Origin of Hydrogel Properties with Small Molecule Kinetic Studies. *Chem. Mater.* **2014**, *26*, 2382−2387.
(10) For recent examples outside the patent literature, see: (a) Jani, G. R.; Vyas, K. B.; Franco, Z. Preparation and antimicrobial activity of *s*-triazine hydrazones of 7-hydroxycoumarin and their metal complexes. *E-J. Chem.* **2009**, *6*, 1228−1232. (b) Kumar, A.; Menon, S. K. Fullerene derivatized *s*-triazine analogues as antimicrobial agents. *Eur. J. Med. Chem.* **2009**, *44*, 2178−2183. (c) Berkoudt, T. W.; Egmose, K. N.; Karst, U.; Kempter, C.; Tolbol, C. G. Air monitoring of aldehydes by use of hydrazine reagents with a triazine backbone. *Anal. Bioanal. Chem.* **2002**, *372*, 639−646.
(11) Simanek, E. E.; Abdou, H.; Lalwani, S.; Lim, J.; Mintzer, M.; Venditto, V. J.; Vittur, B. The 8 year thicket of triazine dendrimers: strategies, targets and applications. *Proc. R. Soc. A* **2010**, *466*, 1445−1468.
(12) An alternative route not pursued here relies on the reaction of $C_3N_3Cl_3$ with hydrazine to arrive at the dichlorotriazine intermediate. See: Polovkovych, S. V.; Karkhut, A. I.; Marintsova, N. G.; Leysk, R. B.; Zimenkovsky, B. S.; Novikov, V. P. Synthesis of New Schiff Bases and Polycyclic Fused Thiopyranothiazoles Containing 4,6-Dichloro-1,3,5-triazine Moiety. *J. Heterocycl. Chem.* **2013**, *50*, 1419−1424.
(13) Patra, S.; Kozura, B.; Huang, A. Y.-T.; Enciso, A. E.; Sun, X.; Hsieh, J.-T.; Kao, C.-L.; Chen, H.-T.; Simanek, E. E. Dendrimers Terminated with Dichlorotriazine Groups Provide a Route to Compositional Diversity. *Org. Lett.* **2013**, *15*, 3808−3811.
(14) Kalia, J.; Raines, R. T. Hydrolytic Stability of Hydrazones and Oximes. *Angew. Chem., Int. Ed.* **2008**, *47*, 7523−7526.
(15) Jencks, W. P. Mechanism and catalysis of simple carbonyl group reactions. *Prog. Phys. Org. Chem.* **1964**, *2*, 63−128.
(16) Wiberg, K. B.; Glaser, J. Resonance interactions in acyclic systems. 4. Stereochemistry, energetics, and electron distributions in 3-center four-π-electron systems A═BC: *J. Am. Chem. Soc.* **1992**, *114*, 841−850.
(17) This traditional argument can be found in, for example: Carey, F. A.; Sundberg, R. J. *Advanced Organic Chemistry*, 5th ed. Springer: New York, 2008; Vol. *A*, pp 650−651.
(18) (a) Becke, A. D. Density-functional exchange-energy approximation with correct asymptotic behavior. *Phys. Rev. A* **1988**, *38*, 3098−3100. (b) Lee, C.; Yang, W.; Parr, R. B. Development of the Colle−Salvetti correlation-energy formula into a functional of the electron density. *Phys. Rev. B* **1988**, *37*, 785−789. (c) Becke, A. D. Density-functional thermochemistry. III. The role of exact exchange. *J. Chem. Phys.* **1993**, *98*, 5648−5652. (d) Stephens, P. J.; Devlin, F. J.; Chalabowski, C. F.; Frisch, M. J. Ab Initio Calculation of Vibrational Absorption and Circular Dichroism Spectra Using Density Functional Force Fields. *J. Phys. Chem.* **1994**, *98*, 11623−11627.
(19) Hehre, W. J.; Ditchfeld, R.; Pople, J. A. Self-consistent molecular orbital methods. XII. Further extensions of Gaussian-type basis sets for use in molecular orbital studies of organic molecules. *J. Chem. Phys.* **1972**, *56*, 2257−2261.
(20) Marenich, A. V.; Cramer, C. J.; Truhlar, D. G. Universal Solvation Model Based on Solute Electron Density and on a Continuum Model of the Solvent Defined by the Bulk Dielectric Constant and Atomic Surface Tensions. *J. Phys. Chem. B* **2009**, *113*, 6378−6396.
(21) Frisch, M. J.; et al. *Gaussian 09*, revision B.01; Gaussian, Inc.: Wallingford, CT, 2009.
(22) Jang, Y. H.; Hwang, S.; Chang, S. B.; Ku, J.; Chung, D. S. Acid Dissociation Constants of Melamine Derivatives from Density Functional Theory Calculations. *J. Phys. Chem. A* **2009**, *113*, 13036−13040.
(23) (a) Hogg, J. L.; Jencks, D. A.; Jencks, W. P. Catalysis of transimination through trapping by acids and bases. *J. Am. Chem. Soc.* **1977**, *14*, 4772−4778. (b) Bokser, A. D.; York, K. A.; Hogg, J. L. Proton inventory investigation of the specific acid-catalyzed hydrolysis of gamma-ethoxy-gamma-butyrolactone. *J. Org. Chem.* **1986**, *51*, 92−94.

DOI: 10.1021/acs.molpharmaceut.5b00205
Mol. Pharmaceutics 2015, 12, 2924−2927

molecules

MDPI

Article

Functionalization of a Triazine Dendrimer Presenting Four Maleimides on the Periphery and a DOTA Group at the Core

Changsuk Lee, Kun Ji and Eric E. Simanek *

Department of Chemistry and Biochemistry, Texas Christian University, Fort Worth, TX 76129, USA; leecs73@hotmail.com (C.L.); kun.ji@tcu.edu (K.J.)

* Correspondence: e.simanek@tcu.edu; Tel.: +1-817-257-5355

Academic Editor: Ashok Kakkar

Received: 28 January 2016 ; Accepted: 26 February 2016 ; Published: 10 March 2016

Abstract: A readily and rapidly accessible triazine dendrimer was manipulated in four steps with 23% overall yield to give a construct displaying four maleimide groups and DOTA. The maleimide groups of the dendrimer are sensitive to hydrolysis under basic conditions. The addition of up to four molecules of water can be observed via mass spectrometry and HPLC. The evolution in the alkene region of the ^{1}H-NMR—the transformation of the maleimide singlet to the appearance of two doublets—is consistent with imide hydrolysis and not the Michael addition. The hydrolysis events that proceeded over hours are sufficiently slower than the desired thiol addition reactions that occur in minutes. The addition of thiols to maleimides can be accomplished in a variety of solvents. The thiols examined derived from cysteine and include the protected amino acid, a protected dipeptide, and native oligopeptides containing either 9 or 18 amino acids. The addition reactions were monitored with HPLC and mass spectrometry in most cases. Complete substitution was observed for small molecule reactants. The model peptides containing nine or eighteen amino acids provided a mixture of products averaging between 3 and 4 substitutions/dendrimer. The functionalization of the chelate group with gadolinium was also accomplished easily.

Keywords: dendrimer; triazine; DOTA; maleimide; peptide; bioconjugate; theranostic

1. Introduction

The term "theranostics" describes molecules that offer both therapeutic and diagnostic capabilities [1–6]. Theranostic small molecules include a reporting group—commonly a chelate for MRI or PET imaging—ligated to a pharmacophore. Theranostic nanoparticles elaborate this design with materials that can offer multivalent displays of the therapeutic and/or diagnostic agent(s), as well as leverage additional properties conveyed with size, including changes in biodistribution and targeting. Theranostic nanoparticles come in many varieties including magnetic [7], silica [8–10], gold/quantum dots [11–13], graphene [14], liposomal [15,16], and polymeric [17,18]. Dendritic materials offer a compelling platform in this area [19,20] given the opportunity to exquisitely control chemistry to manipulate any number of properties displayed across multiple nanoparticle classes, so-called nanoperiodicity [21–23], including size, ligand density and solubility. Versatility is a key criterion for the design of such targets. Here, we report on a tetravalent platform, **1** (Figure 1). Target **1** comprises three different domains: a reporter domain, a functional domain, and a dendritic domain. The reporter domain presents a DOTA group that can host metals for diagnostic applications such as PET or MRI. The functional domain presents four maleimides that can be readily reacted with thiols. The functional domain is linked to the reporter domain through the dendritic domain. Here, the dendritic domain is a small, generation-1 triazine dendron.

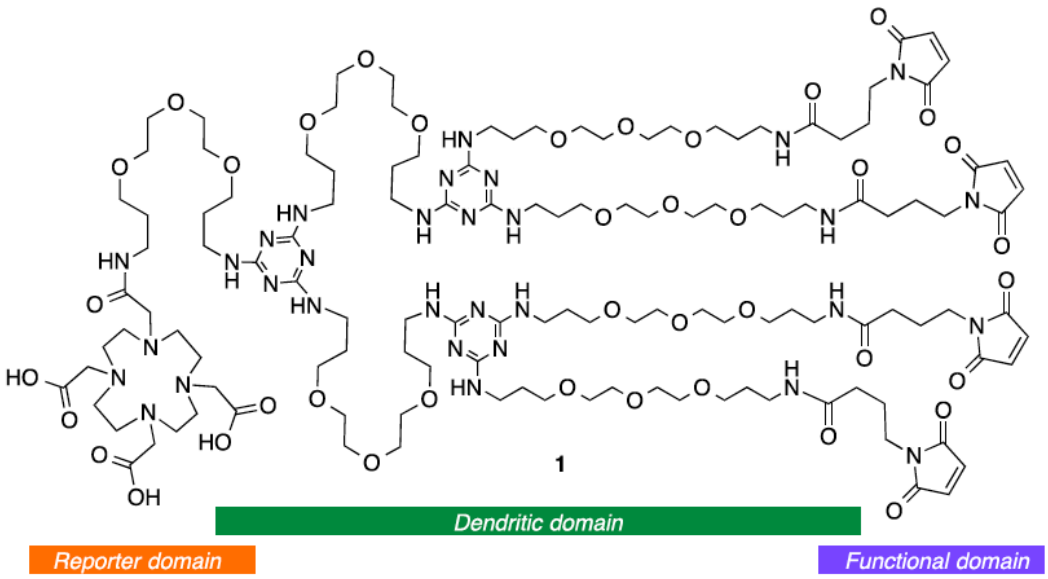

Figure 1. Target **1** with domains identified as reporter domain (**orange**), dendritic domain (**green**) and functional domain (**blue**).

2. Results and Discussion

2.1. Synthesis

The synthesis of **1** is shown in Scheme 1. It commences with the triazine dendron, **2**, which has been previously reported [24]. Intermediate **2** was obtained in less than 24 h using microwave-assisted reactions. The installation of the DOTA-reagent, **3**, was accomplished with HBTU to provide **4** in 43% yield. While mass spectrometry confirmed the structure of the product, the multiple conformations of the DOTA group led to broad signals in the ^{1}H-NMR spectra. The lines corresponding to the seven expected *tert*-butyl groups were well resolved, and integration matched expectation when compared with signature regions of the dendrimer.

To probe generality, and assess opportunities for potential future efforts that elaborate the dendritic portion in the presence of the reporter domain, we explored the feasibility of a two-step deprotection strategy. First, the Boc groups of **4** were selectively removed with a 1:1 mixture of 6 N HCl:MeOH to afford **5** in 79% isolated yield. Second, intermediate **5** was elaborated into a larger G3 dendrimer with 16 terminal groups (see Supplementary Materials). Then, intermediate **6** was obtained directly from **4** with a global deprotection step using a 1:1 mixture of TFA:CH_2Cl_2. Finally, the installation of the maleimides to produce **1** proceeded with 69% yield. This four-step synthetic sequence (starting from **4**) is executed with 23% overall yield. Gadolinium can be incorporated into **1** at this point (see Supplementary Materials).

2.2. Hydrolytic Stability

The hydrolytic stability of **1** in an aqueous solution is of significant concern: Commercially available maleimide crosslinking reagents are moisture sensitive, especially at pH > 7.5. To assess, stability, **1** was added to slightly basic water (pH 7.5) and monitored by mass spectrometry and HPLC. After 4 h, the addition of up to four water molecules was clearly visible by both techniques. HPLC suggests that approximately 10% of **1** remains after 4 h under these slightly basic conditions. Under neutral conditions, however, the hydrolysis is much slower: Analysis of the ^{1}H-NMR suggests only 25% hydrolysis, observed after 2 days.

^{1}H-NMR of the hydrolysis product is consistent with imide hydrolysis to a ring-opened, maleic acid amide. The alkene singlet of **1** appearing at 6.7 ppm is replaced with two doublets at 6.2 and

5.8 ppm (J = 12.4 Hz). Accordingly, only the disappearance of *all* alkene signals during a substitution reaction can be considered evidence for complete substitution of **1** with ligands. The Michael addition reactions of the maleic acid amide derivatives with thiols were unsuccessful under the conditions employed for the conjugates described in the following paragraphs. This hydrolysis reaction—with similar kinetics—has been previously reported in functionalized PAMAM dendrimers [25].

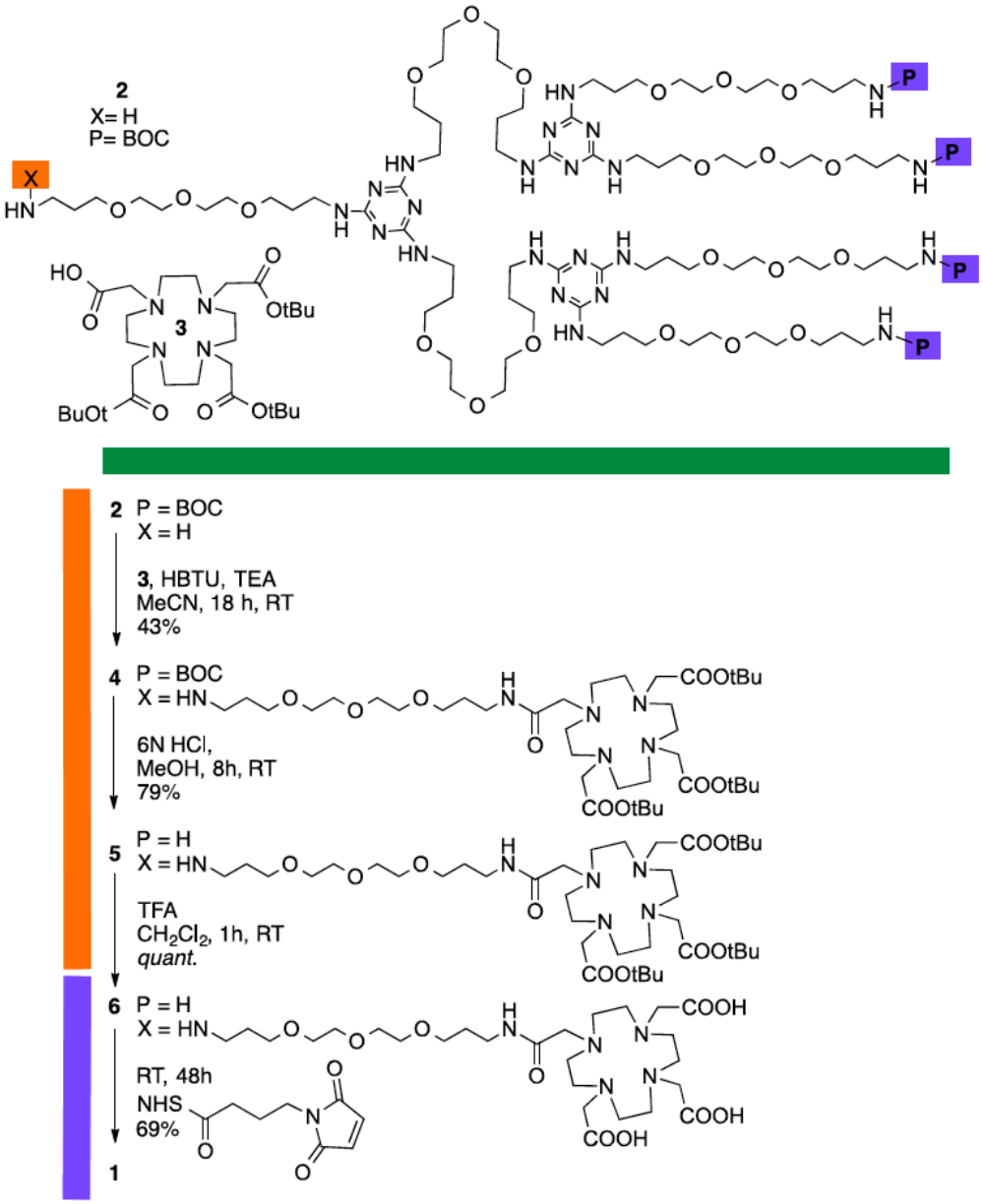

Scheme 1. Synthesis of **1** commencing with reactions at the reported domain (**orange**) and then functional domain (**blue**).

2.3. Conjugation of Small Molecules

Fortunately, and in contrast to hydrolysis, the reaction between the maleimide and a thiol was rapid. The thiols and the model compound **7** that were examined in this study are shown in Figure 2. Hydrophobic **A** and **B** were chosen to examine solubility limitations that might be encountered during conjugation reactions. Oligomers **C** and **D** were chosen to assess the impacts of size on conjugation

efficiency as determined by reaction times and product distributions. Since we predicted that **1** could serve as a building block for libraries, peptides **C** and **D** were used without extensive purification. Specifically, HPLC and MS analysis suggest that each peptide is present in greater than 60% in the crude cocktail obtained after precipitation of the cleavage product derived from a peptide synthesizer. To identify conjugates, the letter indicating the thiol and valency (when appropriate) is appended to the parent maleimide. That is, reaction of **7** and **A** produces **7-A$_1$** (or just **7-A**), whereas the product of three additions of **D** to **1** is identified as **1-D$_3$**.

A FmocCysOMe

B FmocCysTrpOMe

C H_2N-CYGPPPPPG-COOH

D H_2N-CGFQLRQPPLVSRKGEG-COOH

Model **7**

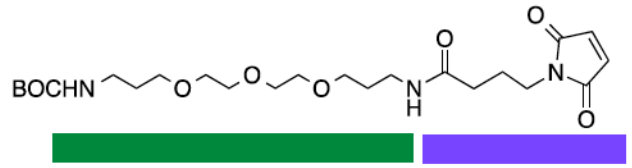

Figure 2. Thiols **A**–**D** in this study and model system **7** which models the dendritic domain (**green**) and functional domain (**blue**).

Compound **7** was prepared as a model to identify indicators of a successful reaction (Figure 2). The reactions of **7** with **A** (FmocCysOMe) and **B** (FmocCysTrpOMe) to yield conjugates **7-A** and **7-B**, respectively, were followed using NMR spectroscopy, mass spectrometry, and HPLC. Here, methylene chloride was used as a reaction solvent due to the limited water solubility of the protected amino acids. NMR spectroscopy provides convenient handles for assessing conjugation. The ^{1}H-NMR spectra showed a shift of the broad multiplet of the β-CH_2 of cysteine from ~3.0 ppm to 3.2 and 3.5 ppm with a pronounced diastereotopic splitting. Unfortunately, this region of the spectra was congested. The signals generated upon addition to the maleimide were more diagnostic. The methylene of the thioether appeared at 3.8 ppm. The adjacent methylene split into a diastereotopic pair at ~2.5 ppm (in an uncrowded region of the spectrum) and 3.1 ppm (in a more crowded region). The ^{13}C-NMR was used to corroborate the addition. The appearance of diastereomers corresponding to the maleimide thioether (~39ppm), imide methylene (~36 ppm) and β-CH_2 of the cysteine residue (~34 ppm) were diagnostic for successful conjugation of the chiral thiol. The data from mass spectrometry and HPLC were consistent with a clean reaction between **7** and **A** or **B**. Mass spectrometry of the conjugates of **7-A** and **7-B** showed the parent ion with minor ions corresponding to the loss of both the Boc and Fmoc groups. Both **7-A** and **7-B** were isolated using column chromatography and obtained with approximately 60% yields. These low yields are attributed to the loss of Fmoc group during isolation.

Oxidation of the thiol offered the potential for a competing side-reaction. The cysteine disulfide of **A** appeared at 3.25 ppm in a crowded region of the ^{1}H-NMR spectrum. However, HPLC analysis provided a clear indication of this compound: The disulfides, thiols and conjugation products **7-A** and **7-B** showed unique retention times (See Supplementary Materials). Oxidation to the disulfide did not appear to be responsible for low yields of isolated materials. Accordingly, no special handling procedures were adopted for latter conjugation reactions.

Advantageously, we were able to perform conjugations with **1** in a range of solvents, because **1** was readily soluble in chloroform, dichloromethane, dioxane, methanol and water. For example, reactions of **1** with hydrophobic models **A** and **B** were performed in a dioxane:dichloromethane mixture. A dioxane:water mixture was used for nonapeptide **C**. For the hydrophilic peptide **D**, the conjugation was performed in water.

Conjugates **1-A$_4$** and **1-B$_4$** were isolated using chromatography with 65% and 54% yields. Mass spectrometry, and HPLC and NMR spectroscopy all provided corroborating data. HPLC showed that the retention times of thiol **A** and the conjugation product **1-A$_4$** were different by approximately

1 min. However, thiol **B** and the product of conjugation, **1-B$_4$**, showed similar retention times. The conjugation reaction using **A** and **B** were readily monitored by electrospray ionization-time of flight mass spectrometry, ESI-TOF MS (Figure 3a,b). Immediately upon mixing reagents, mass spectrometry showed clear evidence of conjugate formation with amino acid **A** reacting faster than dipeptide **B**.

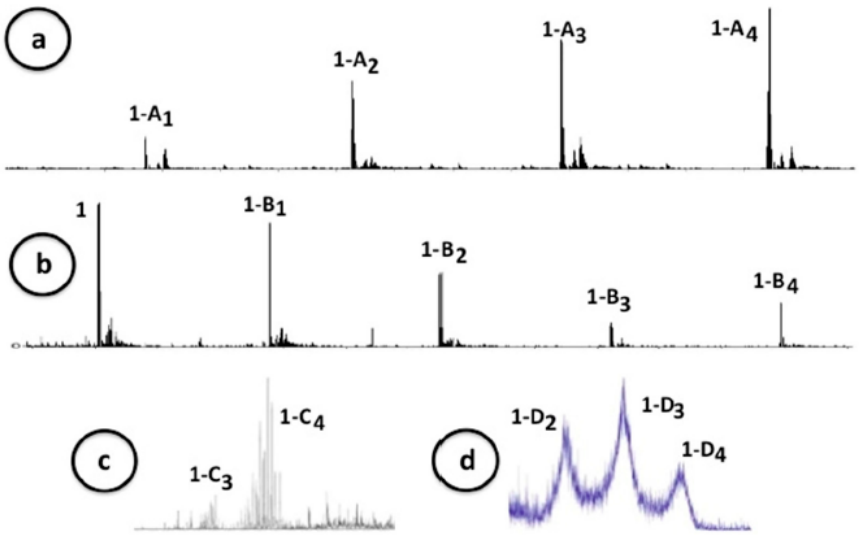

Figure 3. Conjugates **1** with **A** (**a**); **B** (**b**); **C** (**c**) and **D** (**d**). Traces (**a**,**b**) are taken upon the addition of thiol by ESI-TOF MS. Mass scales for these traces are m/z 2900-4400 (**a**) and m/z 2600-5200 (**b**); Traces (**c**,**d**) are taken of the purified product mixture. Mass scales for these traces are m/z 4500–7800 (**c**) and m/z 5000–13000 (**d**). Trace (**d**) was obtained by MALDI-TOF-MS.

2.4. Conjugation of Pepties

The products of conjugation of **1** with nonapeptide **C** were isolated in a multistep sequence. First, the reaction mixture was concentrated to an oil. The oil was then resuspended in deionized water to facilitate membrane filtration with a cellulose centrifugation filter (Ultracell YM3) with a 3 kDa molecular weight cutoff. After multiple rinses, the recovered volume was lyophilized to dryness. Using ^{1}H-NMR, a comparison of the integration of the aromatic signals of the tyrosine with signals derived from the methylene, which was derived from the maleimide at 2.5 ppm (dendrimer), suggests that the product distribution approached the desired **1-C$_4$** target, approximately ~**1-C$_{3.75}$**. Mass spectrometry confirmed a successful reaction (Figure 3c). The presence of multiple lines at lower molecular weights than the target, **1-C$_4$**, is consistent with the use of an impure peptide.

Not surprisingly, these peaks were assignable (Figure 4). The desired product containing four copies of **C** is indicated with *four* green dots. Adducts of **1-C$_4$** with Na^+ and K^+ are shown with blue arrows. For lines corresponding to products with lower molecular weights, one or more of the peptides are missing amino acids. The most abundant ion displays a peptide missing a glycine residue (blue dot). Peptides missing proline (red dot) are also present. For simplicity, we indicate the minimum number of deletions for each peptide. That is, whether the final compound has one deletion in each peptide—or comprises three perfect peptides **C** and a peptide missing four amino acids—is unknown. The necessity of using double couplings during the solid phase synthesis of this proline-rich sequence is also reflected by the presence of a peak corresponding to a product with three copies of **C** and one copy of **C** containing an extra proline residue (purple circle). Given the distribution of products, it is unsurprising that the HPLC trace is broad.

The conjugation of 16-amino acid peptide, **D**, with **1** was followed using HPLC by monitoring the consumption of **1** and the appearance of new species. The reaction products were purified by membrane dialysis. MALDI-TOF mass spectrometry of the isolated product showed peaks

corresponding to **1-D$_2$**, **1-D$_3$**, and **1-D$_4$**. The broadness of the mass spectrum is consistent with both the use of impure peptides and the complications arising from salts of this highly charged peptide. The ^{1}H-NMR spectrum—albeit broad—showed neither maleimide nor maleic acid signals present in the reaction mixture as might be expected from the perceived low conversion rate. Although thiol addition should be faster than that the addition of any other functional group or solvent, steric congestion could retard this desired reaction and afford opportunities for intermolecular reaction of maleimides with amino acid side chains like that of lysine. The extent to which these reaction can occur as a function of lysine residue position will be assessed in a future study. Using ^{1}H-NMR, a comparison of peak areas derived from the aromatic phenylalanine peaks and methylene of maleimide suggests that the product distribution is centered at **1-D$_{3.5}$**, a more favorable ratio than what might be expected from casual inspection of the mass spectrum.

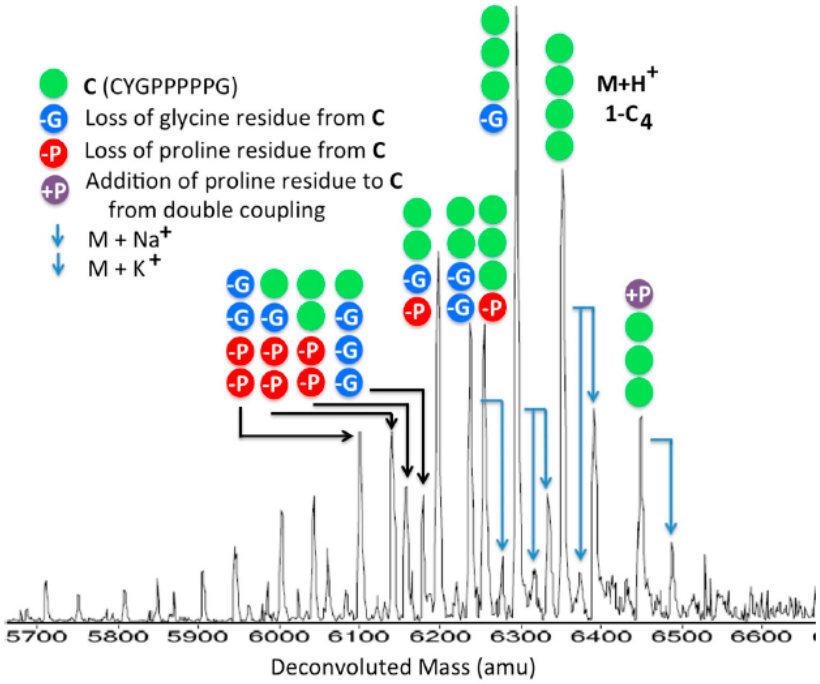

Figure 4. Tentative assignment of the products of conjugation of peptide **C** with **1** to yield **1-C$_4$**.

3. Experimental Section

3.1. General Synthetic Procedures

All chemicals were purchased from Aldrich (St. Louis, MO, USA) and Acros (Fair Lawn, NJ, USA) and used without further purification. All solvents were ACS grade and used without further purification. HPLC was carried out using an Agilent Technologies (Santa Clara, CA, USA) 1260 Infinity system and an Agilent Technologies 1260 Infinity DAD detector. NMR spectra were recorded on a Bruker Ascend 400 MHz spectrometer (Billerica, MA, USA) in $CDCl_3$, CD_3OD, or D_2O. All ESI mass spectral analyses were carried out by an Agilent Technologies 6224 TOF LC/MS system.

The chromatographic system used to measure sample purity consisted of a degasser (Agilent G1379B, Palo Alto, CA, USA), capillary pump (Agilent G1312B), micro well-plate auto sampler (Agilent G1367D), eclipse XDB-C18 column (4.6 mm i.d. × 150 mm, 5 µm, Agilent), and a diode array detector (Agilent G1316B). The mobile phase consisted of water/acetonitrile (A/B, HPLC grade, 0.1% (*w*/*v*) trifluoroacetic acid) at a flow rate of 0.8 mL/min. The elution gradient was 10% MeCN for 5 min, ramp to 90% MeCN in 30 min, and ramp down to 10% MeCN in 15 min. The sample volume injected 5 µL at a concentration 0.1 mg/mL with HPLC-grade MeCN, and detected at 214 nm.

3.2. Synthesis of Dendrimer **1**

To a solution of **6** (31 mg, 0.014 mmol) and DIPEA (20 µL, 0.115 mmol) in dioxane (1 mL), a solution of maleimide–NHS ester (32 mg, 0.115 mmol) in dichloromethane (1 mL) was added at RT then stirred for 48 h. The reaction was concentrated and purified by column chromatography (DCM:MeOH = 97:5 → DCM:MeOH = 8:2) to give **1** (Figure 5) as a foam (28 mg, 69%). ^{1}H-NMR (400 MHz, $CDCl_3$): δ 6.71 (s, 8H), 3.64–3.32 (m, 120H, $CH_2OCH_2CH_2OCH_2CH_2OCH_2$, C_3N_3-$NHCH_2CH_2CH_2O$, DOTA-$CONHCH_2CH_2CH_2O$, $CONHCH_2CH_2CH_2N$, Maleimide-$CONHCH_2CH_2CH_2O$), 2.15 (t, *J* = 7.2, 8H), 1.92 (dt, *J* = 14, 7.2, 8H), 1.89–1.77 (br m, 28H, $OCH_2CH_2CH_2$); ^{13}C-NMR (100 MHz, $CDCl_3$) δ 171.7, 170.9, 134.1, 70.5 (OCH_2CH_2O), 70.2 (OCH_2CH_2O), 70.1 (OCH_2CH_2O), 69.8, 69.2 ($CH_2CH_2CH_2O$), 38.1 ($NH_2CH_2CH_2CH_2O$), 37.7 ($CH_2CH_2CH_2O$), 37.3 (maleimide), 33.6 (maleimide), 29.5 ($NH_2CH_2CH_2CH_2O$), 29.0 ($NH_2CH_2CH_2CH_2O$), 24.8 (maleimide); MS (ESI-TOF) calcd. for $C_{127}H_{214}N_{31}O_{40}$ 2813.5664, found 2813.5751 $[M + H]^+$. Spectra appear in the Supplementary Materials: Figures S1–S5.

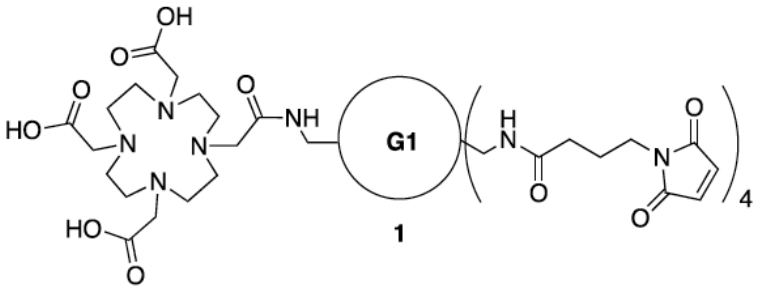

Figure 5. Intermediate **1**.

3.3. Synthesis of Intermediate S1—Maleic Acid Amide of **1**

A solution of **1** (8 mg) in water (1 mL) was adjusted to pH 7–8 with 1 N NaOH at RT then stirred for 18 h. The reaction mixture was lyophilized to give Intermediate **S1** (Figure 6). ^{1}H-NMR (400 MHz, D_2O): δ 6.23 (d, *J* = 12.4 , 4H), 5.83 (d, *J* = 12.4, 4H), 3.55–3.12 (m, 120H, $CH_2OCH_2CH_2OCH_2CH_2OCH_2$, C_3N_3-$NHCH_2CH_2CH_2O$, DOTA-$CONHCH_2CH_2CH_2O$, $CONHCH_2CH_2CH_2N$, Maleimide-$CONHCH_2CH_2CH_2O$), 2.18 (t, *J* = 7.4, 8H), 1.89–1.77 (br m, 36H, $OCH_2CH_2CH_2$, Maleimide); ^{13}C-NMR (100 MHz, D_2O) δ 180.0 (DOTA-acid), 179.9 (DOTA-acid), 175.7 (Maleimide-$CONHCH_2CH_2CH_2O$), 174.3 (DOTA-amide), 173.2 (DOTA-acid), 168.1 (conjugate amide), 165.3 (triazine, conjugate acid), 135.7, 124.9, 69.7, 69.6, 69.5, 69.4, 68.6, 68.4, 38.5 , 37.4, 37.3,36.4, 33.1, 28.9, 28.3, 24.9 (maleimide); MS (ESI-TOF) calcd. for $C_{127}H_{222}N_{31}O_{44}$ 2885.6087, found 2885.6806 $[M + H]^+$. Spectra appear in the Supplementary Materials: Figures S6–S9.

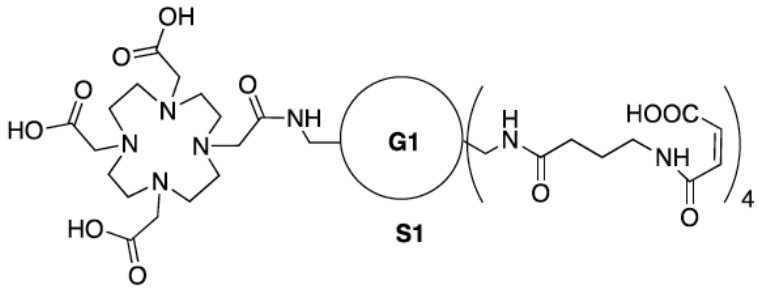

Figure 6. Intermediate **S1**.

3.4. Synthesis of Intermediate **4**

To a solution of **2** (194 mg, 0.09 mmol) and **3** (52 mg, 0.09 mmol) in acetonitrile (8 mL), HBTU (34 mg, 0.09 mmol) was added followed by triethylamine (25 µL, 0.18 mmol) at RT. The reaction

was stirred for 18 h. The reaction was diluted with 30 mL dichloromethane and washed 0.1 N HCl (30 mL), 10% $NaHCO_3$ (30 mL), brine (30 mL), then dried over $MgSO_4$, and concentrated. The crude product was purified by column chromatography (DCM:MeOH = 97:5 → DCM:MeOH = 85:15) to give **4** (Figure 7) as a foam (105 mg, 43%). ^{1}H-NMR (400 MHz, $CDCl_3$): δ 3.68–3.47 (m, 104H, $CH_2OCH_2CH_2OCH_2CH_2OCH_2$, C_3N_3-$NHCH_2CH_2CH_2O$, Dota-$CONHCH_2CH_2CH_2O$), 3.22–3.18 (br m, 8H, $BocNHCH_2$), 1.84–1.72 (m, 28H, $OCH_2CH_2CH_2$), 1.46 (s, 9H), 1.45 (s, 9H), 1.42 (s, 45H); ^{13}C-NMR (100 MHz, CDCl3) δ 176.6 (DOTA-OCO^tBu), 174.4 (DOTA-OCO^tBu), 172.3 (DOTA-OCO^tBu), not found (C_3N_3), 156.0 ($NHCO^tBu$), 81.7 (DOTA-$OC(CH_3)_3$), 78.7 ($C(CH_3)_3$), 70.47 (OCH_2CH_2O), 70.21 (OCH_2CH_2O), 70.17 (OCH_2CH_2O), 70.10 (OCH_2CH_2O), 69.42 ($CH_2CH_2CH_2O$), 69.02 ($CH_2CH_2CH_2O$), 57.5 (DOTA), 56.2 (DOTA), 55.6 (DOTA), 53.5 (DOTA), 41.9 ($NH_2CH_2CH_2CH_2O$), 38.5 ($CH_2CH_2CH_2O$), 38.4 ($CH_2CH_2CH_2O$), 29.6 ($NH_2CH_2CH_2CH_2O$), 29.3 ($NH_2CH_2CH_2CH_2O$), 28.4 ($C(CH_3)_3$), 27.94 (DOTA-$OC(CH_3)_3$), 27.87 (DOTA-$OC(CH_3)_3$); MS (ESI-TOF) calcd. for $C_{127}H_{242}N_{27}O_{36}$ 2721.7936, found 2721.8117 $[M + H]^+$. Spectra appear in the Supplementary Materials: Figures S11–S13.

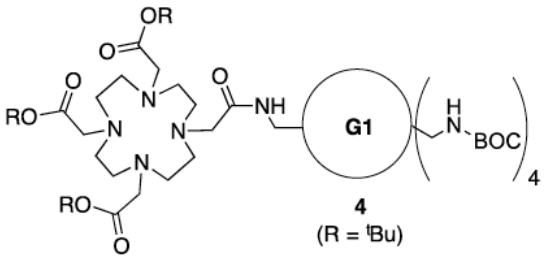

Figure 7. Intermediate 4.

3.5. Synthesis of Intemediate **5**

To a solution of **4** (59 mg, 0.022 mmol) in methanol (2 mL), 6 N HCl (aq) (2 mL) was added at RT then stirred for 8 h. The reaction was diluted with ethyl acetate (10mL) and water (2 mL). Water layer was basifying with 5 N NaOH (aq) then the desired compound was extracted with dichloromethane (10 mL × 8). Combined organic layers was dried over $MgSO_4$, and concentrated to give **5** (40.5 mg of as a clear oil; Figure 8). ^{1}H-NMR (400 MHz, $CDCl_3$): δ 3.63–3.42 (m, 104H, $CH_2OCH_2CH_2OCH_2CH_2OCH_2$, C_3N_3-$NHCH_2CH_2CH_2O$, DOTA-$CONHCH_2CH_2CH_2O$), 3.10 (br s, 8H, NH_2CH_2), 1.96–1.82 (br m, 28H, $OCH_2CH_2CH_2$), 1.45 (s, 27H); ^{13}C-NMR (100 MHz, CDCl3) δ 172.5 (DOTA-OCO^tBu), 171.5 (DOTA-OCO^tBu), 165.8 (C_3N_3), 81.8 (DOTA-$OC(CH_3)_3$), 81.7 (Dota-$OC(CH_3)_3$), 70.54 (OCH_2CH_2O), 70.42 (OCH_2CH_2O), 70.19 (OCH_2CH_2O), 70.11 (OCH_2CH_2O), 69.95 (OCH_2CH_2O), 69.40 ($CH_2CH_2CH_2O$), 69.27 ($CH_2CH_2CH_2O$), 56.1 (Dota), 55.7 (Dota), 55.6 (DOTA), 39.0 ($NH_2CH_2CH_2CH_2O$), 38.1 ($CH_2CH_2CH_2O$), 29.7 ($NH_2CH_2CH_2CH_2O$), 29.5 ($NH_2CH_2CH_2CH_2O$), 29.1 ($NH_2CH_2CH_2CH_2O$), 28.10 (DOTA-$OC(CH_3)_3$), 27.98 (DOTA-$OC(CH_3)_3$); MS (ESI-TOF) calcd for $C_{107}H_{210}N_{27}O_{28}$ 2321.5839, found 2321.6677 $[M + H]^+$. Spectra appear in the Supplementary Materials: Figures S14–S16.

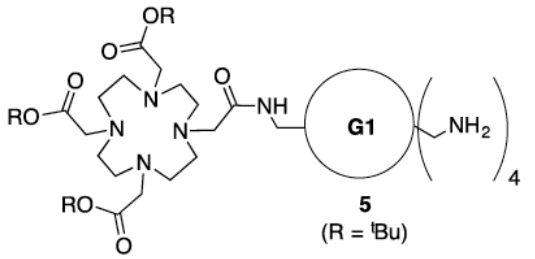

Figure 8. Intermediate 5.

3.6. Synthesis of Intermediate—Generation 3 Dendrimer with DOTA

A solution of **5** (79 mg, 0.034 mmol) and **M** (Macromonomer [24]) (542 mg, 0.27), and DIPEA (71 mL, 0.41 mmol) in THF (3 mL), dioxane (1 mL), *i*-propanol (70%) (0.5 mL) was stirred at 75 °C in a capped vessel for 4 d. The solution was evaporated under vacuum. The residue was dissolved in dichloromethane, washed with brine, dried over $MgSO_4$, and concentrated. The crude product was purified by column chromatography. The crude product was purified by column chromatography (DCM:MeOH = 97:5 → DCM:MeOH = 85:15) to give **S3** (Figure 9) as a foam (92 mg, 27%). ^{1}H-NMR (400 MHz, $CDCl_3$): δ 3.65–3.42 (m, 464H, $CH_2OCH_2CH_2OCH_2CH_2OCH_2$, C_3N_3-$NHCH_2CH_2CH_2O$, Dota-$CONHCH_2CH_2CH_2O$), 3.22–3.19 (br m, 32H, $BocNHCH_2$), 1.81–1.72 (br m, 124H, $OCH_2CH_2CH_2$), 1.47 (s, 9H), 1.45 (s, 9H), 1.44 (s, 9H), 1.42 (s, 144H); ^{13}C-NMR (100 MHz, CDCl3) δ not found (DOTA-OCO^tBu), not found (DOTA-OCO^tBu), not found (DOTA-OCO^tBu), not found (C_3N_3), 156.1 ($NHCO^tBu$), 81.85 (DOTA-$OC(CH_3)_3$), 81.79 (DOTA-$OC(CH_3)_3$), 78.8 ($C(CH_3)_3$), 70.56 (OCH_2CH_2O), 70.28 (OCH_2CH_2O), 70.23 (OCH_2CH_2O), 70.19 (OCH_2CH_2O), 69.52 ($CH_2CH_2CH_2O$), 69.22 ($CH_2CH_2CH_2O$), 69.17 ($CH_2CH_2CH_2O$), not found (DOTA), not found (DOTA), not found (DOTA), 53.4 (DOTA), 41.8 ($NH_2CH_2CH_2CH_2O$), 38.5 ($CH_2CH_2CH_2O$), 38.2 ($CH_2CH_2CH_2O$), 29.67 ($NH_2CH_2CH_2CH_2O$), 29.60 ($NH_2CH_2CH_2CH_2O$), 29.54 ($NH_2CH_2CH_2CH_2O$), 29.33 ($NH_2CH_2CH_2CH_2O$), 28.5 ($C(CH_3)_3$), 28.01 (DOTA-$OC(CH_3)_3$), 27.94 (Dota-$OC(CH_3)_3$); MS (ESI-TOF) calcd for $C_{463}H_{878}N_{111}O_{132}$ 10106.5403, found 10114.2078 $[M + H]^+$. Spectra appear in the Supplementary Materials: Figures S17–S19.

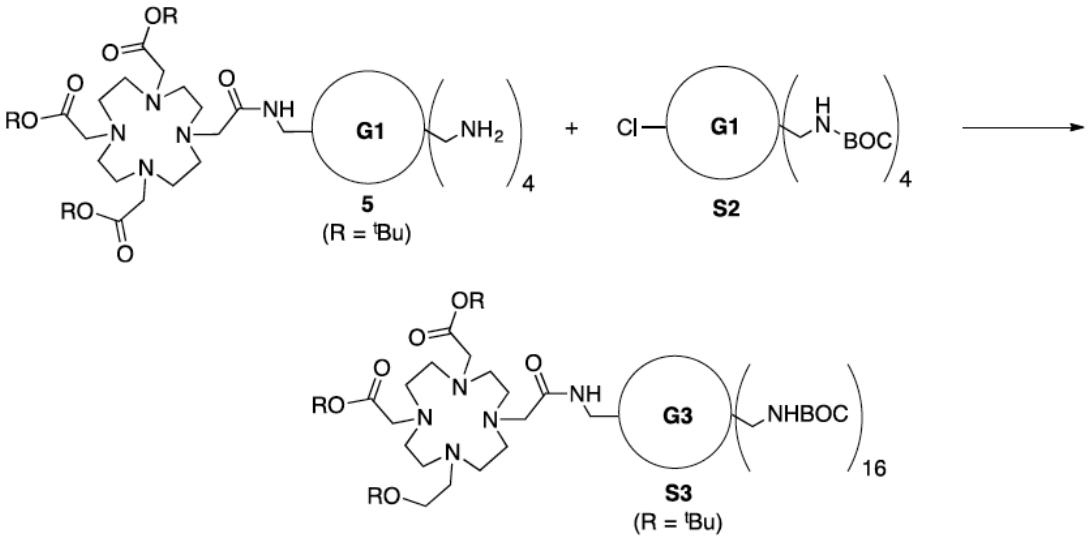

Figure 9. Synthesis of Intermediate S3.

3.7. Synthesis of Intermediate 6

To a solution of **5** (68 mg, 0.029 mmol) in dichloromethane (2 mL), trifluoroacetic acid (2 mL) was added at RT then stirred for 20 h. Susbequently the reaction mixture was evaporated under vacuum. The residue was decanted with diethyl ether (5 mL × 3), and dried under vacuum to give **6** (Figure 10) as a white powder (quantitative). ^{1}H-NMR (400 MHz, CD_3OD): δ 3.55–3.26 (m, 104H, $CH_2OCH_2CH_2OCH_2CH_2OCH_2$, C_3N_3-$NHCH_2CH_2CH_2O$, DOTA-$CONHCH_2CH_2CH_2O$), 2.99 (br t, J = 6.2, 8H, NH_2CH_2), 1.85–1.76 (br m, 28H, $OCH_2CH_2CH_2$); ^{13}C-NMR (100 MHz, CD_3OD) δ 164.8, 157.4 156.4, 71.6, 71.53, 71.50, 71.33, 71.23, 71.21, 70.23, 69.91, 69.76, 69.73, 39.87 , 39.64, 39.44, 39.35, 39.27, 39.19, 38.09, 38.03, 30.86, 30.45, 30.35, 30.19, 30.12; MS (ESI-TOF) calcd. for $C_{95}H_{186}N_{27}O_{28}$ 2153.3961, found 2153.4295 $[M + H]^+$. Spectra appear in the Supplementary Materials: Figures S20–S22.

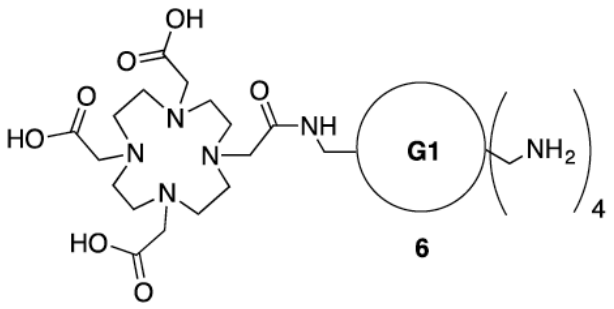

Figure 10. Intermediate **6**.

3.8. Synthesis of Model **7**

To a solution of commercially-available maleimide succinimide ester **S5** (17 mg, 0.06 mmol) in dichloromethane (3.0 mL), a solution of monoBoc amine **S4** (16 mg, 0.05 mmol) in dichloromethane (1.0 mL) was added at RT. The solution was stirred for 3h at RT and evaporated under vacuum. The crude product was purified by column chromatography (DCM:MeOH = 99:1 → DCM:MeOH = 97:3) to give **7** (Figure 11) as a solid (21 mg, 86%). ^{1}H-NMR (400 MHz, $CDCl_3$): δ 6.71 (s, 2H, n), 3.67–3.53 (m, 14H, c, d, e, f, g, h, m), 3.36 (q, *J* = 6.4, 2H, j), 3.23 (q, *J* = 6.4, 2H, a), 2.16 (t, *J* = 6.4, 2H, k), 1.97–1.94 (m, 2H, l), 1.82-1.75 (m, 4H, b, i), 1.43 (s, 9H, Boc) ^{13}C-NMR (100 MHz, $CDCl_3$) δ 171.6, 170.8, 156.0, 134.1, 78.9, 70.5, 70.4, 70.2, 70.1, 69.8, 69.5, 38.4, 37.8, 37.2, 33.6, 29.6, 28.9, 28.4, 24.7; MS (ESI-TOF) calcd. for $C_{23}H_{40}N_3O_8$ 486.2815, found 486.4100 $[M + H]^+$. Spectra appear in the Supplementary Materials: Figures S23–S25.

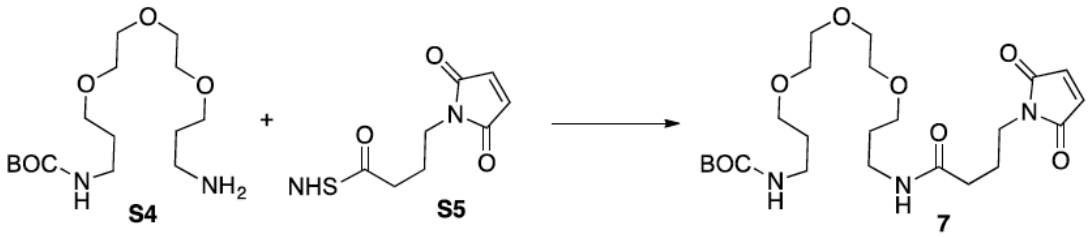

Figure 11. Synthesis of **7**.

3.9. Synthesis of Conjugate **7-A**

To a solution of **1** (35 mg, 0.07 mmol) in dioxane (1.0 mL) a solution of cysteine **A** (28 mg, 0.079) in dichloromethane (1.0 mL) was added at RT. The solution was stirred for 48h at room temperature and evaporated under vacuum. The crude product was purified by column chromatography (DCM = 100 → DCM:MeOH = 95:5) to give **7-A** (Figure 12) as a oil (37 mg, 61%). ^{1}H-NMR (400 MHz, $CDCl_3$): δ 7.76 (d, *J* = 8.0, 2H, FMOC), 7.61 (t, *J* = 6.0, 2H, FMOC), 7.42–7.28 (m, 4H, FMOC), 5.00 (br s, 1H, NH), 4.71–4.68 (m, 1H, p), 4.49–4.41 (m, 2H, FMOC), 4.24 (t, *J* = 6.8 , 1H, FMOC), 3.83–3.75 (m, 1H, n), 3.80 (s, 3H, q), 3.65–3.51 (m, 14H, c, d, e, f, g, h, m), 3.46 (dd, *J* = 14, 6.0, 1H, o), 3.37–3.31 (m, 2H, j), 3.23–3.19 (m, 2H, a), 3.15–3.03 (m, 2H, n′, o), 2.50–2.39 (m, 1H, n′), 2.15 (t, *J* = 7.2, 2H, k), 1.99–1.90 (m, 2H, l), 1.80–1.75 (m, 4H, b, i), 1.43 (s, 9H, BOC) ^{13}C-NMR (100 MHz, $CDCl_3$) δ 176.7, 174.5, 174.3, 171.5 (ester), 170.9 (amide), 156.0 (Boc), 155.9 (FMOC), 143.8, 143.7, 143.6, 141.3, 127.7, 127.1, 127.0, 125.1, 125.0, 119.98, 119.94, 70.4, 70.1, 70.0, 69.7, 69.4, 67.1, 52.9, 52.8, 47.1, 39.6, 38.6, 38.5, 38.4, 37.7, 36.0, 35.6, 33.5, 33.4, 29.6, 28.9, 28.4, 23.6, 23.55; MS (ESI-TOF) calcd. for $C_{42}H_{59}N_4O_{12}S$ 843.3850, found 843.5872 $[M + H]^+$. Spectra appear in the Supplementary Materials: Figures S26–S28.

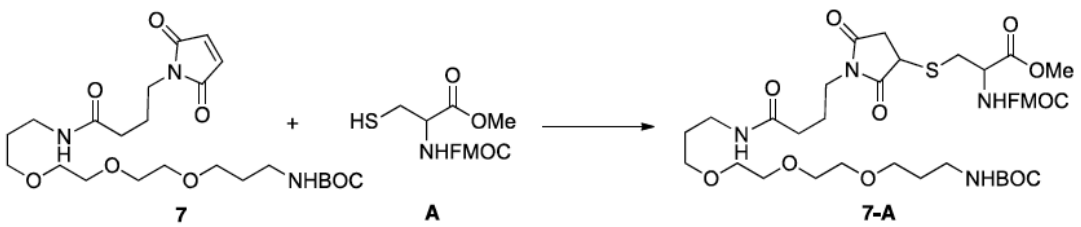

Figure 12. Synthesis of **7-A**.

3.10. Synthesis of Cystine (**S6**)

To a solution of **A** (59 mg, 0.165 mmol) in dichloromethane (4.0 mL), solid iodine (10 mg, 0.082 mmol) was added at RT. The solution was stirred for 2 h at room temperature and evaporated under vacuum. The crude product was purified by column chromatography (Ethyl Acetate: Hexanes = 1:9 → Ethyl Acetate: Hexanes = 3:7) to give **S6** (Figure 13) as white powder (46 mg, 39%). ^{1}H-NMR (400 MHz, $CDCl_3$): δ 7.74 (d, *J* = 7.2, 2H, FMOC), 7.59-7.57 (br s, 2H, FMOC), 7.39–7.27 (m, 4H, FMOC), 5.77 (br d, *J* = 7, 1H, NH), 4.70–4.65 (m, 1H), 4.4–4.39 (m, 2H, FMOC), 4.20 (t, *J* = 7.0, 1H, FMOC), 3.74 (s, 3H), 3.17 (d, *J* = 4.8, 2H); ^{13}C-NMR (100 MHz, $CDCl_3$) δ 170.9, 155.7, 143.8, 143.7, 141.3, 127.8, 127.1, 125.1, 120.0, 67.3, 53.3, 52.9, 47.1, 41.1; MS (ESI-TOF) calcd. for $C_{38}H_{37}N_2O_8S_2$ 713.83898, found 713.3859 $[M + H]^+$. Spectra appear in the Supplementary Materials: Figures S29–S34.

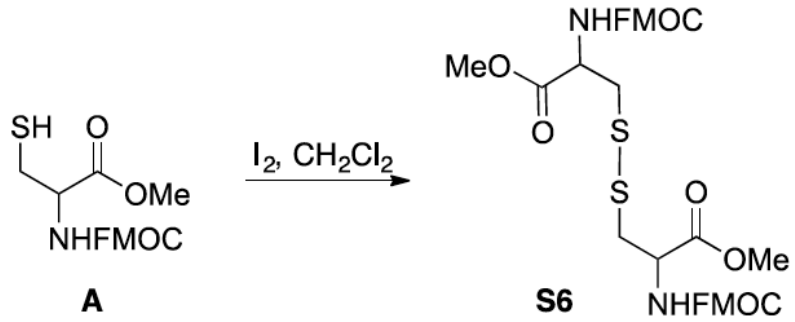

Figure 13. Synthesis of **S6**.

3.11. Synthesis of Conjugate **7-B**

To a solution of **7** (12 mg, 0.025 mmol) in dioxane (1.0 mL), a solution of **B** (18 mg, 0.033) in dichloromethane (1.0 mL) was added at RT. The solution was stirred for 48 h at room temperature and evaporated under vacuum. The crude product was purified by column chromatography (DCM = 100 → DCM:MeOH = 95:3) to give **7-B** (Figure 14) as an oil (16.5 mg, 64%). ^{1}H-NMR (400 MHz, $CDCl_3$): δ 7.75 (t, *J* = 7.6, 2H), 7.58 (d, *J* = 7.1, 2H), 7.52 (t, *J* = 8.5, 1H), 7.42–7.25 (m, 6H), 7.14–7.03 (m, 2H), 4.98–4.84 (m, 2H), 4.69–4.44 (m, 1H), 4.44–4.34 (m, 2H), 4.23–4.17 (m, 1H), 4.04 (br s, 1H), 3.59–3.45 (m, 18H), 3.40–2.80 (m, 9H), 2.47–2.41 (m, 1H), 2.23–2.17 (m, 2H), 2.00–1.86 (m, 2H), 1.79–1.75 (m, 4H), 1.43 (s, 9H) ^{13}C-NMR (100 MHz, $CDCl_3$) δ 178.1, 177.5, 174.6, 174.4, 172.1, 172.0, 171.9, 169.7, 169.6, 156.1, 143.8, 143.7, 141.3, 136.6, 136.4, 127.8, 127.4, 127.3, 127.1, 125.1, 124.1, 121.8, 121.7, 120.0, 119.96, 119.91, 119.2, 119.1, 118.4, 118.3, 111.5, 108.6, 108.2, 79.0, 70.5, 70.2, 70.1, 69.8, 69.4, 67.2, 67.0, 53.4, 52.9, 52.7, 52.5, 52.4, 47.1, 47.06, 40.8, 39.4, 38.8, 38.4, 38.2, 37.9, 36.7, 35.9, 33.3, 33.2, 28.5, 27.4, 23.4, 23.3; MS (ESI-TOF) calcd for $C_{53}H_{69}N_6O_{13}S$ 1029.4643, found 1029.6996 $[M + H]^+$. Spectra appear in the Supplementary Materials: Figures S35–S38.

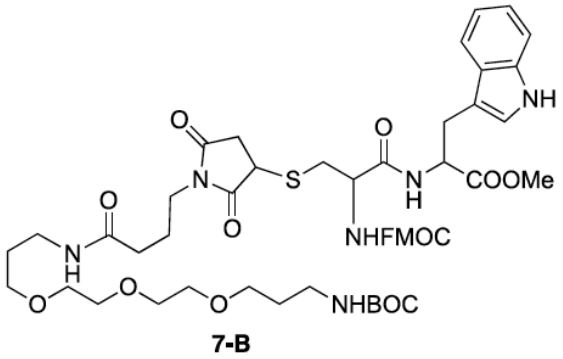

7-B

Figure 14. Intermediate **7-B**.

3.12. Synthesis of Conjugate **1-A$_4$**

To a solution of **1** (26 mg, 0.009 mmol) in dioxane (1.0 mL) a solution of **A** (25 mg, 0.074) in dichloromethane (1.0 mL) was added at RT. The solution was stirred for 48 h at room temperature and evaporated under vacuum. The crude product was purified by column chromatography (DCM = 100 → DCM:MeOH = 9:1) to give **1-A$_4$** (Figure 15) as an oil (25 mg, 65%). ^{1}H-NMR (400 MHz, $CDCl_3$): δ 7.75 (d, *J* = 7.5, 8H, FMOC), 7.61 (t, *J* = 7.2, 8H, FMOC), 7.41–7.29 (m, 16H, FMOC), 4.68 (br s, 4H, p), 4.44–4.40 (m, 8H, FMOC), 4.23 (t, *J* = 7.2 , 4H, FMOC), 3.81–3.70 (m, 4H, n), 3.78 (s, 3H, OCH_3), 3.69–3.10 (m, 128H, a, c, d, e, f, g, h, j, m, n', o), 2.48–2.38 (m, 4H, n'), 2.14 (t, *J* = 6.5, 8H, k), 1.94–1.65 (m, 36H, b, i, l); ^{13}C-NMR (100 MHz, $CDCl_3$) δ 177.0, 176.7, 174.6, 174.4, 171.7, 171.0, 156.0, 143.8, 143.7, 141.3, 127.8, 127.1, 125.2, 11.98, 70.55, 70.46, 70.2, 70.0, 69.7, 69.2, 67.1, 54.2, 53.3, 52.9, 52.8, 47.1, 39.7, 38.7, 38.6, 38.2, 37.7, 36.1, 35.7, 34.4, 33.1, 33.52, 33.46, 29.6, 29.3, 29.0, 23.7, 23.6; MS (ESI-TOF) calcd. for $C_{203}H_{290}N_{35}O_{56}S_4$ 4241.9804, found 4243.7824 $[M + H]^+$. Spectra appear in the Supplementary Materials: Figures S39–S44.

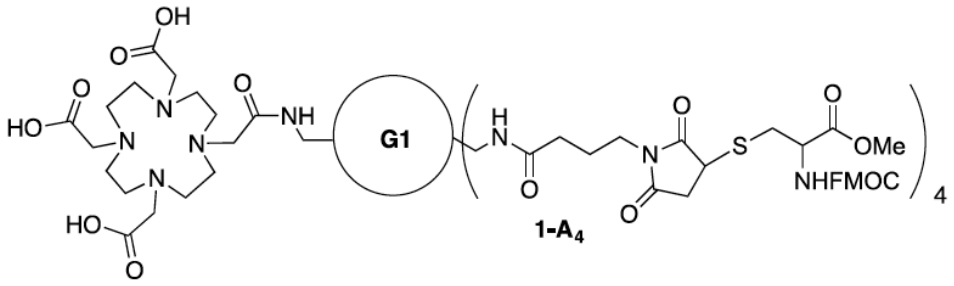

1-A$_4$

Figure 15. Dendrimers **1-A$_4$**.

3.13. Synthesis of Conjugate **1-B$_4$**

To a solution of **1** (11 mg, 0.0025 mmol) in dioxane (1.0 mL) a solution of **B** (17 mg, 0.031 mmol) in dichloromethane (1.0 mL) was added at RT. The solution was stirred for 48h at room temperature and evaporated under vacuum. The crude product was purified by column chromatography (DCM = 100 → DCM:MeOH = 9:1) to give **1-B$_4$** (Figure 16) as an oil (10.5 mg, 54%). ^{1}H-NMR (400 MHz, $CDCl_3$): δ 7.75–7.00 (m, 52H), 4.89–4.01 (m, 20H, p, q, FMOC), 3.46–2.95 (m, 152H, a, c, d, e, f, g, h, j, m, n, o, r, OMe), 2.88-2.81 (m, 4H, n'), 2.37–2.31 (m, 4H, n'), 2.28–2.17 (m, 8H, k), 1.97–1.59 (m, 36H, b, i, l); ^{13}C-NMR (100 MHz, $CDCl_3$) δ 177.9, 177.5, 174.6, 174.5, 172.0, 172.0, 169.9, 156.2, 143.8, 143.7, 141.3, 136.6, 136.4, 127.8, 127.4, 127.1, 125.2, 124.1, 121.6, 120.0, 119.94, 119.1, 118.3, 118.2, 111.6, 108.6, 108.3, 70.4, 70.1, 70.0, 69.8, 69.6,69.1, 67.2, 67.1, 55.1, 53.5, 53.3, 53.0, 52.8, 52.43, 52.38, 47.1, 40.6, 39.4, 38.7, 38.1, 37.9, 37.7, 36.3, 35.9, 33.3, 33.2, 29.7, 29.3, 29.0, 27.4, 23.5, 22.7; MS (ESI-TOF) calcd.

for $C_{247}H_{330}N_{42}O_{60}S_4$ 4986.2976, found 4989.1225 $[M + H]^+$. Spectra appear in the Supplementary Materials: Figures S45–S49.

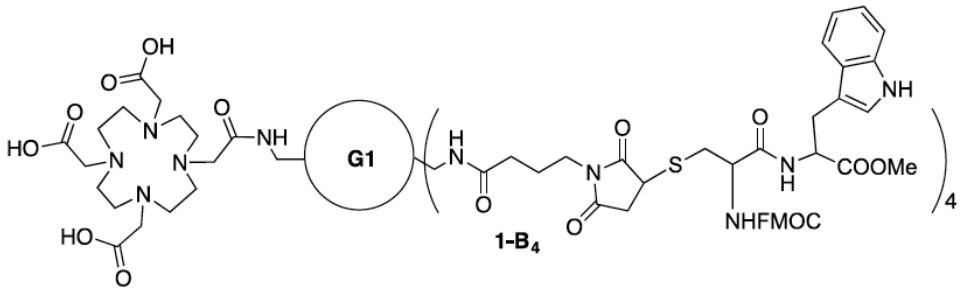

Figure 16. Dendrimer **1-B$_4$**.

3.14. Synthesis of Conjugate **1-C$_4$**

To a solution of maleimide **1** (9.8 mg, 0.0034 mmol) in dioxane (0.5 mL), a solution of CYGPPPPPG **C** (25 mg, 0.0279 mmol) in water (0.5 mL) was added, followed by addition of DIPEA (10 µL, 0.056 mmol) at RT. The solution was stirred for 18h at room temperature and then evaporated under vacuum. The crude product was diluted with deionized water (1.5 mL) and excess amount of peptide was removed from the dendron by centrifugal filtration (3000 MW cut off, 4000 rpm). The residue was washed with deionized water (2 mL) five times and lyophilized to give **1-C$_4$** (Figure 17) as a solid (14 mg, 63%). ^{1}H-NMR (400 MHz, D_2O): δ 7.19–7.06 (m, 8H, x), 6.89–6.73 (m, 8H, y), 4.64–4.57 (m, 20H, t), 4.37–4.34 (m, 4H, q), 4.26–4.22 (m, 4H, p), 3.99–3.86 (m, 8H, s), 3.85–3.68 (m, 32H, n, s, w), 3.65–2.81 (m, 156H, a, c, d, e, f, g, h, m, n′, o, r, w), 2.59–2.51 (m, 4H, n′), 2.31-2.15 (m, 28H, k, u), 2.05–1.65 (m, 96H, b, i, l, u, v); ^{13}C-NMR (100 MHz, D_2O) δ 178.8, 178.7, 176.8, 174.8, 174.7, 174.1, 173.2, 173.1, 171.7, 171.4, 170.85, 170.7, 169.1, 167.1, 166.9, 162.2, 161.9, 154.0, 153.9, 129.8, 129.75, 127.0, 126.8, 117.0, 114.6, 114.1, 71.3, 68.9, 68.65, 67.8, 67.6, 67.5, 65.8, 61.7, 60.2, 59.7, 58.5, 57.8, 55.7, 55.0, 54.7, 54.6, 51.7, 50.9, 50.0, 47.5, 47.4, 46.9, 46.8, 46.2, 42.0, 41.9, 40.8, 37.8, 37.0, 35.7, 35.4, 34.8, 32.1, 28.5, 27.6, 27.3, 27.1, 23.9, 23.5, 22.2; MS (ESI-TOF) calcd. for $C_{291}H_{442}N_{67}O_{84}S_4$ 6347.1257, found 6295.1574 $[M + H]^+$. Spectra appear in the Supplementary Materials: Figures S50–S55.

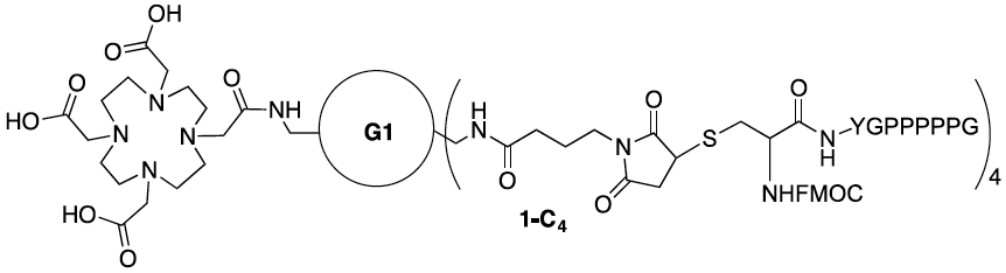

Figure 17. Dendrimer **1-C$_4$**.

3.15. Synthesis of Conjugate **1-D$_4$**

To a solution of **1** (9.1 mg, 0.0032 mmol) in water (0.5 mL), a solution of CGFQLRQPPLVPSRKGEG, **D** (51 mg, 0.026 mmol) in water (0.5 mL) was added followed by addition of 0.1 N NaOH (adjust pH ~ 7–8). The solution was stirred for 18 h at RT before diluting with deionized water (1.0 mL). Excess peptide was removed by centrifugal filtration (3000 MW cut off, 4000 rpm). The residue was washed with deionized water (2 mL) five times and lyophilized to give **1-D$_4$** (Figure 18) as a solid (19.7 mg,

57%). ^{1}H-NMR (400 MHz, D_2O): δ 7.25–7.13 (m, 20H, 2), 4.61–4.49 (m, 8H, r, x), 4.39–4.22 (m, 52H, p, s(2), t(2), u(2), v(3), w, y, z), 3.95–.2.90 (m, 224H, a, c, d, e, f, g, h, j, m, n, n′, o, q(3), 1, 10(2), 11(3), 16, 20), 2.58–2.52 (m, 4H, n′), 2.33–2.13 (m, 44H, k, 4(2), 13(3), 22), 2.13–1.34 (m, 168H, b, i, l, 3(2), 5(2), 6(2), 8(2), 9(2), 12(3), 13(3), 14, 17, 18, 19, 21), 0.92–0.78 (m, 72H, 7(2), 15) ^{13}C-NMR (100 MHz, D_2O) δ 181.0, 179.4, 179.2, 177.7, 176.2, 174.8, 174.3, 174.1, 173.8, 173.3, 173.2, 173.0, 172.4, 171.8, 171.6, 171.2, 170.7, 170.4, 169.8, 156.7, 136.1, 129.2, 128.7, 127.2, 69.7, 69.4, 68.5, 68.4, 61.0, 60. 5, 60.0, 58.8, 56.8, 56.4, 55.8, 55.5, 55.0, 53.9, 53.5, 53.2, 53.0, 52.7, 52.5, 50.8, 48.3, 47.9, 47.7, 43.5, 42.5, 40.5, 39.7, 39.1, 38.5, 37.7, 37.1, 36.5, 33.4, 32.9, 31.0, 30.7, 30.2, 30.1, 29.5, 29.3, 28.6, 28.4, 28.2, 27.8, 27.0, 26.2, 24.7, 24.4, 23.0, 22.2, 22.0, 21.9, 21.1, 21.0, 18.3, 17.6; MS (MALDI-TOF) calcd. for $C_{471}H_{777}N_{139}O_{136}S_4$ 10684., found 10662. Spectra appear in the Supplementary Materials: Figures S56–S60.

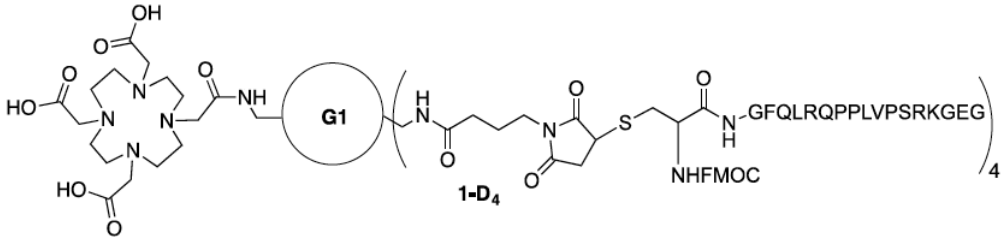

Figure 18. Dendrimer **1-D$_4$**.

4. Conclusions

In conclusion, **1** represents a valuable platform for the pursuit of theranostic applications. Mass spectrometry provides evidence that, upon metallation with gadolinium, **1-Gd** can be reacted with **A** to yield **1-A$_4$-Gd**. This construct and related conjugates will be described in due course. While poly(maleimides) are commercially available (Toronto Research Chemicals), the cost and lack of a chelating-group for imaging applications represent limitations overcome by **1**. Both the synthetic and conjugation chemistry described here are straightforward and can be affected with a minimum of effort. However, the extent to which these reactions proceed is dependent on the size and composition of the thiol. Tetravalent displays of large peptides have proven difficult to push to completion. Critically, conjugation can be accomplished in a range of solvents—from organic solvents to aqueous solutions—to incorporate a range of thiol-containing species. The value of this conjugation strategy—maleimide and thiol—over alternatives has been reported: Wangler *et al.* showed that thiol-maleimide couplings proceed more effectively than oxime formation or copper-catalyzed cycloadditions [26]. Finally, we note that, when the flexible dendritic domains are fully extended, **1** places ligands in the corners of a rectangular array measuring ~2.5 nm by ~4.2 nm.

Supplementary Materials: The following are available online at: http://www.mdpi.com/1420-3049/21/3/335/s1; ESI-TOF MS, ^{1}H-NMR, ^{13}C-NMR and Stability test.

Acknowledgments: We thank the Robert A. Welch Foundation (P-0008), the DOD (W81XWH-12-1-0338) and the NIH (R01 CA 159144) for support.

Author Contributions: C.S.L. and E.E.S. conceived and designed the experiments; C.S.L. performed a majority of the experiments; K.J. assisted in the preparation of peptides and conjugation reactions. All contributed to the preparation of the paper.

Conflicts of Interest: The authors declare no conflict of interest.

References

1. McCarthy, J.R.; Weissleder, R. Multifunctional magnetic nanoparticles for targeted imaging and therapy. *Adv. Drug Deliv. Rev.* **2008**, *60*, 1241–1251. [CrossRef] [PubMed]
2. Janib, S.M.; Moses, A.S.; MacKay, J.A. Imaging and drug delivery using theranostic nanoparticles. *Adv. Drug Deliv. Rev.* **2010**, *62*, 1052–1063. [CrossRef] [PubMed]

3. Kelkar, S.S.; Reineke, T.M. Theranostics: Combining imaging and therapy. *Bioconjug. Chem.* **2011**, *22*, 1879–1903. [CrossRef] [PubMed]
4. Duncan, R.; Gaspar, R. Nanomedicine(s) under the microscope. *Mol. Pharm.* **2011**, *8*, 2101–2141. [CrossRef] [PubMed]
5. Jokerst, J.V.; Gambhir, S.S. Molecular imaging with theranostic nanoparticles. *Acc. Chem. Res.* **2011**, *44*, 1050–1060. [CrossRef] [PubMed]
6. Yu, M.K.; Park, J.; Jon, S. Targeting strategies for multifunctional nanoparticles in cancer imaging and therapy. *Theranostics* **2012**, *2*, 43–44. [CrossRef] [PubMed]
7. Lartigue, L.; Innocenti, C.; Kalaivani, T.; Awwad, A.; Sanchez Duque, M.D.M.; Guari, Y.; Larionova, J.; Guerin, C.; Montero, J.-L.G.; Barragan-Montero, V.; *et al*. Water-dispersible sugar-coated iron oxide nanoparticles. An evaluation of their relaxometric and magnetic hyperthermia properties. *J. Am. Chem. Soc.* **2011**, *133*, 10459–10472. [CrossRef] [PubMed]
8. Lee, J.E.; Lee, N.; Kim, T.; Kim, J.; Hyeon, T. Multifunctional mesoporous silica nanocomposite nanoparticles for theranostic applications. *Acc. Chem. Res.* **2011**, *44*, 893–902. [CrossRef] [PubMed]
9. Cheng, S.-H.; Lee, C.-H.; Chen, M.-C.; Souris, J.S.; Tseng, F.-G.; Yang, C.-S.; Mou, C.-Y.; Chen, C.-T.; Lo, L.-W.J. Tri-functionalization of mesoporous silica nanoparticles for comprehensive cancer theranostics-the trio of imaging, targeting and therapy. *Mater. Chem.* **2010**, *20*, 6149–6157. [CrossRef]
10. Jain, T.K.; Foy, S.P.; Erokwu, B.; Dimitrijevic, S.; Flask, C.A.; Labhasetwar, V. Magnetic resonance imaging of multifunctional pluronic stabilized iron-oxide nanoparticles in tumor-bearing mice. *Biomaterials* **2009**, *30*, 6748–6756. [CrossRef] [PubMed]
11. Moon, G.D.; Choi, S.-W.; Cai, X.; Li, W.; Cho, E.C.; Jeong, U.; Wang, L.V.; Xia, Y. A new theranostic system based on gold nanocages and phase-change materials with unique features for photoacoustic imaging and controlled release. *J. Am. Chem. Soc.* **2011**, *133*, 4762–4765. [CrossRef] [PubMed]
12. Ho, Y.-P.; Leong, K.W. Quantum dot-based theranostics. *Nanoscale* **2010**, *2*, 60–68. [CrossRef] [PubMed]
13. Ke, H.; Wang, J.; Dai, Z.; Jin, Y.; Qu, E.; Xing, Z.; Guo, C.; Yue, X.; Liu, J. Gold-nanoshelled microcapsules: A theranostic agent for ultrasound contrast imaging and photothermal therapy. *Angew. Chem. Int. Ed. Eng.* **2011**, *50*, 3017–3021. [CrossRef] [PubMed]
14. Yang, K.; Feng, L.; Shi, X.; Liu, Z. Nano-graphene in biomedicine: Theranostic applications. *Chem. Soc. Rev.* **2013**, *42*, 530–547. [CrossRef] [PubMed]
15. Al-Jamal, W.T.; Al-Jamal, K.T.; Bomans, P.H.; Frederik, P.M.; Kostarelos, K. Functionalized-quantum-dot-liposome hybrids as multimodal nanoparticles for cancer. *Small* **2008**, *4*, 1406–1415. [CrossRef] [PubMed]
16. Al-Jamal, W.T.; Kostarelos, K. Liposomes: From a clinically established drug delivery system to a nanoparticle platform for theranostic nanomedicine. *Acc. Chem. Res.* **2011**, *44*, 1094–1104. [CrossRef] [PubMed]
17. Li, X.; Qian, Y.; Liu, T.; Hu, X.; Zhang, G.; You, Y.; Liu, S. Amphiphilic multiarm star block copolymer-based multifunctional unimolecular micelles for cancer targeted drug delivery and magnetic resonance imaging. *Biomaterials* **2011**, *32*, 6595–6805. [CrossRef] [PubMed]
18. Shi, J.; Xiao, Z.; Kamaly, N.; Farokhzad, O.C. Self-assembled targeted nanoparticles: Evolution of technologies and bench to bedside translation. *Acc. Chem. Res.* **2011**, *44*, 1123–1134. [CrossRef] [PubMed]
19. Shukla, R.; Thomas, T.P.; Peters, J.; Kotlyar, A.; Myc, A.; Bakers, J.R., Jr. Tumor angiogenic vasculature targeting with PAMAM dendrimer-RGD conjugates. *Chem. Comm.* **2005**, 5739–5741. [CrossRef] [PubMed]
20. Li, Y.; He, H.; Jia, X.; Lu, W.-L.; Lou, J.; Wei, Y. A dual-targeting nanocarrier based on poly(amidoamine) dendrimers conjugated with transferrin and tamoxifen for treating brain gliomas. *Biomaterials* **2012**, *33*, 3899–3908. [CrossRef] [PubMed]
21. Tomalia, D.A. In quest of a systematic framework for unifying and defining nanoscience. *J. Nanopart. Res.* **2009**, *11*, 1251–1310. [CrossRef] [PubMed]
22. Tomalia, D.A.; Khanna, S.N. A systematic framework and nanoperiodic concept for unifying nanoscience: Hard/Soft nanoelements, superatoms, meta-atoms, new emerging properties, periodic property patterns, and predictive mendeleev-like nanoperiodic tables. *Chem. Rev.* **2016**, *116*, 2705–2774. [CrossRef] [PubMed]
23. Kannan, R.M.; Nance, E.; Kannan, S.; Tomalia, D.A. Emerging concepts in dendrimer-based nanomedicine: From design principles to clinical applications. *J. Internal Med.* **2014**, *276*, 579–617. [CrossRef] [PubMed]
24. Enciso, A.E.; Abid, Z.M.; Simanek, E.E. Rapid, semi-automated convergent synthesis of low generation triazine dendrimers using microwave assisted reactions. *Polym. Chem.* **2014**, *5*, 4635–4640. [CrossRef]

25. Gray, W.D.; Wu, R.J.; Yin, X.; Zhou, J.; Davis, M.E.; Luo, Y. Dendrimeric bowties featuring hemispheric-selective decoration of ligands for microRNA-based therapy. *Biomacromolecules* **2013**, *14*, 101–109. [CrossRef] [PubMed]
26. Wängler, C.; Mashauer, S.; Prante, O.; Schafer, M.; Schmirrmacher, R.; Bartenstein, P.; Eisenhut, M.; Wängler, B. Multimerization of cRGD peptides by click chemistry: Synthetic strategies, chemical limitations, and influence on biological properties. *ChemBioChem* **2010**, *11*, 2168–2181. [CrossRef] [PubMed]

Sample Availability: Samples of the compounds are available from the authors.

molecules

MDPI

Article

Thermoregulated Coacervation, Metal-Encapsulation and Nanoparticle Synthesis in Novel Triazine Dendrimers

Fermín Ramírez-Crescencio [1], Alan E. Enciso [2], Mirza Hasan [2], Viviana C. P. da Costa [2], Onofrio Annunziata [2], Rocío Redón [1], Jeffery L. Coffer [2] and Eric E. Simanek [2,*]

[1] Centro de Ciencias Aplicadas y Desarrollo Tecnológico, Universidad Nacional Autónoma de México, Cd. Universitaria, A.P. 70–186, C.P., Cd. Mx. 04510, Mexico; qfermin@gmail.com (F.R.-C.); rredon@unam.mx (R.R.)

[2] Department of Chemistry & Biochemistry, Texas Christian University, Fort Worth, TX 76129, USA; a.encisobarros@tcu.edu (A.E.E.); mirza.hasan@tcu.edu (M.H.); v.costa@tcu.edu (V.C.P.C.); o.annunziata@tcu.edu (O.A.); j.coffer@tcu.edu (J.L.C.)

* Correspondence: e.simanek@tcu.edu; Tel.: +1-817-257-5355

Academic Editor: Ashok Kakkar

Received: 9 March 2016; Accepted: 28 April 2016; Published: 11 May 2016

Abstract: The synthesis and solubility behaviors of four generation five (G5) triazine dendrimers are studied. While the underivatized cationic dendrimer is soluble in water, the acetylated and propanoylated derivatives undergo coacervation in water upon increasing temperature. Occurring around room temperature, this behavior is related to a liquid-liquid phase transition with a lower critical solution temperature (LCST) and is explained by differences in composition, notably, the hydrophobic nature of the terminal groups. Interestingly, the water solubility of the acetylated dendrimer is affected by the addition of selected metal ions. Titrating solutions of acetylated dendrimer at temperatures below the LCST with gold or palladium ions promoted precipitation, but platinum, iridium, and copper did not. Gold nanoparticles having diameters of 2.5 $\pm$ 0.8 nm can be obtained from solutions of the acetylated dendrimer at concentrations of gold less than that required to induce precipitation by treating the solution with sodium borohydride.

Keywords: dendrimer; triazine; LLPS; LCST; thermoresponsive; nanoparticle, gold

1. Introduction

The temperature-induced, reversible coacervation of macromolecules in solution is a result of liquid-liquid phase separation (LLPS) [1]. Depending on the chemical nature of macromolecule and solvent, LLPS may be induced either by decreasing or increasing temperature. The corresponding temperature-composition phase diagrams will exhibit either an upper critical solution temperature (UCST) or a lower critical solution temperature (LCST), respectively.

This phase transition has been extensively investigated for solutions of linear polymers due to their importance for mixture thermodynamics, separation technologies, self-assembly processes, catalysis and the preparation of thermoresponsive materials [1–5]. However, corresponding studies on dendrimer solutions are scarce [6], which is surprising given the significant overlap between the scopes of dendrimers and LLPS applications. In the case of catalysis, a thermoregulated formation of coacervates of dendrimers could be employed to separate these nanoreactors from the reaction products. In the case of extraction, LLPS could be used to separate the molecules sequestered by the host dendrimers from solution with applications to purification and drug loading. Finally, the coupling of coacervation with chemical crosslinking could be applied to produce crosslinked coacervates with high guest loading capacity, relevant to drug delivery applications.

Our own interest rests in triazine dendrimers [7]. Recent interest in metal nanoparticles led to the serendipitous discovery of dendrimers displaying LLPS behaviors. Specifically, two of these systems undergo reversible opacification upon increasing temperature, characteristic of the LCST type of behavior. To our knowledge, no previous LLPS study has been reported for solutions of triazine dendrimers.

2. Results and Discussion

2.1. Design and Synthesis

The compounds examined in this study derive from **1** (Figure 1), a generation 5 triazine dendrimer composed of triazines linked by 4,7,10-trioxodecanediamine and piperazine [8–10]. Like **1**, dendrimers **2**, **3**, and **4** are generation 5 dendrimers with 96 end groups and molecular weights of approximately 40 kDa. The compound numbers (**2**, **3**, **4**) conveniently reflect the number of carbons in their acyl groups (acetyl, propanoyl, isobutanoyl).

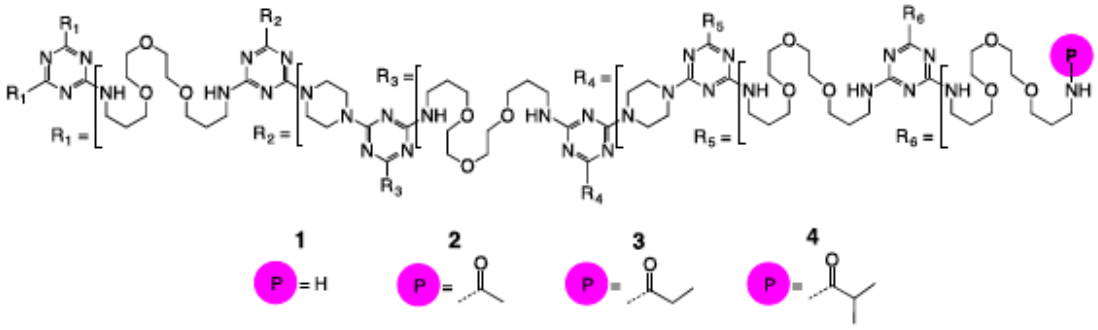

Figure 1. The molecules used in this study.

Generation 5 dendrimers were chosen because this generation shows an onset of globular structure with high degrees of porosity and diameters measuring 6 nm [10]. This size was considered ideal for the creation of dendrimer-encapsulated nanoparticles, the initial impetus for this work [11–24]. The choice of linkers reflects a balance of needs for reactivity during synthesis (piperazine groups) [25,26] and water solubility (4,7,10-trioxodecanediamine) [8–10,27]. Additionally, polyethyleneglycol tethers have been shown to influence Au nanoparticle formation and stability [19,20].

The acetylated dendrimer, **2**, was the first target based on literature precedent. Wang *et al*. have shown that acetylated PAMAM dendrimers lead to the formation of dendrimer-encapsulated nanoparticles that are more biocompatible [22]. Pietsch has shown that acetylation leads to better control over nanoparticle size and shape [23].

To arrive at **2**, progenitor **1** was acetylated with acetic anhydride. Indeed, to arrive at **3** and **4**, **1** was subjected the commercially available acid anhydrides as well. The preparation of **1** relied on condensing two published molecules, **5** and **6** (Figure 2) to yield **7**. Both **5** and **6** are available by a rapid, microwave and macromonomer-mediate synthesis [8,9]. In addition to providing water solubility, these building blocks were perceived to yield dendrimers that were both large and flexible with pores envisioned to support nanoparticle growth. The reaction is facilitated by the presentation of secondary amines (piperazine) on **5** that show higher reactivity than primary amines [25,26] for monochlorotriazines like **6**. Upon isolation of **7**, a BOC-derivative displaying no water solubility, **1** can be obtained by treatment with acid.

During the course of manipulating **2**, we observed an LCST in water. Manipulating the LCST of a system is commonly done by affecting the hydrophobic/hydrophilic balance. In polyacrylamides, for example, the LCST of a polymer comprising *N*-isopropyl groups can be increased by introducing *N*-ethyl groups or decreased by introducing isobutyl groups [28]. To probe the impact that the acyl group has on LCST, the acetylated dendrimer, **2**, was compared with those presenting propanoyl

groups, **3**, and isobutanoyl groups, **4**. Like **1**, **4** was insoluble in water at room temperature, precluding further analysis.

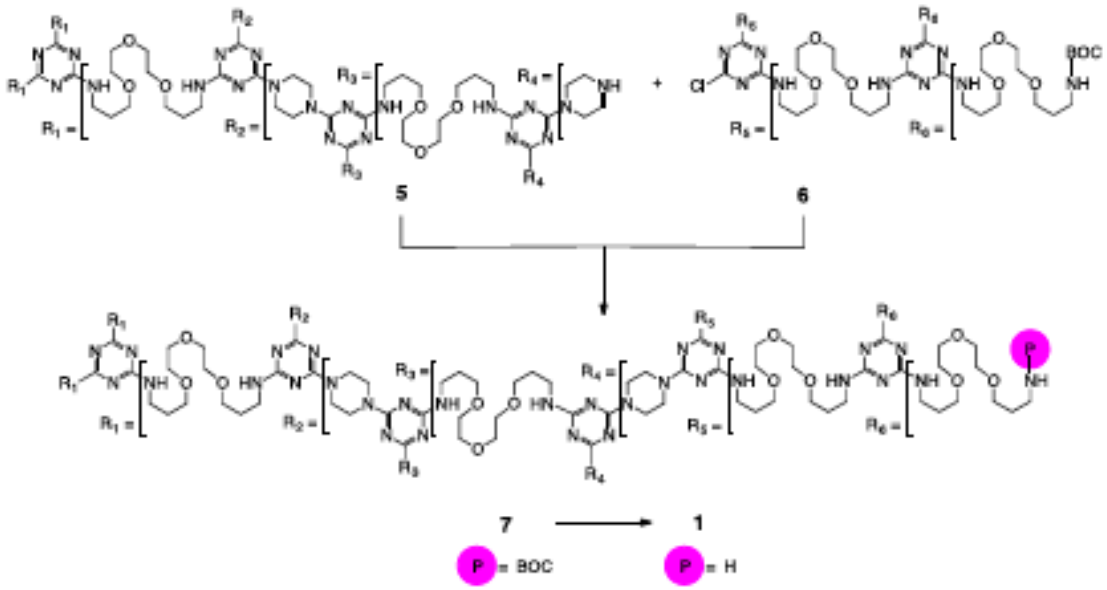

Figure 2. The synthesis of **1** relies on the use of **5** and **6** [12].

2.2. *Liquid-Liquid Phase Separation (LLPS) Temperatures*

LLPS temperatures, T_{ph}, were determined using the turbidity method described in the Experimental Section. The temperature-induced opacification of aqueous solutions of **2** and **3** at 4 mg/mL are shown in Figure 3. We obtain T_{ph} = 28 °C for **2** and T_{ph} = 20 °C for **3**.

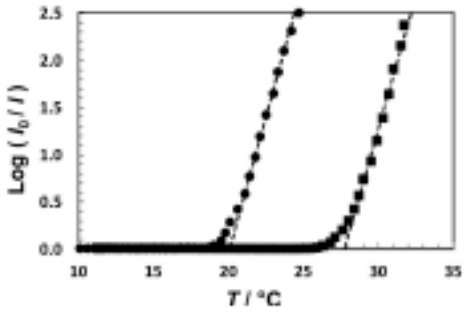

Figure 3. Temperature-turbidity profiles for aqueous solutions of **2** (squares) and **3** (circles). The dendrimer concentration is 4 mg/mL in both cases. The dashes lines, which are linear fits through the data with Log (I_0/I) > 0.5, show the values of T_{ph} = 20 °C (**3**) and T_{ph} = 28 °C (**2**) extrapolated at Log (I_0/I) = 0.

LCST behavior is observed for aqueous solutions of polyethylene glycol (PEG) [29]. At room temperature, water is a good solvent for this polymer due to the formation of hydrogen bonds between the PEG ethoxy groups and water molecules. As temperature increases, water becomes a poorer solvent for PEG, thereby leading to LLPS [30]. In our case, PEG-like linkers are used between triazines to enhance water solubility of these dendrimers at room temperature. The observed LCST type of behavior is attributed to the PEG-like domains of our triazine dendrimers. As temperature increases, the hydration of the PEG-like linkers decreases [31], and the solubility of triazine dendrimers is expected to reduce giving rise to LLPS. Similar desolvation behavior of the PEG-like domains has been observed in computational models of these and other dendrimers [32].

The actual location of the LLPS temperature is expected to strongly depend on the chemical nature of the dendrimer terminal groups. That the value of T_{ph} in the case of **3** is lower than that in the case of **2** correlates with the higher hydrophobicity of the propanoyl group compared to that of the acetyl group. Furthermore, our analysis suggests that the LLPS of aqueous solutions of **4** should be located at lower temperatures, consistent with the observed poor solubility of **4** in water. In summary, our findings show that the modifications of the terminal groups of these triazine dendrimers can be used to modulate the LLPS temperature around room temperature.

2.3. *Influence of Metal Ions on Solubility of* **2**

Dendrimer **2** was chosen for hosting nanoparticles because the LCST was sufficiently high to facilitate their synthesis. However, upon adding approximately 100 mole equivalents of gold in the form of $HAuCl_4$-$3H_2O$ to solutions of **2**, a precipitate formed. While we recognize that the equivalence point is close to the number of end groups, additional studies will be required to ascertain the mechanistic basis for this coincidence. A similar behavior was seen with additions of Na_2PdCl_4. In contrast, titrated additions of K_2PtCl_4, $IrCl_3{\cdot}xH_2O$, or $CuSO_4{\cdot}5H_2O$ did not promote precipitation. The selectivity observed could be useful, as the separation of gold or palladium from copper is of some interest in the recycling of microelectronic waste streams [33–36]. Simple sequestration strategies are also attracting attention [37,38]. Dendrimers are largely unexplored in this capacity, but the scalable synthesis of triazines makes such opportunities of interest.

2.4. *Formation of Nanoparticles*

At low molar ratios of Au^{3+}: Dendrimer (approximately 60:1), soluble dendrimer-encapsulated nanoparticles could be prepared by the addition of sodium borohydride, a reagent required to generate Au at room temperature. Figure 4 summarizes the results of these experiments. The mean diameters of these particles was 2.55 ± 0.84 nm. The particles are red in solution and UV-Vis spectroscopy reveals an absorption maximum at 510 nm, consistent with the well-known surface plasmon of gold. Preliminary experiments show that nanoparticles of palladium, platinum, iridium and copper are also accessible, but these studies are preliminary and will be reported in due course. For gold nanoparticles, we note that not only is the particle size reasonably homogeneous, but the spacing between the particles is very similar and close to 6 nm, the diameter of the dendrimer. That is, the micrograph is consistent with a single gold nanoparticle encapsulated within a single globular macromolecule that sterically separates it from its neighbor. Additional experiments will be required to bear out this hypothesis.

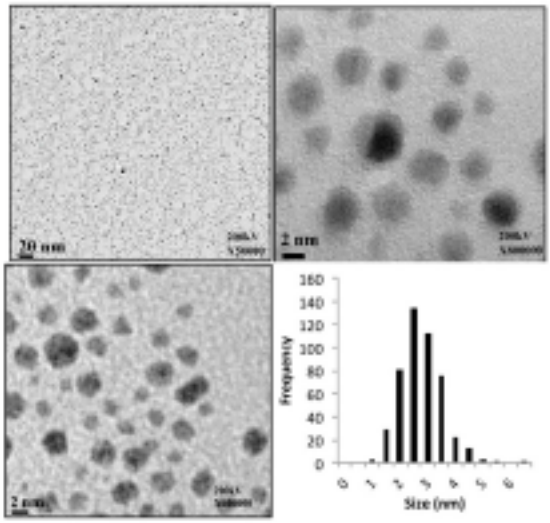

Figure 4. A TEM micrographs at three magnifications of dendrimer-encapsulated gold nanoparticles derived from **2** and the distribution of their sizes.

3. Materials and Methods

3.1. General Experimental

All reagents were used as received. Methanol, dichloromethane, dioxane, diethylether, acetic anhydride, $HAuCl_4$, D_2O, $CDCl_3$ (Sigma-Aldrich, St. Louis, MO, USA); triethylamine (TEA), DIPEA, Na_2PdCl_4, K_2PtCl_4, $IrCl_3 \cdot x\ H_2O$ (Pressure Chemical, Pittsburgh, PA, USA). Microwave reactions were carried on using a CEM SP Discover microwave (CEM Corporation, Matthews, NC, USA). NMR experiments were conducted on a Bruker 400 Ascend spectrometer (Bruker, Billerica, MA, USA); UV-Vis spectra were obtained on an Agilent 8453(Agilent, Santa Clara, CA, USA) were recorded at room temperature in water 18 mΩ. The NMR data listed shows the theoretical number of protons expected for the molecule reported. Error prevents an accurate assessment of the true numbers, but integration of the spectra corroborate this expectation.

3.2. Preparation of **1**

A solution of **7** (0.2605 g, 4 µmol) in dioxane (6 mL) was mixed with HCl conc. (3 mL) and heated 3 min at 60 °C using dynamic mode. Afterwards, solvent was evaporated under vacuum and residue dissolved in water; pH was adjusted to 12 using 5 M NaOH (aq). The product was extracted with dichloromethane and, after solvent evaporation, deprotected dendrimer was obtained as a white thick oil (0.2069 g, quantitative yield). ^{1}H-NMR (400 MHz, D_2O) δ 3.77–3.11 (m, 2592H, $C\underline{H}_2OC\underline{H}_2C\underline{H}_2OC\underline{H}_2C\underline{H}_2OC\underline{H}_2$, C_3N_3-$NHC\underline{H}_2CH_2CH_2O$, C_3N_3-$NC\underline{H}_2C\underline{H}_2N$), δ 2.74–2.92 (br, 192H, $NH_2C\underline{H}_2$), δ 1.86–1.59 (br, 636H, $OCH_2C\underline{H}_2CH_2NH$); ^{13}C-NMR (100 MHz, $CDCl_3$) δ 166.06 ($\underline{C}_3N_3$), δ 165.14 ($\underline{C}_3N_3$), δ 70.57 ($O\underline{C}H_2\underline{C}H_2O$), δ 70.16 (two lines, $O\underline{C}H_2\underline{C}H_2O$), δ 69.42 ($NHCH_2CH_2\underline{C}H_2O$), δ 69.28 ($NHCH_2CH_2\underline{C}H_2O$), δ 43.01 ($N\underline{C}H_2\underline{C}H_2N$), δ 39.50 ($NH\underline{C}H_2CH_2CH_2O$), δ 38.08 ($NH\underline{C}H_2CH_2CH_2O$), δ 33.12 ($NHCH_2\underline{C}H_2CH_2O$), δ 29.68 ($NHCH_2\underline{C}H_2CH_2O$); MS (MALDI-TOF) calcd for $C_{1992}H_{3834}N_{660}O_{677}$ 44639.60, found 40742.54. See the Supplementary Materials (Figures S4–S6) for the NMR and MS data of **1**.

3.3. Preparation of **2**

A mixture of **1** (0.0917 g, 2 µmol), acetic anhydride (93 µL, 985 µmol) and triethylamine (165 µL, 1183 µmol) in methanol (13 mL) was stirred overnight at room temperature. Afterwards, solvent was evaporated and residue dissolved in water; then, impurities were filtered off using ultracentrifugation (30 min, 14,000 rpm) and product was washed two more times with pure water. After liophylization, a pale yellow sticky solid was obtained (0.0497g, 50% yield). ^{1}H-NMR (400 MHz, D_2O) δ 3.12–3.60 (m, 2592H, $C\underline{H}_2OC\underline{H}_2C\underline{H}_2OC\underline{H}_2C\underline{H}_2OC\underline{H}_2$, C_3N_3-$NHC\underline{H}_2CH_2CH_2O$, C_3N_3-$NC\underline{H}_2C\underline{H}_2N$), δ 3.05–3.12 (t, 192H $AcNHC\underline{H}_2$), δ 1.57–1.77 (br, 636H, $OCH_2C\underline{H}_2CH_2NH$), δ 1.84 (s, 288H, $COC\underline{H}_3$); ^{13}C-NMR (100 MHz, D_2O) δ 173.44 ($\underline{C}O$), δ 164.76 (br, $\underline{C}_3N_3$), δ 69.70 ($O\underline{C}H_2\underline{C}H_2O$), δ 69.42 (two lines, $O\underline{C}H_2\underline{C}H_2O$), δ 68.64 ($NHCH_2CH_2\underline{C}H_2O$), δ 68.45 ($NHCH_2CH_2\underline{C}H_2O$), δ 42.88 ($N\underline{C}H_2\underline{C}H_2N$), δ 37.50 ($NH\underline{C}H_2CH_2CH_2O$), δ 36.49 ($NH\underline{C}H_2CH_2CH_2O$), δ 28.96 ($NHCH_2\underline{C}H_2CH_2O$), δ 28.35 ($NHCH_2\underline{C}H_2CH_2O$), δ 21.89 ($\underline{C}(CO)$); MS (MALDI-TOF) calcd for $C_{2184}H_{4026}N_{660}O_{573}$ 48672.62, found 40652.96. See the Supplementary Materials (Figures S7–S9) for the NMR and MS data of **2**.

3.4. Preparation of **3**

A mixture of **1** (0.039 g, 0.873 µmol), propionic anhydride (53 µL, 419 µmol) and triethylamine (70 µL, 503 µmol) in methanol (10 mL) was stirred overnight at room temperature. Afterwards, solvent was evaporated and residue dissolved in water; then, impurities were filtered off using ultracentrifugation (30 min, 14,000 rpm) and product was washed two more times with pure water. After liophylization, a pale yellow sticky solid was obtained (0.009 g, 21% yield). ^{1}H-NMR (400 MHz, D_2O) δ 3.10–3.60 (m, 2592H, $C\underline{H}_2OC\underline{H}_2C\underline{H}_2OC\underline{H}_2C\underline{H}_2OC\underline{H}_2$, C_3N_3-$NHC\underline{H}_2CH_2CH_2O$, C_3N_3-$NC\underline{H}_2C\underline{H}_2N$), δ 2.10–2.04 (m, 192H $CH_3C\underline{H}_2CONHC\underline{H}_2$), δ 1.45–1.95 (br, 636H, $OCH_2C\underline{H}_2CH_2NH$), δ 0.91–0.97 (t, 288H, $COCH_2C\underline{H}_3$); ^{13}C-NMR (100 MHz, D_2O)

δ 176.6 (CO),δ 165.2 (br, C_3N_3), δ 69.7 (OCH_2CH_2O), δ 69.4 (two lines, OCH_2CH_2O), δ 68.5 ($NHCH_2CH_2CH_2O$), δ 42.88 (NCH_2CH_2N), δ 37.4 ($NHCH_2CH_2CH_2O$), δ 36.4 ($NHCH_2CH_2CH_2O$), δ 29.1 ($NHCH_2CH_2CH_2O$), δ 29.0 ($NHCH_2CH_2CH_2O$), δ 28.4 (CH_3CH_2CON), δ 9.7 (CH_3CH_2CON); MS (MALDI-TOF) calcd for $C_{2280}H_{4218}N_{660}O_{573}$ 50018.12, found 47376.9. See the Supplementary Materials (Figures S10–S12) for the NMR and MS data of **3**.

3.5. *Preparation of* **4**

A mixture of **1** (0.039 g, 0.873 μmol), isobutyric anhydride (100 μL, 603 μmol) and triethylamine (14 μL, 100μmol) in methanol (10 mL) was heated overnight at 40 °C Afterwards, solvent was evaporated and residue dispersed in water; then, impurities were filtered off using ultracentrifugation (30 min, 14,000 rpm) and product was washed two more times with pure water. After lyophylization, a pale yellow sticky solid was obtained (0.029g, 65% yield). ^{1}H-NMR (400 MHz, D_2O) δ 3.21–3.60 (m, 2592H, $CH_2OCH_2CH_2OCH_2CH_2OCH_2$, C_3N_3-$NHCH_2CH_2CH_2O$, C_3N_3-NCH_2CH_2N), δ 3.05–3.22 (m, 192H $CH_3CH_2CONHCH_2$), δ 2.31–2.38 (m, 96, $CH(CH_3)_2$) , δ 1.64–1.73 (br, 636H, $OCH_2CH_2CH_2NH$), δ 0.99–0.97 (d, 576H, $CH(CH_3)_2$); ^{13}C-NMR (100 MHz, D_2O) δ 180.0 (CO),δ 165.2 (br, C_3N_3), δ 69.7 (OCH_2CH_2O), δ 69.5 (OCH_2CH_2O), δ 69.4 (OCH_2CH_2O), δ 68.5 ($NHCH_2CH_2CH_2O$), δ 42.88 (NCH_2CH_2N), δ 38.2 ($NHCH_2CH_2CH_2O$), δ 37.6 ($NHCH_2CH_2CH_2O$), δ 35.1 ($CH(CH_3)_2$), δ 28.7 ($NHCH_2CH_2CH_2O$), δ 18.7 ($CH(CH_3)_2$); MS (MALDI-TOF) calcd for $C_{2376}H_{4506}N_{660}O_{573}$ 51460.37, not found. See the Supplementary Materials (Figures S13 and S14) for the NMR spectra of **4**.

3.6. *Preparation of* **7**

Synthesis of **7** was accomplished following an analogous procedure to the one reported for Enciso *et al* [9]. A solution of 5 (0.0711g, 9 μmol) in methanol (0.5 mL) was mixed with another solution of 6 (0.9157 g, 461 μmol) in dioxane (4 mL), and DIPEA (0.2 mL, 1148 μmol) was added. Then mixture was heated for 6 h at 95 °C. Solvent was evaporated and product impurities were removed washing the crude several times with diethyl ether. A white solid, **7**, was obtained (0.3681 g, 71% yield). ^{1}H-NMR (400 MHz, $CDCl_3$) δ 3.25–3.95 (m, 2592H, $CH_2OCH_2CH_2OCH_2CH_2OCH_2$, C_3N_3-$NHCH_2CH_2CH_2O$, C_3N_3-NCH_2CH_2N), δ 3.02–3.25 (br, 192H $BocNHCH_2$), δ 1.54–1.96 (br, 636H, $OCH_2CH_2CH_2NH$), δ 1.38 (s, 864H, $C(CH_3)_3$); ^{13}C-NMR (100 MHz, $CDCl_3$) δ 164.56 (br, C_3N_3), δ 156.04 (CO), δ 78.77 ($C(CH_3)_3$), δ 70.53 (OCH_2CH_2O), δ 70.15 (two lines, OCH_2CH_2O), δ 69.48 ($NHCH_2CH_2CH_2O$), δ 69.15 ($NHCH_2CH_2CH_2O$), δ 43.0 (NCH_2CH_2N), δ 38.24 ($NHCH_2CH_2CH_2O$), δ 38.45($NHCH_2CH_2CH_2O$), δ 29.58 ($NHCH_2CH_2CH_2O$), δ 29.46 ($NHCH_2CH_2CH_2O$), δ 28.44 ($C(CH_3)_3$); MS (MALDI-TOF) calcd for $C_{2472}H_{4602}N_{660}O_{669}$ 54244.64, found 50180.07. See the Supplementary Materials (Figures S1–S3) for the NMR and MS data of **7**.

3.7. *Measurement of the Cloud Point*

The phase separation temperature, T_{ph}, was determined by measuring the turbidity of binary dendrimer-water samples as function of temperature. A binary dendrimer-water homogenous sample with a dendrimer concentration of 4 mg/mL was prepared by mixing known amounts of water and dendrimer. The turbidity meter is comprised of a programmable circulating bath (1197P, VWR), a calibrated thermocouple (±0.1 °C), a homemade optical cell, where the initially-transparent sample (optical path of 0.4 cm) and a thermocouple probe are located. Collimated light from a solid state laser (633 nm, 5 mW, Coherent) passes through the sample and its transmittance is recorded by a photodiode detector coupled with a computer-interfaced optical meter (1835-C Newport). After recording the transmitted intensity of the transparent sample, I_o, the temperature of the bath is changed at a constant rate of ±0.5 °C/min and the transmitted intensity, I, is recorded as a function of temperature, T. We identify T_{ph} as the temperature at which a sharp decrease in intensity is observed (see Figure 3).

3.8. Titrations

A stock solution of **2** (0.0184 g, 0.37 µmol) in water (3 mL) were prepared. For every complexation experiment, 100 µL of stock solution were diluted with 900 µL of water in a 1 mL quartz cuvette to yield a dendrimer concentration (1.25×10^{-5} M). Aqueous solutions of metal salts (typically at $10\times$ lower concentration) were freshly prepared and added under stirring using a micropipette; no more than 100 µL were added to the dendrimer solution to avoid dilution effects; mixtures were allowed to equilibrate 10 minutes (Cu, Pt, Ir, and Au) or 15 min (Pd).

3.9. Nanoparticle Synthesis

The same stock solution of metal-dendrimer (**2**) titration experiments was used. For every reduction experiment 100 µL of stock solution were diluted with 900 µL of water in a 1 mL quartz cuvette. Aqueous solutions of metal precursors were freshly prepared and added under stirring using a micropipette (30 µL, 60 metal equivalents). Mixture was left to equilibrate for a period of 15 min before $NaBH_4$ were added (20 µL, metal to $NaBH_4$ ratio 1:4) under vigorous stirring. The procedure was carried out at room temperature.

3.10. Electron Microscopy

Samples of dendrimer-encapsulated gold nanoparticles were analyzed using transmission electron microscopy (JEOL Ltd., Tokyo, Japan) on a JEOL JEM-2100 operating at 200 kV. Approximately 50 µL of a given sample was applied to a carbon-coated copper grid and allowed to air dry.

4. Conclusions

Aqueous solutions of some generation 5 triazine dendrimers display LLPS with an LCST type of behavior. The LCST of these materials can be varied with the choice of terminal acyl group: Acetylated dendrimers remain soluble at higher temperatures than propanoylated dendrimers. Curiously, the LCST appears to be affected by the addition of some metal ions, but not others. Indeed, this behavior could translate into strategies for the selective recovery of some precious metal salts like gold and palladium in the presence of less valuable ones such as copper. Gold nanoparticles can still be achieved, however, by performing the reduction at concentrations below which precipitation occurs.

Supplementary Materials: Supplementary materials can be accessed at: http://www.mdpi.com/1420-3049/21/5/599/s1.

Acknowledgments: Eric E. Simanek thanks the Robert A. Welch Foundation (P-0008) and DOD (W81XWH-12-1-0338) for support. Fermín Ramírez-Crescencio and Rocío Redón thank CONACyT for a fellowship (227152–332714) and funding (167356). Rocío Redón also thanks PAPIIT for support (IN117514). Jeffery L. Coffer also thanks the Robert A. Welch Foundation for financial support (Grant P-1212).

Author Contributions: F.R.-Z. and A.E.E. conceived and executed the experiments under the direction of R.R. and E.E.S., respectively. M.H. collected the TEM micrographs under the supervision of J.L.C., V.C.P.C. performed the measurements of LCST under the direction of O.A. All authors contributed to the preparation of the manuscript.

Conflicts of Interest: The authors declare no conflict of interest.

Abbreviations

The following abbreviations are used in this manuscript:

DEN	Dendrimer-encapsulated nanoparticle
G5	Generation 5
LCST	Lower critical solution temperature
LLPS	Liquid-liquid phase separation
PAMAM	Polyamidoamine
PPI	Polypropyleneimine

$NaBH_4$	Sodium tetrahydroborane
TEM	Transmission electron microscopy

References

1. Albertsson, P.A. *Partition of Cell Particles and Macromolecules*; Wiley: New York, NY, USA, 1986.
2. Zhang, Y.; Cremer, P.S. Chemistry of Hofmeister Anions and Osmolytes. *Annu. Rev. Phys. Chem.* **2010**, *61*, 63–83. [CrossRef] [PubMed]
3. Lima, A.C.; Sher, P.; Mano, J.F. Production methodologies of polymeric and hydrogel particles for drug delivery applications. *Expert Opin. Drug Deliv.* **2012**, *9*, 231–248. [CrossRef] [PubMed]
4. Keating, C.D. Aqueous Phase Separation as a Possible Route to Compartmentalization of Biological Molecules. *Acc. Chem. Res.* **2012**, *45*, 2114–2124. [CrossRef] [PubMed]
5. Elbert, D.L. Liquid-liquid two-phase systems for the production of porous hydrogels and hydrogel microspheres for biomedical applications: A tutorial review. *Acta. Biomater.* **2011**, *7*, 31–56. [CrossRef] [PubMed]
6. Da Costa, V.C.P.; Annunziata, O. Unusual liquid–liquid phase transition in aqueous mixtures of a well-known dendrimer. *Phys. Chem. Chem. Phys.* **2015**, *17*, 28818–28829. [CrossRef] [PubMed]
7. Simanek, E.E.; Abdou, H.; Lalwani, S.; Lim, J.; Mintzer, M.; Venditto, V.J.; Vittur, B. The 8 year thicket of triazinedendrimers: Strategies, targets and applications. *Proc. R. Soc. A* **2010**, *466*, 1445–1468. [CrossRef]
8. Enciso, E.; Abid, Z.M.; Simanek, E.E. Rapid, semi-automated convergent synthesis of low generation triazine dendrimers using microwave assisted reactions. *Polym. Chem.* **2014**, *5*, 4635–4640. [CrossRef]
9. Enciso, A.E.; Ramirez-Crescencio, F.; Zeiser, M.; Redon, R.; Simanek, E.E. Accelerated synthesis of large generation triazine dendrimers using microwave assisted reactions: A 24 hours challenge. *Polym. Chem.* **2015**, *6*, 5219–5224. [CrossRef]
10. Lim, J.; Pavan, G.M.; Annunziata, O.; Simanek, E.E. Experimental and Computational Evidence for an Inversion in Guest Capacity in High-Generation Triazine Dendrimer Hosts. *J. Am. Chem. Soc.* **2012**, *134*, 1942–1945. [CrossRef] [PubMed]
11. Zhao, M.; Sun, L.; Crooks, R.M. Preparation of Cu Nanoclusters within Dendrimer Templates. *J. Am. Chem. Soc.* **1998**, *120*, 4877–4878. [CrossRef]
12. Zhao, P.; Feng, X.; Huang, D.; Yang, G.; Astruc, D. Basic concepts and recent advances in nitrophenol reduction by gold- and other transition metal nanoparticles. *Coord. Chem. Rev.* **2015**, *287*, 114–136. [CrossRef]
13. Yamamoto, K.; Imaoka, T. Precision Synthesis of Subnanoparticles Using Dendrimers as a Superatom Synthesizer. *Acc. Chem. Res.* **2014**, *47*, 1127–1136. [CrossRef] [PubMed]
14. Nemanashi, M.; Meijboom, R. Synthesis and characterization of Cu, Ag and Au dendrimer-encapsulated nanoparticles and their application in the reduction of 4-nitrophenol to 4-aminophenol. *J. Colloid Interface Sci.* **2013**, *389*, 260–267. [CrossRef] [PubMed]
15. Esumi, K.; Isono, R.; Yoshimura, T. Preparation of PAMAM and PPI metal (Silver, Platinum, and Palladium) nanocomposites and their catalytic activities for reduction of 4-nitrophenol. *Langmuir* **2004**, *20*, 237–243. [CrossRef] [PubMed]
16. Wang, D.; Astruc, D. Dendritic catalysis-Basic concepts and recent trends. *Coord. Chem. Rev.* **2013**, *257*, 2317–2334. [CrossRef]
17. Myers, V.S.; Weir, M.G.; Carino, E.V.; Yancey, D.F.; Pande, S.; Crooks, R.M. Dendrimer-encapsulated nanoparticles: New synthetic and characterization methods and catalytic applications. *Chem. Sci.* **2011**, *2*, 1632–1646. [CrossRef]
18. Crooks, R.M.; Zhao, M.; Sun, L.; Chechik, V.; Yeung, L.K. Dendrimer-Encapsulated Metal Nanoparticles: Synthesis, Characterization, and Applications to Catalysis. *Acc. Chem. Res.* **2001**, *34*, 181–190. [CrossRef] [PubMed]
19. Boisselier, E.; Diallo, A.K.; Salmon, L.; Ruiz, J.; Astruc, D. Gold nanoparticles synthesis and stabilization via new "clicked" polyethyleneglycoldendrimers. *Chem. Commun.* **2008**, *39*, 4819–4821. [CrossRef] [PubMed]
20. Li, N.; Echeverría, M.; Moya, S.; Ruiz, J.; Astruc, D. "Click" Synthesis of Nona-PEG-branched Triazole Dendrimers and Stabilization of Gold Nanoparticles That Efficiently Catalyze *p*-Nitrophenol Reduction. *Inorg. Chem.* **2014**, *53*, 6954–6961. [CrossRef] [PubMed]

21. Deraedt, C.; Salmon, L.; Astruc, D. "Click" Dendrimer-Stabilized Palladium Nanoparticles as a Green Catalyst Down to Parts per Million for Efficient C-C Cross-Coupling Reactions and Reduction of 4-Nitrophenol. *Adv. Synth. Catal.* **2014**, *356*, 2525–2538. [CrossRef]
22. Wang, X.; Zhang, Y.; Li, T.; Tian, W.; Zhang, Q.; Cheng, Y. Generation 9 Polyamidoamine Dendrimer Encapsulated Platinum Nanoparticle Mimics Catalase Size, Shape, and Catalytic Activity. *Langmuir* **2013**, *29*, 5262–5270. [CrossRef] [PubMed]
23. Pietsch, T.; Appelhans, D.; Gindy, N.; Voit, B.; Fahmi, A. Oligosaccharide-modified dendrimers for templating gold nanoparticles: Tailoring the particle size as a function of dendrimer generation and size structure. *Colloids Surf. A Physicochem. Eng. Asp.* **2009**, *341*, 93–102. [CrossRef]
24. Golpidas, K.R.; Whitesell, J.K.; Fox, M.A. Synthesis, Characterization, and Catalytic Applications of a Palladium-Nanoparticle-Cored Dendrimer. *Nano. Lett.* **2003**, *3*, 1757–1760. [CrossRef]
25. Steffensen, M.B.; Simanek, E.E. Chemoselective building blocks for dendrimers from relative reactivity data. *Org. Lett.* **2003**, *5*, 2359–2361. [CrossRef] [PubMed]
26. Moreno, K.X.; Simanek, E.E. Identification of Diamine Linkers with Differing Reactivity and their Application in the Synthesis of a Melamine Dendrimers. *Tetrahedron Lett.* **2008**, *49*, 1152–1154. [CrossRef] [PubMed]
27. Lim, J.; Kostiainen, M.; Maly, J.; da Costa, V.C.; Annunziata, O.; Pavan, G.M.; Simanek, E.E. Synthesis of Large Dendrimers with the Dimensions of Small Viruses. *J. Am. Chem. Soc.* **2013**, *135*, 4660–4663. [CrossRef] [PubMed]
28. Bergbreiter, D.E. Using soluble polymers to recover catalysts and ligand. *Chem. Rev.* **2002**, *102*, 3345–3383. [CrossRef] [PubMed]
29. Malcolm, G.N.; Rowlinson, J.S. The Thermodynamic Properties of Aqueous Solutions of Polyethylene Glycol, Polypropylene Glycol and Dioxane. *Trans. Faraday Soc.* **1957**, *53*, 921–931. [CrossRef]
30. Matsuyama, A.; Tanaka, F. Theory of Solvation-Induced Reentrant Phase Separation in Polymer Solutions. *Phys. Rev. Lett.* **1990**, *65*, 341–344. [CrossRef] [PubMed]
31. Dormidontova, E.E. Role of Competitive PEO-Water and Water-Water Hydrogen Bonding in Aqueous Solution PEO Behavior. *Macromolecules* **2002**, *35*, 987–1001. [CrossRef]
32. Simanek, E.E.; Enciso, A.E.; Pavan, G.M. Computational design principles for the discovery of bioactive dendrimers: [s]-triazines and other examples. *Expert Opin. Drug Discov.* **2013**, *8*, 1057–1069. [CrossRef] [PubMed]
33. Fogarasi, S.; Imre-Lucaci, F.; Imre-Lucaci, A.; Ilea, P. Copper recovery and gold enrichment from waste printed circuit boards by mediated electrochemical oxidation. *J. Hazard. Mater.* **2014**, *273*, 215–221. [CrossRef] [PubMed]
34. Ha, V.H.; Lee, J.C.; Huyhn, T.H.; Jeong, J.; Pandey, B.D. Optimizing the thiosulfate leaching of gold from printed circuit boards of discarded mobile phone. *Hydrometallurgy* **2014**, *149*, 118–126. [CrossRef]
35. Zhang, Z.Y.; Zhang, F.S. Selective recovery of palladium from waste printed circuit boards by a novel non-acid process. *J. Hazard. Mater.* **2014**, *279*, 46–51. [CrossRef] [PubMed]
36. Deng, S.; Tang, H.; Xiao, G. Regenerating Method and Process for Recycling Rare Precious Metals from Electronic Wastes. CN 103397186-A, 20 November 2013.
37. Tong, S.; Jia, Q.; Song, N.; Zhou, W.; Duan, T.; Bao, C. Determination of gold(III) and palladium(II) in mine samples by cloud point extraction preconcentration coupled with flame atomic absorption spectrometry. *Microchim. Acta* **2011**, *172*, 95–102.
38. Behbahani, M.; Gorji, T.; Mahyari, M.; Salarian, M.; Bagheri, A.; Shaabani, A. Application of Polypropylene Amine Dendrimers (POPAM)-Grafted MWCNTs Hybrid Materials as a New Sorbent for Solid-Phase Extraction and Trace Determination of Gold(III) and Palladium(II) in Food and Environmental Samples. *Food Anal. Methods* **2014**, *7*, 957–966. [CrossRef]

Sample Availability: Not Available.

THE JOURNAL OF PHYSICAL CHEMISTRY C

Article

pubs.acs.org/JPCC

Intrinsic Fluorescence of Triazine Dendrimers Provides a New Approach to Study Dendrimer Structure and Conformational Dynamics

Sangram Raut,[†] Alan E. Enciso,[‡] Giovanni M. Pavan,[*,§] Changsuk Lee,[‡] Akop Yepremyan,[‡] Donald A. Tomalia,[∥] Eric E. Simanek,[*,‡] and Zygmunt Gryczynski[*,†]

[†]Department of Physics and Astronomy, Texas Christian University, Fort Worth, Texas 76129, United States,

[‡]Department of Chemistry and Biochemistry, Texas Christian University, Fort Worth Texas 76129, United States,

[§]Department of Innovative Technologies, University of Applied Sciences and Arts of Southern Switzerland, Manno 6928, Switzerland

[∥]NanoSynthons, LLC and the National Dendrimer and Nanotechnology Center, Mount Pleasant, Michigan 48858, United States

Supporting Information

ABSTRACT: We present basic spectroscopic studies of 5 triazine dendrimers ranging from generations one through nine, **G1**, **G3**, **G5**, **G7**, and **G9**, based on the intrinsic fluorescence of these molecules. The extinction spectra of each generation can be separated into two components; the absorption spectra from triazine chromophores and Rayleigh scattering by dendrimer particles. Rayleigh scattering into the UV spectral range is significant and may contribute more than 50% to the measured light attenuation (extinction) for larger dendrimer generations. Deviations from the Rayleigh model at long wavelengths (where the triazine chromophore does not absorb) are clear indications of dendrimer aggregation. These larger particles can be eliminated by dilution and sonication. Importantly, this model system represents a comprehensive case study where the intrinsic fluorescence of the dendrimer when combined with insights from molecular dynamics (MD) simulations can be utilized to probe molecular conformations and dynamics. Experimental results from fluorescence lifetimes, time-resolved anisotropies, and diffusional quenching indicate an increasingly compact core as size increases from **G1** to **G5**. This trend is reversed for **G7** and **G9** generations, which present more extended, and porous structures, less dense cores, and a denser peripheries. Simulations corroborate this picture and better anchor intuition of the behavior of these molecules.

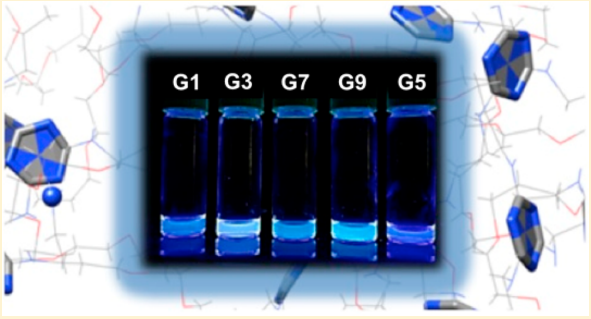

INTRODUCTION

Unique intrinsically fluorescent protein properties have not only been recognized by a Nobel Prize in 2008,[1] but also have led to a plethora of critical diagnostic, therapeutic, and imaging applications in the medical and life sciences fields.[2] Driven largely by the presence of fluorescent tryptophan, tyrosine, or phenylalanine moieties in their compositions, these intrinsic fluorescence properties have been exploited extensively as an important tool and strategy for probing internal protein structure.[3] It is notable that these fluorescence events occur on a time scale that allows articulate quantitation and monitoring of critical dynamics associated with protein folding, conformational transitions, protein denaturation, and local environmental effects, as well as external protein interactions and aggregation phenomena.[3,4] Many of these important issues have been reviewed in detail elsewhere.[3−5]

Considering the widely recognized "protein mimicry" features exhibited by dendrimers,[6−8] it was indeed surprising to find that the use of these intrinsically fluorescent protein-type protocols have not yet been reported for the characterization of their internal structure and dynamics. Dendrimers are highly branched polymers that adopt globular structures at higher generations reaching protein and even viral dimensions. Explored for more than three decades,[9−11] energies have focused on synthetic methodologies, biophysical characterization, and applications in fields ranging from materials to medical sciences.[7,12,13] Since their conception, the interaction of dendrimers with light has been an area of intense interest.[14,15] Most dendrimer classes have been scrutinized including PAMAM,[16] polyureas,[17] polyphenylenes,[18,19] phosphorus-containing dendrimers,[20] polyarylacetylenes,[21] and more recently even those derived from DNA.[22] Notable early reports included the incorporation of azobenzene dyes as

Received: November 4, 2016
Revised: February 26, 2017
Published: February 27, 2017

DOI: 10.1021/acs.jpcc.6b11110
J. Phys. Chem. C 2017, 121, 6946−6954

Chart 1. Triazine Dendrimers Used in This Study

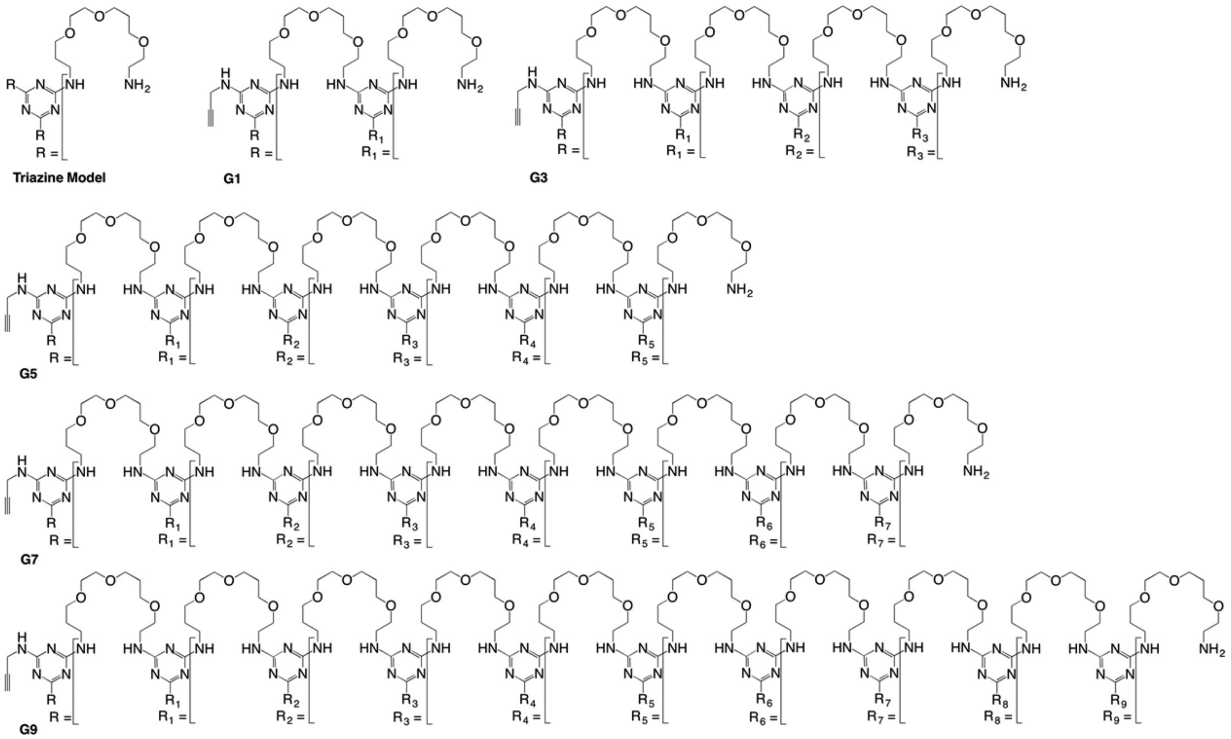

probes of structure[23] and derivatization with photoresponsive groups for light harvesting[24] or imaging applications.[25]

Light has been used to probe structure through the use of solvatochromic probes[26,27] and with dyes including pyrene,[28] Rubipy and fluorescein.[29] In these cases, photoactive groups were explicitly engineered into these structures. To these ends, dendrimers are attractive candidates as the placement of groups can be controlled with synthesis. More recently, however, energies have turned to exploring the intrinsic fluorescence of dendrimers to probe structure and guide function. PAMAM dendrimers have been of notable interest due to their widespread adoption.[30]

Triazine dendrimers have been of particular interest for many years due to their synthetic accessibility and the potential for exquisite control over composition.[31] This control derives from the systematic substitution of the triazine nucleus. When amines are used as nucleophiles, a melamine is the result. Melamine fluorescence has been well studied and used for its detection.[32] However, the intrinsic fluorescence of triazine dendrimers has been ignored. Given the potential of these molecules for applications in both materials science[33] and medicine,[34] a thorough study of these behaviors was undertaken. Herein, we present the first report characterizing spectroscopic and fluorescence properties of triazine dendrimers spanning generations 1 to 9 (Chart 1). The data inform both the structure and dynamic properties of these macromolecules. Specifically, steady state and time-resolved fluorescence were complemented with computational models to reveal the emergence of behaviors (both structural and dynamic) over many different dendrimer generations.

MATERIALS AND METHODS

Spectroscopic Measurements. UV−vis absorption and fluorescence spectra were obtained using an Agilent 60 Bio UV−visible Spectrophotometer and Cary Eclipse Spectrofluorometer (Varian Inc.), respectively. The absorption measurements were done using a custom-designed cuvette with a 4 cm path length and low volume (0.8 mL). The fluorescence measurements of **G1−G9** were done in 0.4 cm × 1 cm cuvettes at room temperature in water. To evaluate the quantum yield, extinction spectra of dendrimers were collected and decomposed to absorption traces and Rayleigh scattering traces to obtain scatter-free absorption spectra. At higher generation, dendrimers are larger particles (up to 10 nm diameter) that significantly scatter light at shorter wavelength range, especially at the UV range. This deconvultion procedure is necessary to obtain true absorption of dendrimer chromophores at any given wavelength. The analysis (see the Supporting Information, SI, for details) was followed by measuring the integrated fluorescence intensity of the sample. A solution of anthranilic acid was used as a quantum yield reference (quantum yield: 0.60) to evaluate quantum yield of various dendrimer generations.[35] Emission spectra were collected using 320 nm excitation and scanning the emission spectrum from 340 to 600 nm. Fluorescence lifetime was measured on a FluoTime 300 Fluorometer (PicoQuant, Inc.) using a 375 nm diode laser. The fluorometer was equipped with an ultrafast microchannel plate photomultiplier detector (MCPPMT) from Hamamatsu, Inc. The fluorescence lifetimes were measured in the magic angle (54.70) condition and data analyzed using FluoFit4 program from PicoQuant, Inc. (Germany) using multiexponential fitting model:

DOI: 10.1021/acs.jpcc.6b11110
J. Phys. Chem. C 2017, 121, 6946−6954

$$I(t) = \sum_i \alpha_i e^{-t/\tau_i} \quad (1)$$

where, α_i is the amplitude of the decay of the i^{th} component at time t and τ_i is the lifetime of the i^{th} component. The intensity weighted average lifetimes (τ_{avg}) were calculated using following equation;

$$\tau_{avg} = \sum_i f_i \tau_i, \quad \text{where } f_i = \frac{\alpha_i \tau_i}{\sum_i \alpha_i \tau_i} \quad (2)$$

Time resolved anisotropy measurements were done with the same FT300 fluorometer (Picoquant GmbH, Germany) using 375 nm excitation diode laser (PicoQuant) operated at 5 MHz repetition rate. The emission was observed at 420 nm supported with long pass 405 nm filter to eliminate any residual sample scattering. The resolution was kept at 4 ps per channel, and the pulse width was less than 100 ps. Fluorescence intensity decays were collected while orienting the emission polarizer in vertical and horizontal position respective to the vertically oriented excitation polarizer for measuring anisotropy decays. The vertical (parallel) and horizontal (perpendicular) intensity decays were used to calculate the time dependent anisotropy using the following:

$$r(t) = \frac{I_{parallel}(t) - I_{perpendicular}(t)}{I_{parallel}(t) + 2I_{perpendicular}(t)} \quad (3)$$

The obtained anisotropy decay was analyzed using Fluofit 4.0 provided by Picoquant GmbH, Germany, and fitted using the following formula:

$$r(t) = \sum r_i e^{-t/\phi_i} \quad (4)$$

where, $r(t)$ is the time-dependent total anisotropy decay, r_i is the fractional anisotropy amplitude associated with i^{th} component, φ_i is the rotational correlation time. Measured anisotropy decays can be fitted with up to four exponential components, but in our case, sufficient quality of the fit was reached already with either one or two components. Particle size was estimated from the recovered rotational correlation times for each dendrimer (see the SI for details). Fluorescence quenching experiments were done by measuring the emission spectra of each dendrimer solution with increasing concentration of potassium iodide (KI) as a quencher.

RESULTS AND DISCUSSION

Design and Synthesis. The triazine dendrimers used in this study have been previously described.[34] Briefly, they are derived from iterative additions of macromonomer, **M**, to the growing dendrimer thus providing two generations per reaction sequence (Table 1). To arrive at the generation 1 dendrimer, **G1**, **M** was reacted with propargyl amine. Deprotection yields the water-soluble tetra-amine. Reaction of **G1** with **M** and deprotection yields **G3** with 16 end groups. Iteration of this two-step protocol yields **G5**, **G7**, and **G9**.

Macromonomer **M** derives from a multistep reaction sequence from commercially available diamine and cyanuric chloride. The chemistry used to provide this critical building block is attractive due to its cost and ease of synthesis for scale up, stability in different environments (pH, polarity) and long shelf life.

Spectral Deconvolution and Rayleigh Scattering Corrections. The extinction spectra of dendrimers **G1**−**G9** are shown in Figure 1. Each spectrum shows a small bump in the region between 300 and 400 nm. Sometimes ignored, the extinction spectrum of each dendrimer is a composite of both absorption and scattering in the sample. With sizes ranging from 1 to 20 nm, **G1**−**G9** demonstrates sizes that would significantly out-scatter light, especially at the UV range. Since this size range is significantly smaller than the wavelength of used light (>300 nm) the scattering should obey Rayleigh's law. Since the absorption of the dendrimer's chromophores starts below 450 nm, the spectral range from 500 to 850 nm represents loss of transmitted light intensity due to out-scattering. This portion of the spectra can be fit to the Rayleigh dependence ($1/\lambda^4$) that in a later step can be extended to shorter wavelengths.

The difference between the measured extinction and predicted (fitted) scattering represents the true absorption for the dendrimer. It is this spectrum that can and should be used for calculations of quantum yield and other parameters. The magnitude of this correction is significant, especially for larger generation dendrimers. An example, **G9**, is shown in Figure 2 to demonstrate that the real absorption after spectral deconvolution is less than half of measured extinction. This procedure also allows dendrimer aggregation to be probed. A

Table 1. Building Blocks of the Triazine Dendrimers Used in This Study, and Parameters for the Theoretical Composition of These Targets and Size Data[a]

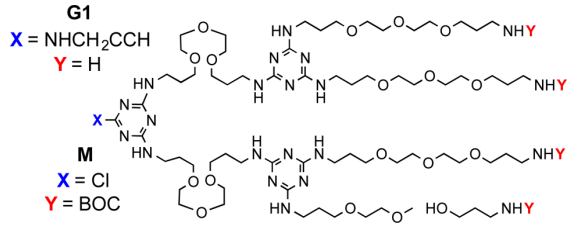

cmpd	triazines	ends	MW[theo]	d^{DLS}	density[b]	density[c]
G1	3	4	1602	na	0.75	0.34
G3	15	16	7790	3.7	0.68	0.29
G5	63	64	33 000	8.0	0.4	0.12
G7	255	256	131 000	13.7	0.37	0.1
G9	1023	1024	528 000	21.4	0.37	0.1

[a]"Triazines" refer to the number of triazine rings in the structure. "Ends" refer to the number of end groups. "MW (Daltons)" is the molecular weight. The diameter from dynamic light scattering, d^{DLS}, is reported in nanometers. Two calculations of density (Daltons/Å^3) are provided. [b]From the radius of gyration. [c]From the hydrodynamic radius. See text for details.

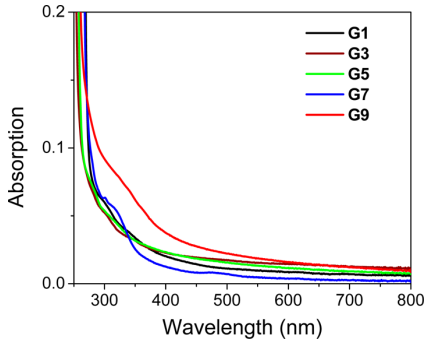

Figure 1. Measured extinction spectrum of dendrimers **G1**−**G9**.

DOI: 10.1021/acs.jpcc.6b11110
J. Phys. Chem. C 2017, 121, 6946−6954

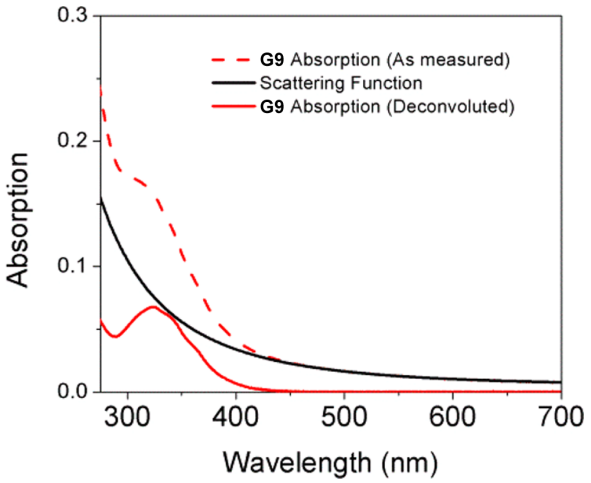

Figure 2. Deconvolution of a measured absorption spectra (**G9**).

poor fit to the Rayleigh dependence in the long wavelength range of the spectrum indicates the presence of larger particles for which the requirement (that $\lambda \gg$ than particle size) does not hold. In such cases, sample dilution and sonication typically improves the fit greatly. All the samples were measured at low concentrations to avoid possible aggregation. In addition, the spectra corrected for scattering match well with measured excitation spectra (shown in Figure 3 and SI), offering additional evidence that deconvolution yields proper dendrimer absorptions. Additional details of the Rayleigh scattering fitting function and the underlying theory are provided in the SI.

Excitation/Emission Spectra. The measured fluorescence emission and excitation spectra of each dendrimer are shown in Figure 3. They reveal that the long wavelength excitation peak varied between 322 and 342 nm while the emission peak changed from 384 to 416 nm.

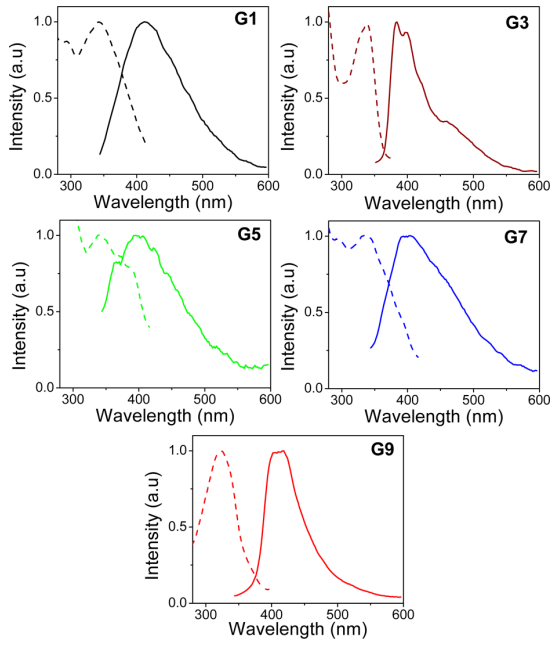

Figure 3. Fluorescence excitation and emission spectra of **G1**−**G9**. Photograph shows the fluorescence of dendrimers under UV light (366 nm) excitation.

Individual peaks for excitation and emission are provided in Table 2. The overlap between excitation and emission changes also. The Stokes shift increases from **G3** to **G9** suggesting an increasing energy gap for excitation and emission with increasing generation of dendrimers. The observation supports the belief that the structure is changing across the series. The fluorescence quantum yields (QY) measured are shown in Table 2 along with radiative (K_r) and nonradiative (K_{nr}) rates. The QY in all cases were less 10%. The K_{nr} which is an indicator of nonradiative/nonfluorescence losses increases up to **G5** and then decreases for **G7** and **G9** corroborating structural changes across the series.

Fluorescence Lifetimes. Fluorescence lifetime measures the average time spent in the excited state by a fluorophore and gives information about the radiative (fluorescence) and nonradiative losses after the excitation event. With the measured intensity decays and quantum yields, radiative and nonradiative deactivation rates can be calculated. Information such as heterogeneity of environments, energy transfer, and quenching can be extracted from such measurements.

Figure 4 shows the fluorescence intensity decays of **G1**−**G9**. Table 3 lists all the parameters derived from fitting the individual intensity decays to a multiexponential model. The need for four exponential components (τ_1−τ_4) to satisfy fit quality indicates the presence of very heterogenic triazine environments within the dendrimers as compared to that of a monomeric chromophore. The lifetime values of τ_1−τ_4 represent four triazine excited state environments; from highly quenched τ_1 to longer lived, well-stabilized species τ_4. Interestingly, the average environments for these populations (for short-lived triazine population, τ_1, for example) seem to be similar across all the generations.

The values α_1−α_4 represent the relative populations of each of these four species (which sum to unity). The picture that emerges from the collected data suggests that a majority of the interactions between triazines (hypothesized now) are fast and fleeting, τ_1 and α_1, respectively, while the long-lived states are less populated, τ_4 and α_4, respectively.

Specifically, the fluorescence lifetimes vary from about 100 ps to over 10 ns. In addition, τ_1 and τ_2 contribute ∼80% in amplitude toward the overall excited state decay in all cases. The intensity weighted contributions of these two, short-lived species (see SI) reveals that they contribute little to the overall fluorescence. The majority of the observed steady state fluorescence intensity is due to the two long lifetime components. We hypothesize that processes like electron transfer between amine groups and triazines, or between triazines, could be at work at a specific distance. The hypothesis that triazines are close together is supported by MD simulations appearing later in the text.

The long lifetime components allow slower dynamics of the dendrimers structure to be monitored by measuring time-resolved anisotropy decays and calculating correlation times for these macromolecules. This is possible because the intensity weighted fractional intensity contribution of α_4 or long lifetime component (τ_4) is more than 25% in total fluorescence intensity (see SI). The average amplitude weighted lifetime, τ_{avg}, dropped from 1.34 ns for **G1** to 0.48 ns for **G5** and then recovered slightly for **G7** and **G9**. This lifetime change from **G1** to **G5** decreases and again from **G5** to **G9** increases suggesting

DOI: 10.1021/acs.jpcc.6b11110
J. Phys. Chem. C 2017, 121, 6946−6954

Table 2. Excitation and Emission Properties of Traizine Dendrimers

sample	exc. peak (nm)	ems. peak (nm)	stokes shift (nm)	quantum yield (%)	K_r (s^{-1}) × 10^{-9}	K_{nr} (s^{-1}) × 10^{-9}
G1	342	412	70	4.1 ± 0.38	0.03	0.72
G3	338	384	46	8.2 ± 0.65	0.12	1.31
G5	342	400	58	3.4 ± 0.30	0.07	2.01
G7	338	400	62	2.8 ± 0.50	0.04	1.38
G9	322	416	94	8.1 ± 0.60	0.11	1.23

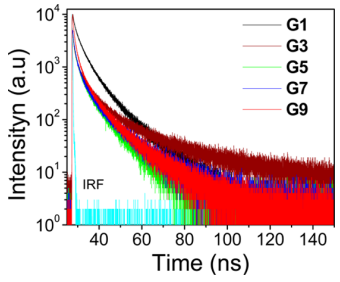

Figure 4. Fluorescence intensity decays of **G1**−**G9**.

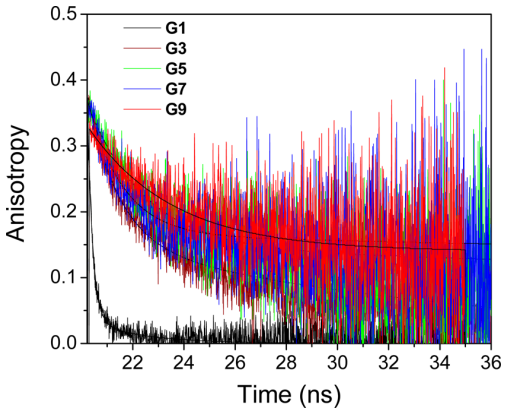

Figure 5. Fluorescence anisotropy decays of **G1**−**G9**.

marked changes in dendrimer structure across different generations. This behavior is consistent with a collapse of structure down to **G5**, and then an expansion and growth to **G9**.

Table 3 also reports the lifetime of a single, trisubstituted triazine. A four-component model was employed to facilitate direct comparisons with the dendrimers. The three peripheral amines in this molecule could lead to interactions (electron transfer) with triazine ring and the appearance of different environments, as could the conformation isomerism provided by hindered rotation around the aromatic-exocyclic amine bond. The fingerprint value most interesting to us is τ_{avg}, which is similar to **G1** and used as a reference to ascertain the change in lifetime going from monomeric unit to higher generation dendrimer. Interestingly, a drop of both the intensity and amplitude averaged lifetimes for **G5** may suggest more compact environment for this macromolecule.

Rotational correlation times corroborate fluorescent lifetime predictions and argue for collapsed, small **G3** and **G5** dendrimers and extended, large **G7** and **G9** dendrimers. The presence of long lifetime components opens the opportunity to further look into slow dendrimer dynamics and rotational correlation times of dendrimers by measuring the time-resolved fluorescence anisotropy decays.

Figure 5 shows the anisotropy decays for **G1**−**G9**. The fitted parameters for these decays are shown in Table 4. The rotational correlation time is the time required for an angular transition moment reorientation (in practice molecule rotation) of 1 rad (~57.30). It becomes apparent that such measurement can be correlated with the molecular rotational diffusion and molecule size/weight given all other parameter such as temperature and viscosity are constant. The recovered rotational correlation times (φ) from the anisotropy decays correlate very well with the increasing molecular weight of dendrimers. Moreover, estimated particle size from anisotropy measurements (Table 4) matches well with the size measured using dynamic light scattering in Table 1.

For **G1**, only one component was required to fit the decay with a measured correlation time of 240 ps due to its small size. However, all other samples needed two components—a fast and slow component—to fit the data. The faster component (φ_1) can be ascribed to the local internal motion of the dendrimer domains/branches, while longer component (φ_2) is due to the global motion/tumbling of entire dendrimer molecule.

In the case of **G3** and **G5**, the majority of the anisotropy is contributed by the longer correlation time component (r_2) suggesting that the triazine groups of these dendrimers are compact/closely packed. Specifically, in the case of **G3** and **G5**, 60% and 71%, respectively, of anisotropy decay is due to the longer correlation time or global motion. This behavior is consistent with the data reported in Table 1, showing that the density of **G3** is higher than that of large generations.

Table 3. Fitting Parameters for the Fluorescence Intensity Decay of G1−G9[a]

type[b]	τ_1 (ns)	τ_2 (ns)	τ_3 (ns)	τ_4 (ns)	α_1	α_2	α_3	α_4	τ avg amp (ns)	τ avg int (ns)	χ^2
triazine	0.12	0.75	3.00	7.80	0.39	0.36	0.20	0.05	1.32	3.90	0.94
G1	0.09	0.84	3.40	11.2	0.58	0.19	0.18	0.04	1.34	6.00	0.95
G3	0.09	0.75	3.60	14.5	0.72	0.20	0.07	0.01	0.70	5.30	1.01
G5	0.07	0.55	2.40	8.40	0.73	0.17	0.08	0.02	0.48	3.55	1.02
G7	0.10	0.70	2.80	10.0	0.67	0.21	0.10	0.02	0.70	4.12	1.15
G9	0.12	0.76	3.20	12.3	0.65	0.25	0.09	0.01	0.75	4.70	0.96

[a] τ_1, τ_2, τ_3, and τ_4 are lifetime components, α_1, α_2, α_3, and α_4 are respective amplitudes, χ^2 is chi square value. [b] The triazine sample was measured in dichloromethane (DCM) and **G1**−**G9** were measured in DI water.

DOI: 10.1021/acs.jpcc.6b11110
J. Phys. Chem. C 2017, 121, 6946−6954

Table 4. Fitted Parameters for Anisotropy Decays of G1−G9[a]

sample	r_0	r_1	r_2	ϕ_1 (ns)	ϕ_2 (ns)	χ^2	SS r	size diameter (nm)
triazine	0.24	0.24		0.26 ± 0.01		1.18	0.020	NA
G1	0.30	0.30		0.24 ± 0.02		1.20	0.015	1.23 ± 0.22
G3	0.35	0.14	0.21	0.81 ± 0.05	5.90 ± 0.34	2.60	0.15	3.60 ± 0.27
G5	0.38	0.11	0.27	1.30 ± 0.17	15.00 ± 1.7	2.60	0.24	5.00 ± 1.18
G7	0.36	0.22	0.14	1.70 ± 0.22	654 ± NA	3.10	0.20	17.20 ± NA
G9	0.33	0.18	0.14	3.40 ± 0.38	1000 ± NA	2.24	0.22	19.88 ± NA

[a]The r_0 anisotropy at zero time, r_1 and r_2 are anisotropy components, ϕ_1 and ϕ_2 are rotational correlation times in picoseconds, χ^2 is chi square value, SS r is steady state anisotropy.

However, in the case of **G7** and **G9**, the short component (r_1) contributes more to the total anisotropy suggesting the slightly relaxed nature of these dendrimer which allows greater mobility of dendrimer domains/branches. The long correlation components for **G3** and **G5** of 5.9 and 15 ns, respectively, correlate very well with overall molecule masses of 7.8 kDa and 33 kDa. It is important to note that the longer components for **G7** and **G9** do not have standard error values due to the uncertainty in determining the precise correlation time. This shortcoming is due to the significantly longer correlation times as compared to the fluorescence lifetimes ($\varphi \gg \tau$). In effect there are no photons/signal left after complete decay of the fluorescence (in this case about 50 ns after the excitation pulse).

Collected Evidence for a Structural Transition at G5. Multiple lines of evidence point to a structural change at **G5**. The steady state anisotropy (SS r) quickly increases from **G1** to **G5** from 0.015 to 0.24, and then slightly drops for **G7** and **G9** in spite of much larger overall size. Similarly, the anisotropy at time zero (r_0) increases from 0.3 for **G1** to 0.38 for **G5** again suggesting very compact structure of **G5** with immobilized chromophores. The anisotropy measurements show progressive initial anisotropy (r_0) increase from **G1** to **G5** then drop for **G7** and further drop for **G9**. The initial, significant increase of r_0 and steady state anisotropy from **G1** to **G5** following slight lowering of r_0 and steady state anisotropy for **G7** and **G9** clearly indicate internal structural changes that allow for more internal mobility in the larger generation dendrimers.

Quenching by KI as a Probe of Structure. One elegant way for probing the porosity of the macromolecule is to use a small molecule quencher that can diffuse to the chromophore through the macromolecular structure.[36] To test different generations of dendrimers we used well-known quencher KI, which works through a charge transfer mechanism.[37] Figure 6 shows the results of KI quenching. The left panel shows the Stern−Volmer plots for the dendrimers while the right panel shows the percent quenching of each generation after treating with 200 mM of KI. Dendrimer **G1** was quenched about 90%, a value consistent with the behavior of a flexible small molecule that is exposed to KI. However, quenching decreases for **G3** and **G5**, attributed to reduced accessibility to internal triazines consistent with the collapsed/compact structure predicted earlier from lifetime and anisotropy data.

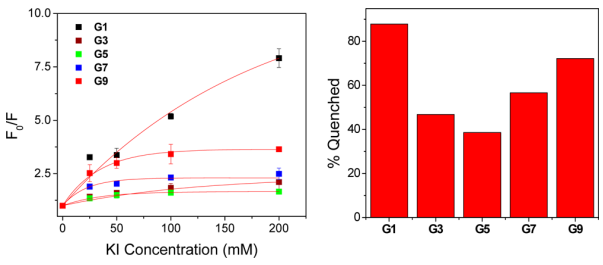

Figure 6. Stern−Volmer plots for dendrimer quenching in terms of recorded intensities (left) and percent quenching (right) of each dendrimer sample using 200 mM KI (n = 3).

The quenching efficiency of KI increases for **G7** and **G9**. This behavior is consistent with an extended conformation predicted for these larger generation molecules. This enhanced quenching may be due to the greater availability of larger numbers of triazines on surface or better accessibility of KI to the interior of the dendrimer. The computational analysis which follows corroborates the inferences drawn from the lifetime, anisotropy and KI quenching measurements.

***In Silico* Characterization of Dendrimers in Solution.** We have used all-atom molecular dynamics (MD) simulations to model the different generations of dendrimers in solution (Figure 7). The creation of the dendrimer models and the simulation procedure followed the same procedures previously reported for the computational study of dendrimers in solution.[38,39] Dendrimers **G1−G9** were immersed in a simulation box filled of explicit TIP3P[40] water molecules and 150 mM NaCl. The dendrimer structures were simulated for 200 ns of MD in NPT periodic boundary conditions using AMBER 12.[41] Complete detail of the modeled systems and of simulation protocol is available in the SI.

During the MD runs, **G1** and **G3** assume a globular-like configuration with a dense core and flexible surface. **G5** behaves similarly, albeit this dendrimer appears to be less spherical and more heterogeneous upon collapse. In contrast, **G7** and **G9** remain porous and open to the penetration of solvent (Figure 7a). This behavior is likely due to the effect of electrostatic repulsion of the peripheral groups. At neutral pH, the terminal amino groups of the dendrimers are assumed to be protonated, and electrostatic repulsion between the branches increases together with the generation.

The radial distribution functions ($g(r)$) shown in Figure 7c provide information on the relative probability for finding dendrimer's atoms as a function of the distance from the dendrimer's center. The $g(r)$ data clearly shows that while smaller generations (i.e., **G1**) have a relatively higher dense core (high $g(r)$ peaks at short distance from the dendrimer's center) and flexible surface, **G9** has much denser surface and less dense core. This calculation is consistent with the comparison between the radii of gyration (R_g) obtained from the MD simulations with the hydrodynamic radius (R_h) obtained from DLS (see Table 1). In fact, while for a sphere of uniform density a R_h/R_g ratio of ∼1.3 is expected, the R_h/R_g ratio is known to increase for fractal structures having surface denser than the interior.[42,43]

DOI: 10.1021/acs.jpcc.6b11110
J. Phys. Chem. C 2017, 121, 6946−6954

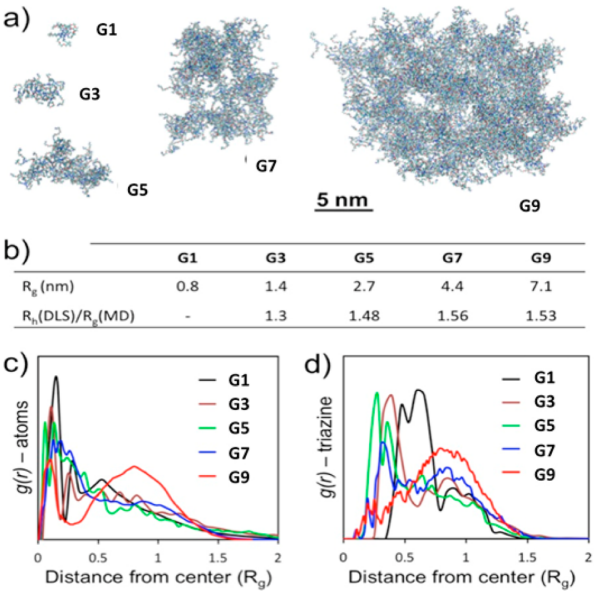

Figure 7. MD structural characterization. (a) Equilibrated structures for the dendrimers in aqueous solution. (b) Radii of gyration (R_g, in nm) for the dendrimers in solution extracted from the MD simulations, and R_h(DLS)/R_g(MD) ratios. A sphere has typical $R_h/R_g \approx 1.3$, while R_h/R_g increases when the mass density is uniform in the sphere, and higher close to the surface. (c,d) Radial distribution functions ($g(r)$) of the dendrimer's atoms (c) and of the triazine groups (d) with respect to the dendrimers's centers. Distances are reported in R_g units to facilitate comparison between different size dendrimers.

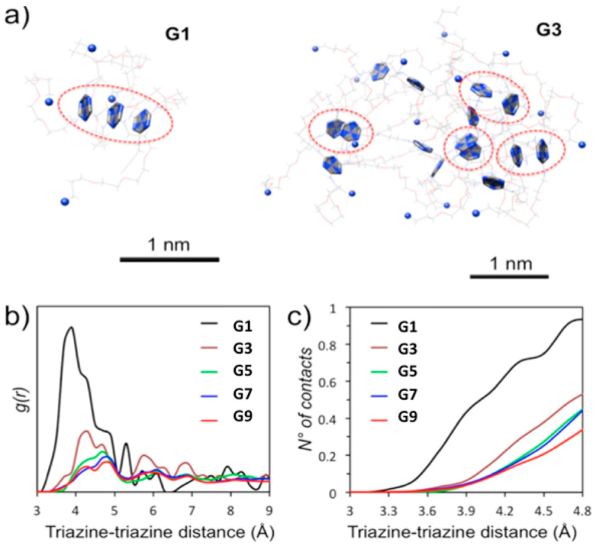

Figure 8. Triazine interactions in the dendrimers. (a) Details of triazine–triazine interactions (red dotted ovals) in the equilibrated configurations of **G1** and **G3** (final MD snapshots). (b) Radial distribution functions ($g(r)$) of the triazines with respect to themselves as a function of the distance: High peaks at short distance are indicators of persistent triazine–triazine interaction. (c) Average number of triazine neighbors as a function of the distance from the triazines in the different dendrimers.

Moreover, Figure 7d shows the $g(r)$ for the triazine groups as a function of the distance from the center, providing an indication of the relative probability for finding triazine groups in different regions of the dendrimers. For **G9**, triazines are more densely located at the proximity of the surface ($g(r)$ peak close to R_g). While **G7** shows relatively high probability for finding triazines close to the surface, these are more densely packed in the interior in the case of **G3** and **G5**, which is well consistent with the quenching results discussed above. G1 shows intermediate behavior. However, this dendrimer is so small and dynamic that triazines can be in contact with the external solvent even when located close to the center.

Computational Models Reveal Triazine–Triazine Interactions. From the MD simulations, the extent of triazine–triazine interactions in the different dendrimer scaffolds can be quantified. Figure 8a shows ordered triazine aggregates observed in models of **G1** and **G3** during the MD runs. Similar experimental results were obtained by other groups using naphthalene labeled dendrimer where naphthalene interaction led to excimers.[43] These are dynamically formed and more or less stable/persistent during the simulation.

The $g(r)$ of the triazines (calculated respect to themselves) provides a quantification of the persistence of triazine–triazine interactions. In fact, high $g(r)$ peaks at short-range are indicators of relatively stable interaction between the triazines (hydrophobic, aromatic).[44] Shown in Figure 8b, evidence of a persistent triazine–triazine interaction is present only in the case of **G1**. In fact, Figure 8c (the number of triazine–triazine contacts as a function of intertriazine distance) shows that in the smaller dendrimers each triazine has on average one triazine neighbor at short distance (<5 Å) during the MD. On the other hand, this number readily decreases for increasing generations.

CONCLUSIONS

The intrinsic fluorescence of triazine dendrimers provides an opportunity to probe structure in the absence of external labels. The picture that emerges from numerous lines of evidence is that structural collapse continues to **G5** after which the dendrimers **G7** and **G9** appear to be extended porous structures. The large size of these architectures leads to significant contributions of Rayleigh scattering to the measured extinction spectra with strong out-scattering of transmitted light in the UV spectral range. The recovered absorption spectra after subtracting Rayleigh scattering correlate well with measured fluorescence excitation spectra. The deconvolution procedure offers an additional probe for the presence of dendrimer aggregates.

More specifically, the intrinsic fluorescence of triazine dendrimers presents complex intensity decays with fluorescence lifetimes spreading from 10 ps to over 10 ns. The significant presence of very long lifetime components opens new possibilities for studying molecular dynamics of dendrimer molecules up to the **G9** generation. Fluorescence intensity and anisotropy decays clearly indicate conformational rearrangements yielding increasingly compact structures when going from **G1** to **G5** and significant structural relaxation when increasing to **G7** and then **G9**. These experimental finding are confirmed with theoretical molecular dynamics simulations.

ASSOCIATED CONTENT

Supporting Information

The Supporting Information is available free of charge on the ACS Publications website at DOI: 10.1021/acs.jpcc.6b11110.

DOI: 10.1021/acs.jpcc.6b11110
J. Phys. Chem. C 2017, 121, 6946–6954

Spectra and experimental details for fluorescence and computational efforts (PDF)

AUTHOR INFORMATION

Corresponding Authors

*E-mail: giovanni.pavan@supsi.ch (G.M.P.).
*E-mail: e.simanek@tcu.edu (E.E.S.).
*E-mail: z.gryczynski@tcu.edu (Z.G.).

ORCID

Giovanni M. Pavan: 0000-0002-3473-8471
Eric E. Simanek: 0000-0002-3195-4523

Author Contributions

The manuscript was written through contributions of all authors. All authors have given approval to the final version of the manuscript.

Notes

The authors declare no competing financial interest.

ACKNOWLEDGMENTS

We thank the Robert A. Welch Foundation (P-0008), the National Institutes of Health (R01EB12003; R01CA159144), and the DOD (W81XWH-12-1-0338) for support.

REFERENCES

(1) Schultz, C. Fluorescent revelations. *Chem. Biol.* **2009**, *16*, 107−111.
(2) Davidson, M. W.; Campbell, R. E. Engineered fluorescent proteins: innovations and applications. *Nat. Methods* **2009**, *6*, 713−717.
(3) Royer, C. *A.* Probing protein folding and conformational transitions with fluorescence. *Chem. Rev.* **2006**, *106*, 1769−1784.
(4) Schlick, K. H.; Lange, C. K.; Gillispie, G. D.; Cloninger, M. J. Characterization of protein aggregation via intrinsic fluorescence lifetime. *J. Am. Chem. Soc.* **2009**, *131*, 16608−16609.
(5) Vivian, J. T.; Callis, P. R. Mechanisms of tryptophan fluorescence shifts in proteins. *Biophys. J.* **2001**, *80*, 2093−2109.
(6) Tomalia, D.; Huang, B.; Swanson, D.; Brothers, H.; Klimash. Structure control within poly (amidoamine) dendrimers: size, shape and regio-chemical mimicry of globular proteins. *Tetrahedron* **2003**, *59*, 3799−3813.
(7) Tomalia, D. A.; Christensen, J. B.; Boas, U. In *Dendrimers, Dendrons, And Dendritic Polymers: Discovery, Applications, And the Future*; Cambridge University Press: Cambridge, 2012.
(8) Jang, W.-D.; Kamruzzaman Selim, K. M.; Lee, C.; Kang, I. Bioinspired application of dendrimers: from bio-mimicry to biomedical applications. *Prog. Polym. Sci.* **2009**, *34*, 1−23.
(9) Tomalia, D. A.; Baker, H.; Dewald, J.; Hall, M.; Kallos, G.; Martin, S.; Roeck, J.; Ryder, J.; Smith, P. A new class of polymers: starburst-dendritic macromolecules. *Polym. J.* **1985**, *17*, 117−132.
(10) Newkome, G. R.; Yao, Z.; Baker, G. R.; Gupta, V. K. Micelles. Part 1. Cascade molecules: a new approach to micelles. A [27]-arborol. *J. Org. Chem.* **1985**, *50*, 2003−2004.
(11) Buhleier, E.; Vögtle, F. Überbrückung des anthrachinons in 1,8-stellung. *Chem. Ber.* **1978**, *111*, 2729−2731.
(12) Caminade, A.; Turrin, C.; Laurent, R.; Ouali, A.; Delavaux-Nicot, B. In *Dendrimers: Towards Catalytic, Material and Biomedical Uses*; John Wiley & Sons: New York, 2011.
(13) Tomalia, D. A.; Cheng, Y. In *Dendrimer-Based Drug Delivery Systems: From Theory to Practice*; John Wiley & Sons: New York, 2012; Vol. *18*.
(14) Astruc, D.; Boisselier, E.; Ornelas, C. Dendrimers designed for functions: from physical, photophysical, and supramolecular properties to applications in sensing, catalysis, molecular electronics, photonics, and nanomedicine. *Chem. Rev.* **2010**, *110*, 1857−1959.
(15) Lo, S.; Burn, P. L. Development of dendrimers: macromolecules for use in organic light-emitting diodes and solar cells. *Chem. Rev.* **2007**, *107*, 1097−1116.
(16) Wang, D.; Imae, T. Fluorescence emission from dendrimers and its pH dependence. *J. Am. Chem. Soc.* **2004**, *126*, 13204−13205.
(17) Restani, R. B.; Morgado, P. I.; Ribeiro, M. P.; Correia, I. J.; Aguiar-Ricardo, A.; Bonifácio, V. D. Biocompatible polyurea dendrimers with pH-dependent fluorescence. *Angew. Chem., Int. Ed.* **2012**, *51*, 5162−5165.
(18) Liu, D.; De Feyter, S.; Cotlet, M.; Stefan, A.; Wiesler, U.; Herrmann, A.; Grebel-Koehler, D.; Qu, J.; Müllen, K.; De Schryver, F. C. Fluorescence and intramolecular energy transfer in polyphenylene dendrimers. *Macromolecules* **2003**, *36*, 5918−5925.
(19) Tabuchi, M.; Momotake, A.; Kanna, Y.; Nishimura, Y.; Arai, T. Extremely efficient and long lifetime fluorescence of cis-stilbene contained in a rigid dendrimer. *Photochem. Photobiol. Sci.* **2011**, *10*, 1521−1523.
(20) Majoral, J.; Caminade, A. Dendrimers containing heteroatoms (si, p, B, ge, or bi). *Chem. Rev.* **1999**, *99*, 845−880.
(21) Feng, F.; Lee, S. H.; Cho, S. W.; Kömürlü, S.; McCarley, T. D.; Roitberg, A.; Kleiman, V. D.; Schanze, K. S. Conjugated polyelectrolyte dendrimers: aggregation, photophysics, and amplified quenching. *Langmuir* **2012**, *28*, 16679−16691.
(22) Xuan, F.; Hsing, I. Triggering hairpin-free chain-branching growth of fluorescent DNA dendrimers for nonlinear hybridization chain reaction. *J. Am. Chem. Soc.* **2014**, *136*, 9810−9813.
(23) Junge, D. M.; McGrath, D. V. Photoresponsive dendrimers. *Chem. Commun.* **1997**, 857−858.
(24) Koskela, J. E.; Liljeström, V.; Lim, J.; Simanek, E. E.; Ras, R. H.; Priimagi, A.; Kostiainen, M. A. Light-fuelled transport of large dendrimers and proteins. *J. Am. Chem. Soc.* **2014**, *136*, 6850−6853.
(25) Esipova, T. V.; Ye, X.; Collins, J. E.; Sakadzic, S.; Mandeville, E. T.; Murray, C. B.; Vinogradov, S. A. Dendritic upconverting nanoparticles enable in vivo multiphoton microscopy with low-power continuous wave sources. *Proc. Natl. Acad. Sci. U. S. A.* **2012**, *109*, 20826−20831.
(26) Pistolis, G.; Malliaris, A.; Paleos, C.; Tsiourvas, D. Study of poly (amidoamine) starburst dendrimers by fluorescence probing. *Langmuir* **1997**, *13*, 5870−5875.
(27) Hawker, C. J.; Wooley, K. L.; Frechet, J. M. Solvatochromism as a probe of the microenvironment in dendritic polyethers: transition from an extended to a globular structure. *J. Am. Chem. Soc.* **1993**, *115*, 4375−4376.
(28) Sideratou, Z.; Tsiourvas, D.; Paleos, C. Quaternized poly (propylene imine) dendrimers as novel pH-sensitive controlled-release systems. *Langmuir* **2000**, *16*, 1766−1769.
(29) Jockusch, S.; Ramirez, J.; Sanghvi, K.; Nociti, R.; Turro, N. J.; Tomalia, D. A. Comparison of nitrogen core and ethylenediamine core starburst dendrimers through photochemical and spectroscopic probes. *Macromolecules* **1999**, *32*, 4419−4423.
(30) Larson, C. L.; Tucker, S. A. Intrinsic fluorescence of carboxylate-terminated polyamido amine dendrimers. *Appl. Spectrosc.* **2001**, *55*, 679−683.
(31) Lim, J.; Simanek, E. E. Triazine dendrimers as drug delivery systems: From synthesis to therapy. *Adv. Drug Delivery Rev.* **2012**, *64*, 826−835.
(32) Yang, C.; Liu, Y.; Li, L.; Zhang, F. Studying on the steady-state and time-resolved fluorescence characteristics of melamine. *Spectrochim. Acta, Part A* **2010**, *75*, 1329−1332.
(33) Lim, J.; Pavan, G. M.; Annunziata, O.; Simanek, E. E. Experimental and computational evidence for an inversion in guest capacity in high-generation triazine dendrimer hosts. *J. Am. Chem. Soc.* **2012**, *134*, 1942−1945.
(34) Lim, J.; Kostiainen, M.; Maly, J.; da Costa, V. C.; Annunziata, O.; Pavan, G. M.; Simanek, E. E. Synthesis of large dendrimers with the dimensions of small viruses. *J. Am. Chem. Soc.* **2013**, *135*, 4660−4663.
(35) Raut, S.; Heck, A.; Vishwanatha, J.; Sarkar, P.; Mody, A.; Luchowski, R.; Gryczynski, Z.; Gryczynski, I. Fluorescent properties of

DOI: 10.1021/acs.jpcc.6b11110
J. Phys. Chem. C 2017, 121, 6946−6954

antioxidant cysteine ABZ analogue. *J. Photochem. Photobiol., B* **2011**, *102*, 241−245.
(36) Eftink, M. R.; Ghiron, C. A. Fluorescence quenching studies with proteins. *Anal. Biochem.* **1981**, *114*, 199−227.
(37) Pownall, H. J.; Smith, L. C. Fluorescence quenching of anthracene in charged micelles by pyridinium and iodide ions. *Biochemistry* **1974**, *13*, 2594−2597.
(38) Enciso, A. E.; Garzoni, M.; Pavan, G. M.; Simanek, E. E. Influence of linker groups on the solubility of triazine dendrimers. *New J. Chem.* **2015**, *39*, 1247−1252.
(39) Caminade, A. M.; Fruchon, S.; Turrin, C. O.; Poupot, M.; Ouali, A.; Maraval, A.; Garzoni, M.; Maly, M.; Furer, V.; Kovalenko, V.; Majoral, J. P.; Pavan, G. M.; Poupot, R. The key role of the scaffold on the efficiency of dendrimer nanodrugs. *Nat. Commun.* **2015**, *6*, 7722.
(40) Jorgensen, L.; Chandrasekhar, J.; Madura, J. D.; Impey, R. W.; Klein, M. L. Comparison of simple potential functions for simulating liquid water. *J. Chem. Phys.* **1983**, *79*, 926−935.
(41) Case, D.; Darden, T.; Cheatham, T.; Simmerling, C.; Wang, J.; Duke, R.; Luo, R.; Walker, R.; Zhang, W.; Merz, K. *AMBER 12*; University of California: San Francisco, 2012.
(42) Van Saarloos, W. On the hydrodynamic radius of fractal aggregates. *Phys. A* **1987**, *147*, 280−296.
(43) Ghaddar, T. H.; Whitesell, J. K.; Fox, M. A. Excimer formation in a naphthalene-labeled dendrimer. *J. Phys. Chem. B* **2001**, *105*, 8729−8731.
(44) Munkhbat, O.; Garzoni, M.; Raghupathi, K. R.; Pavan, G. M.; Thayumanavan, S. Role of aromatic interactions in temperature-sensitive amphiphilic supramolecular assemblies. *Langmuir* **2016**, *32*, 2874−2881.

DOI: 10.1021/acs.jpcc.6b11110
J. Phys. Chem. C 2017, 121, 6946−6954

Nanoscale

PAPER

View Article Online
View Journal | View Issue

Cite this: *Nanoscale*, 2017, **9**, 3128

Facile synthesis of stable, water soluble, dendron-coated gold nanoparticles†

Alan E. Enciso,[a] Giovanni Doni,[b] Riccardo Nifosì,[c] Ferruccio Palazzesi,[d,e] Roberto Gonzalez,[a] Amy A. Ellsworth,[f] Jeffery L. Coffer,[a] Amy V. Walker,[f,g] Giovanni M. Pavan,[h] Ahmed A. Mohamed[a,i] and Eric E. Simanek[a]

Received 15th December 2016,
Accepted 29th January 2017

DOI: 10.1039/c6nr09679d

rsc.li/nanoscale

Upon reduction with sodium borohydride, diazonium tetrachloroaurate salts of triazine dendrons yield dendron-coated gold nanoparticles connected by a gold–carbon bond. These robust nanoparticles are stable in water and toluene solutions for longer than one year and present surface groups that can be reacted to change surface chemistry and manipulate solubility. Molecular modeling was used to provide insight on the hydration of the nanoparticles and their observed solubilties.

Motivated by applications in biomedical[1] and materials[2] sciences, modifications to the organic layer surrounding metal nanoparticles have focused on improving stability and increasing functional complexity.[3] Originally, citrate or surfactants like CTAB (cetyl trimethylammonium bromide) passivated the surface of gold nanoparticles (AuNPs), but the desire for increased stability led to the emergence of thiol-terminated organics.[4] The structure of these organics evolved from simple hydrocarbons to those bearing functional ligands and drugs including paclitaxel,[5] oxaliplatin,[6] and doxorubicin.[7] Installation of these functionalities relies primarily on either synthetic manipulation of a reactive AuNP surface[5] or ligand exchange with the passivating groups of the AuNP.[6,7]

Significant advances have been made by dissecting the challenge into that of stability[8] and functionalization of organics decorating nanoparticles. For example, strategies to increase the versatility of these scaffolds and orthogonality for suitable post-preparative conjugation with bioactive molecules have led to the creation of water soluble AuNPs with clickable linkages[9] or maleamides.[10] These constructs have been prepared by multiple routes including retro-Diels–Alder chemistry.[11] Research efforts in this area have resulted in commercially available products.[12] Still, other strategies for derivatization of the nanoparticle surface are being pursued. Notable amongst them are the use of covalent Au–C bonds. The groups of Crudden and Johnson have both described the use of carbene ligands.[13] Johnson has shown that these ligands can be subjected to ROMP-chemistry, while Crudden installs azides amenable to click chemistry.

Reduction of diazonium tetrachloroaurate salts offers an alternative strategy to carbenes,[14] and indeed these reductive strategies prove quite general for functionalization of species besides metal nanoparticles. For example Tour and coworkers use these methods to derivatize single walled carbon nanotubes.[15] The construction of nanoparticles with a Au–C linked organic shell using this strategy has been limited to simple organic molecules including perfluoro-octyl benzene,[14] nitrobenzene,[14] and phenylnitrile.[14] Only recently have large organics been appended. In pioneering efforts using macromolecules, Kumar and Gopidas successfully installed Frechet-dendrons (G1–G4) on AuNPs to arrive at materials soluble in toluene.[16] The route relied on the use of TOAB (tetraoctylammonium bromide) in a surfactant-mediated AuNP synthesis and subsequent ligand exchange with the reduced diazonium species. Reduced dependence on additives, improved water solubility and the increased ease of functionalization of the organic coating serve as metrics to measure future efforts. Inspired by these challenges, we describe a strategy that incorporates dendritic molecules that are amenable to functionalization to provide water-soluble AuNPs.

The synthetic strategy shown in Scheme 1 relies on a one-pot reaction and facile purification. Dendrons of varying gen-

[a]*Department of Chemistry, Texas Christian University, Fort Worth, TX 76109, USA*
[b]*Department of Physics, King's College, London Strand, London WC2R 2NS, UK*
[c]*NEST, Istituto Nanoscienze-CNR and Scuola Normale Superiore, Pisa, Italy*
[d]*Department of Chemistry and Applied Biosciences, Eidgenössische Technische Hochschule Zürich, CH-8093 Zurich, Switzerland*
[e]*Facoltá di Informatica, Istituto di Scienze Computazionali, Universitá della Svizzera Italiana, CH-6900 Lugano, Switzerland*
[f]*Department of Chemistry and Biochemistry, University of Texas at Dallas, Richardson, TX, 75080, USA*
[g]*Department of Materials Science and Engineering, University of Texas at Dallas, Richardson, TX, 75080, USA*
[h]*Department of Innovative Technologies, University of Applied Sciences and Arts of Southern Switzerland, Galleria 2, Via Cantonale 2c, CH-6928 Manno, Switzerland*
[i]*Department of Chemistry, University of Sharjah, Sharjah, United Arab Emirates*

† Electronic supplementary information (ESI) available: Synthetic and computational methods, spectra, 70 pages. See DOI: 10.1039/c6nr09679d

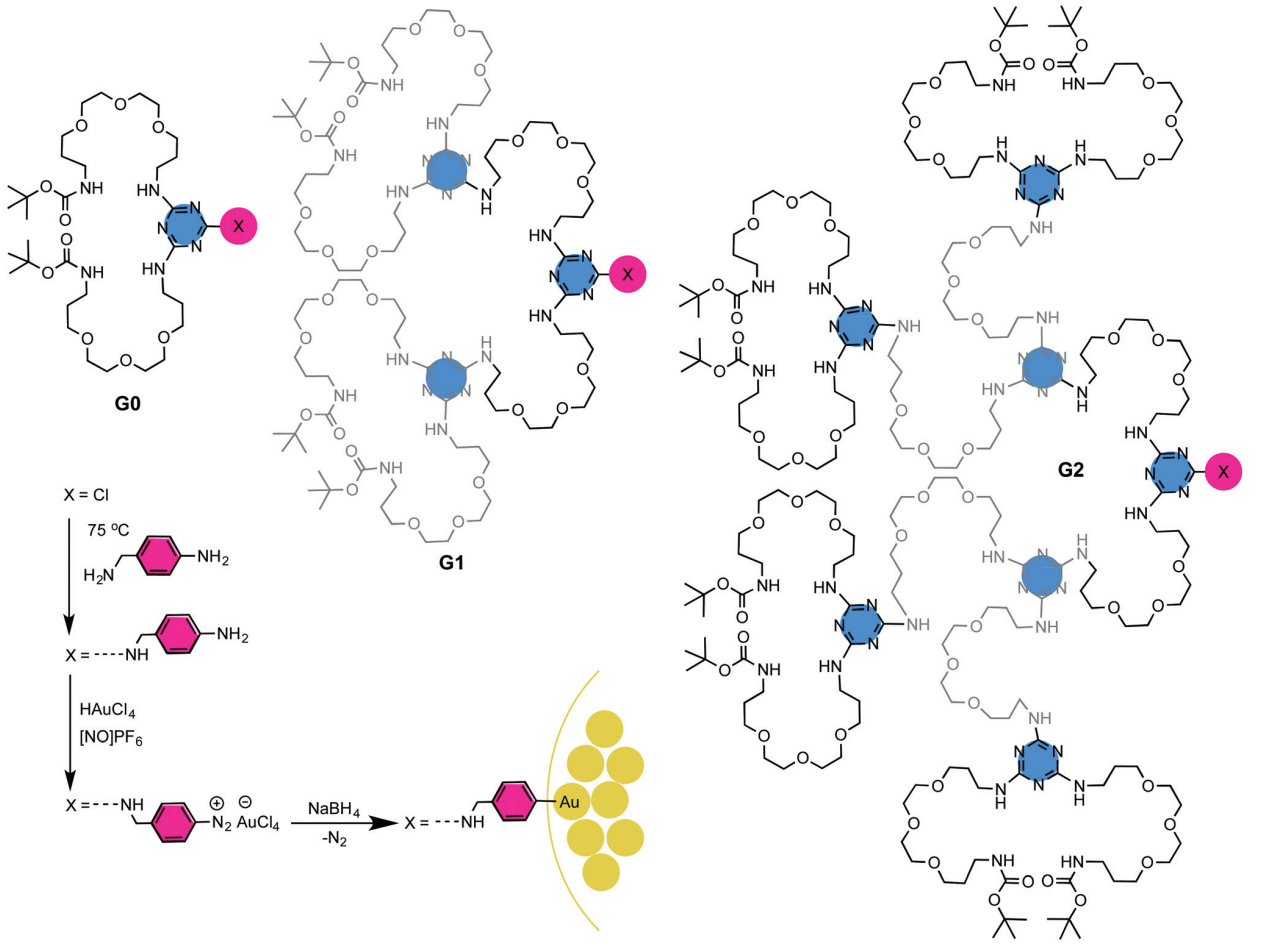

Scheme 1 Dendrimers used in this study (**G0**–**G2**) and the synthetic route adopted. For clarity, the bond and atom labels for the zero and second layers appear in black, bonds and atom labels for the first layer appear in dark gray.

eration with an aniline focus are protonated with tetrachloroauric acid before oxidation to the diazonium salt with nitrosonium hexafluorophosphate. Following precipitation with ether and resuspension in acetonitrile, treatment of the resulting mixture with sodium borohydride yields the desired nanoparticles.

The dendrons are readily available from commercially available reagents.[17] To promote AuNP solubility in organic solvents and aqueous solutions, triazines are linked with the hydrophilic and flexible 4,7,10-trioxa-1,14-tridecanediamine groups. The last step of the synthesis installs the aniline group through selective substitution of the monochlorotriazine by the benzylic amine of *p*-aminobenzylamine. Starting from the mono-BOC protected diamine, the G0, G1 and G2 dendrons are available in 2,4, and 6 steps in 83%, 83% and 80% overall yields, respectively.

Formation of the diazonium salt from the aniline can be monitored by NMR spectroscopy with the expected downfield shift of the aromatic protons (approximately ~1.4 ppm)[18] as well as carbon lines. Corroborating data from FTIR spectroscopy shows the appearance of an N≡N stretch at 2279 cm^{-1}. A 1 : 1 ratio of $HAuCl_4$ and aniline is employed in the conversion. The ^1H NMR reveals partial deprotection of the BOC-groups which is most pronounced for G0 and decreases to G2. Formation of the diazonium salt produces a color change: the off-white aniline yields a light maroon solid upon reaction. This observation is consistent with other reports.[16]

Upon addition of $NaBH_4$, the solution derived from G0 turns deep purple while those derived from G1 and G2 turn ruby red with absorption maxima at 533 nm, 517 nm, and 515 nm, respectively (Fig. 1). The absorption spectra are provided (ESI Fig. 32, 34 and 36†). The nanoparticles are isolated by filtration and washed with acetonitrile. Of note, the method adopted for synthesis has not been successful when water is used instead of acetonitrile.[14] NMR analysis shows evidence for the presence of dendrimer with signals assignable to the flexible, hydrophilic linker and BOC groups. Consistent with other reports, the signals of the aromatic linking region are not observed.[16]

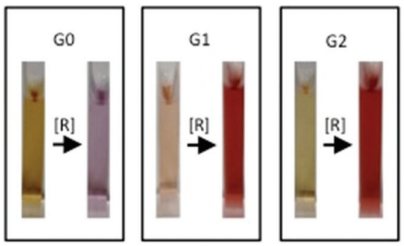

Fig. 1 Photographs of G0, G1 and G2 and the products of reduction [R], G0@Au, G1@Au and G2@Au.

The initial nanoparticles produced—G0@Au, G1@Au, and G2@Au—show different solubility behavior that reflects the state of end group derivatization: that is, BOC groups are lost during preparation of the nanoparticles. The extent of this loss is reflected in the solubility of these materials in either water or toluene. When added to a biphasic mixture of toluene and water, G0@Au migrates to the aqueous phase while G1@Au and G2@Au migrate to the organic phase. The 1 : 1 ratio of tetrachloroauric acid to dendron led to almost complete deprotection of the two BOC groups during the synthesis of G0@Au based on analysis by ^{1}H NMR. Reduced levels of deprotection are seen with G1@Au and G2@Au.

The state of protection/deprotection can be manipulated with synthesis. Treatment of G0@Au with BOC-anhydride led to a product that partitioned into the toluene phase. Indeed, no effort was made to find conditions to control deprotection as it is straightforward to remedy the problem. Treatment of G1@Au and G2@Au with trifluoroacetic acid led to products that partitioned into water. The relative solubilities of the amine-terminated G0@Au, G1@Au and G2@Au in water showed no clear trend. G1@Au was most soluble in water. G1@Au can be dried and subsequently redissolved. Upon drying either G0@Au or G2@Au, neither of these materials can be redissolved in water. Computation was used to further investigate these solubility differences (*vide infra*).

To provide a preliminary assessment of stability, samples of nanoparticles were heated in acetonitrile for 30 minutes at 70 °C with stirring, sonicated for 20 minutes, or centrifuged for 20 minutes at 4000 rpm. Using absorption spectroscopy and monitoring signal between 750 nm and 900 nm as a reporter of aggregation, both heating and sonication had pronounced affects on G0@Au wherein increased aggregation was observed. These affects were markedly diminished for G1@Au, and not observed for G2@Au. After initial isolation, centrifugation does not lead to additional loss of signal in either G0@Au or G1@Au.

Transmission electron microscopy provides a size distribution for G0@Au, G1@Au and G2@Au (Table 1). The two larger dendrons yield smaller gold nanoparticles. The images are presented in Fig. 2. These particles were stored in acetonitrile at 4 °C for one year before resubjecting them to TEM analysis. No appreciable difference is observed in size before and after this storage period.

Table 1 TEM analysis of nanoparticle size (nm)

Time	G0@Au	G1@Au	G2@Au
Fresh	10.3 ± 3.6	6.4 ± 1.4	7.7 ± 1.9
Aged	9.8 ± 3.4	7.1 ± 1.8	7.8 ± 2.0

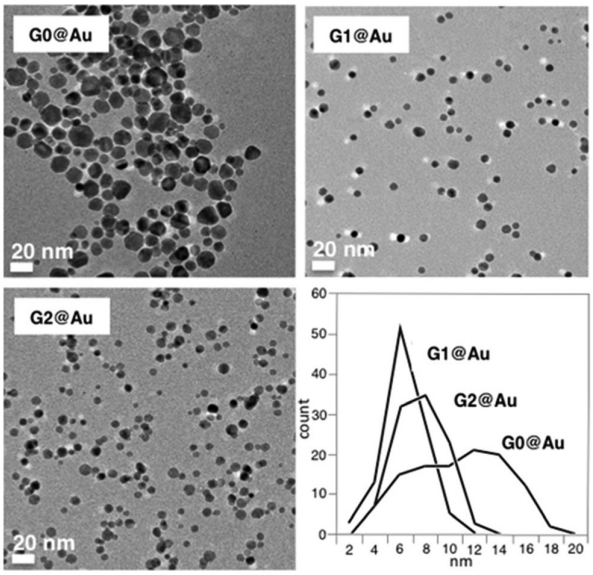

Fig. 2 TEM images of the G0@Au, G1@Au and G2@Au systems and a histogram of sizes after aging for 1 year.

Explicit in Scheme 1, but experimentally illusive, is the presence of a Au–C bond at the nanoparticle–dendrimer interface. To probe these interfaces, all three nanoparticle systems were subjected to both X-ray photoelectron spectroscopy (XPS) and secondary ion mass spectrometry (SIMS). Evidence for this bond, however, proved difficult to unambiguously ascertain, presumably as a consequence of increasing carbon content with increasing dendrimer shell thickness. The experimental limits of analysis depths for SIMS and XPS are typically 5 nm and 5–10 nm, respectively. Indeed, SIMS analysis of G0@Au shows fragments clearly consistent with Au–C bonds (ESI Fig. 50–52†), but such species were not detectable in the case of G1@Au and G2@Au. SIMS data also indicate an organic layer of increasing thickness going from G0@Au to G1@Au to G2@Au. This influence of shell thickness is also manifested in our ability to detect Au signals in the XPS spectra in G0@Au and G1@Au, but not in the case of G2@Au.

Molecular models for the three systems were created in a stepwise fashion. First, the Au nanoparticles (NPs) were created having dimensions consistent with the average size observed in the experiments (diameters of 9.8 nm, 7.1 nm and 7.8 nm for G0@Au, G1@Au and G2@Au respectively). Exploiting the intrinsic symmetry of the NP systems, our models are restricted to half-nanoparticles. Moreover, the half-NP models were created as hollow (see Fig. 3)—save a single

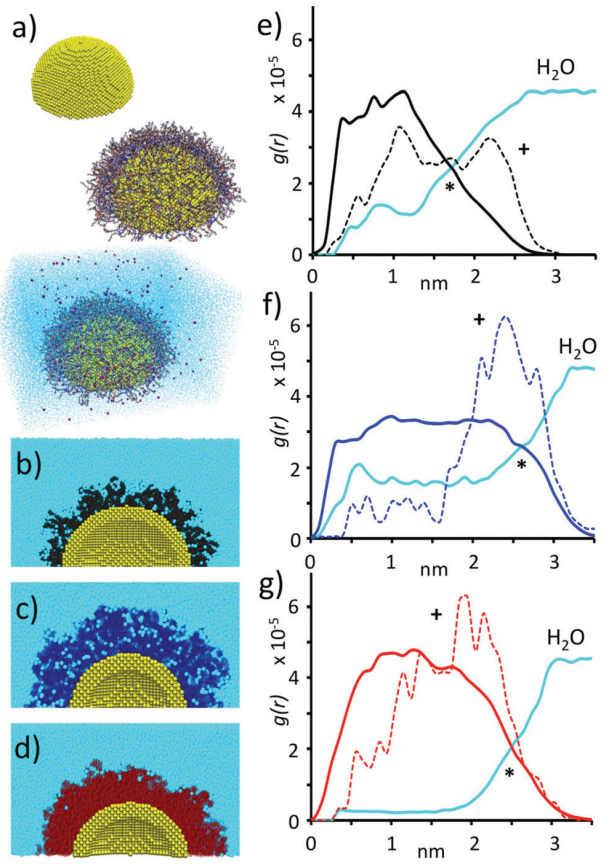

Fig. 3 MD simulations of the dendron–NP systems in solution. (a) Building the molecular models (Au atoms in yellow, the dendrons in native colors – C: grey, O: red, N, blue and H: white –, water in cyan and Na^+ ions in purple). (b–d) Section of the G0@Au (b), G1@Au (c) and G2@Au (d) equilibrated systems. (e–g) Radial distribution functions $g(r)$ of the G0 (e), G1 (f) and G2 (g) dendrons, water and dendrons peripheral charges (origin of the x axis identify the NP surface) wherein the solid lines are dendrimer, the dashed lines are surface charges (labeled '+') and cyan line is water. The 'surface of the nanoparticle' is defined at the '*'.

central atom (to facilitate the radial distribution functions $g(r)$ calculations) – in order to decrease the computational burden.

The dendrons grafting density on the Au–NP surface is controlled by crowding effects and intermolecular interactions in the organic layer.[19] Given the large excess of dendrons present in the experiments (1 : 1 stoichiometry between dendrons and Au atoms), a variable number of G0, G1 and G2 dendrons were grafted onto the NP models consistent with the maximum achievable density for each system (see ESI† for details). The obtained G0@Au, G1@Au and G2@Au systems (modeled as terminal ammonium ions with neutralizing Cl^-) were then equilibrated in explicit water[20] molecules (Fig. 3a) by means of all-atom molecular dynamics (MD) simulations using the GROMACS 4.5.7 software.[21] Additional computational details are available in the ESI.†

Fig. 3b–d report sections of the equilibrated G0@Au, G1@Au and G2@Au systems, and show different levels of hydration in the three cases. Seen in Fig. 3d, the G2 organic layer covering the NP is so dense that water penetration is prevented. Hydration is higher for G0@Au (Fig. 3b), and markedly increased in the case of G1@Au (Fig. 3c). Information on the levels of hydration in the three systems can be obtained from the radial distribution functions, $g(r)$, reported in Fig. 3e–g. The $g(r)$ plots indicate the relative probability of finding dendron atoms or water molecules as a function of the distance from the NP surface (the origin in the x axis).

We identify the surface of the organic layer as the point where the $g(r)$ of the dendrons (solid colored lines) intersects that of water (cyan lines). At distances greater than this point (labeled * in Fig. 3d–f), there is more water than organic. The greater water solubility of G1@Au over G0@Au and G2@Au can be rationalized. The $g(r)$ data in Fig. 3f shows that water penetrates deeper into the organic layer of G1@Au, resulting in uniform hydration. In stark contrast, water is largely excluded from G2@Au. G0@Au is somehow intermediate. Moreover, the $g(r)$ of the surface groups of the dendrons (Fig. 3e–g: dotted lines) indicates the differential distributions of the peripheral charges in these particles. For G1@Au, the dendrons' charged groups are preferentially displayed at the surface of the NP (Fig. 3f: dotted $g(r)$ peak), while the cationic surface groups are significantly backfolded in both G0@Au (Fig. 3e) and G2@Au (Fig. 3g). While there is no apparent trend between solubility and dendron generation, computation suggests that degree of hydration correlates with water solubility.

Data from XPS and SIMS corroborate some elements of the computational models generated even though these vacuum techniques may not adequately capture the solvated model. As previously stated, SIMS data indicate an organic layer of increasing thickness going from G0@Au to G1@Au to G2@Au. The lack of a signal for Au by XPS for G2@Au is consistent with this result. The computational model predicts an increase from G0@Au to G1@Au, but with G2@Au being similar to G1@Au. The difference between SIMS and computation could derive from the role of solvation: that is, models of G1@Au match the size of G2@Au due in part to water molecules. Loss of waters upon desiccation would lead to the observed size trend seen in SIMS. Alternatively, the lack of water penetration for the G2 system in the simulation may reflect a more dense dendrimer shell, which is consistent with a more challenging detection of Au species (or Au–C bonds) in XPS and SIMS.

In summary, the use of triazine dendrons with a diazonium salt of gold tetrachloroaurate at the core can give rise to shell nanoparticles that likely, but not unambiguously, comprise a Au–C linkage in an additive-free synthesis. Indeed, alternatives such as Au–N bond formation, noncovalent association, or some combination of all of these processes could be occuring. These nanoparticles are highly stable, staying readily dispersed and of similar size for periods greater than one year. The properties of these materials can be tuned by manipulating the surface chemistry, or other structural parameters, of the dendron. As indicated here, the removal or uncontrolled loss of BOC groups provides evidence for this manipulation although future studies will focus on a more robust protecting

group. Indeed, either organic soluble or water soluble materials can be prepared. A more resilient protecting group could be considered for future work as interest in such constructs, especially in biological media, have been described.[22] The dimensions of the nanoparticles reported here are similar to middle to large-generation triazine dendrimers (G7–G9).[23] While not reaching the size of viruses, the synthetic burden associated with the preparation of these nanoparticles is greatly reduced in comparison to triazine dendrimers.[24] Interestingly, similar challenges to solubility arise at these dimensions independent of whether the nanoparticle is wholly organic or a composite as reported here—increasing evidence for the concept of nanoperiodicity.[25]

We thank the Robert A. Welch Foundation (P-0008; P-1212) and DoD (W81XWH-12-1-0338) for support.

Notes and references

1 R. R. Arvizo, S. Saha, E. Wang, D. Robertson, R. Bhattacharya and P. Mukherjee, *Proc. Natl. Acad. Sci. U. S. A.*, 2013, **110**, 6700–6705; E. C. Dreaden, A. M. Alkilany, X. Huang, C. J. Murphy and M. A. El-Sayed, *Chem. Soc. Rev.*, 2012, **41**, 2740–2779; B. S. S. Gruirgis, C. S. Cunha, I. Gomez, M. Cavadas, I. Silva, G. Doria, G. L. Blatch, P. V. Baptista, E. Pereira, H. M. E. Azzazy, M. M. Mota, M. Prudencio and R. Franco, *Anal. Bioanal. Chem.*, 2012, **402**, 1019–1027.

2 V. Biju, *Chem. Soc. Rev.*, 2014, **43**, 744–764.

3 R. A. Sperling and W. J. Parak, *Philos. Trans. R. Soc. London, Ser. A*, 2010, **368**, 1333–1383.

4 M. Brust, M. Walker, D. Bethell, D. J. Schiffrin and R. Whyman, *J. Chem. Soc., Chem. Commun.*, 1994, 801–802.

5 J. D. Gibson, B. P. Khanal and E. R. Zubarev, *J. Am. Chem. Soc.*, 2007, **129**, 11653–11661.

6 S. D. Brown, P. Nativo, J.-A. Smith, D. Stirling, P. R. Edwards, B. Venugopal, D. J. Flint, J. A. Plumb, D. Graham and N. J. Wheate, *J. Am. Chem. Soc.*, 2010, **132**, 4678–4684; S. Dhar, W. L. Daniel, D. A. Giljohann, C. A. Mirkin and S. J. Lippard, *J. Am. Chem. Soc.*, 2009, **131**, 14652–14653.

7 T.-M. Sun, Y.-C. Wang, F. Wang, J.-Z. Du, C.-Q. Mao, C.-Y. Sun, R.-Z. Tang, Y. Liu, J. Zhu, Y.-H. Zhu, X.-Z. Yang and J. Wang, *Biomaterials*, 2014, **35**, 836–845; J. P. Hermes, F. Sander, U. Fluch, T. Peterle, D. Thompson, R. Urbani, T. Pfohl and M. Mayor, *J. Am. Chem. Soc.*, 2012, **134**, 14674–14677.

8 J. Gao, X. Huang, H. Liu, F. Zan and J. Ren, *Langmuir*, 2012, **28**, 446471; D. Zopes, B. Stein, S. Mathur and C. Graf, *Langmuir*, 2013, **29**, 11217–11226.

9 E. Boisselier, L. Salmon, J. Ruiz and D. Astruc, *Chem. Commun.*, 2008, **44**, 5788–5790.

10 J. Zhu, C. Waengler, B. Lennox and R. Schirrmacher, *Langmuir*, 2012, **28**, 5508–5512; E. Oh, J. B. Blanco-Canosa, I. L. Medintz, P. E. Dawson and H. Mattoussi, *Small*, 2010, **6**, 1273–1278.

11 P. Gobbo and M. S. Workentin, *Langmuir*, 2012, **28**, 12357–12363.

12 J. I. Cutler, E. Auyeung and C. A. Mirkin, *J. Am. Chem. Soc.*, 2012, **134**, 1376–1391.

13 C. M. Crudden, J. H. Horton, I. I. Ebralidze, O. V. Zenkina, A. B. McLean, B. Drevniok, Z. She, H.-B. Kraatz, N. J. Mosey, T. Seki, E. C. Keske, J. D. Leake, A. Rousin-Webb and G. Wu, *Nat. Chem.*, 2014, **6**, 409–414; A. V. Zhukhovitskiy, M. G. Mavros, T. V. Voorhis and J. A. Johnson, *J. Am. Chem. Soc.*, 2013, **135**, 7418–7421.

14 L. Laurentius, S. R. Stoyanov, S. Gusarov, A. Kovalenko, R. Du, G. P. Lopinski and M. T. McDermott, *ACS Nano*, 2011, **5**, 4219–4227; A. Mesnage, X. Lefevre, P. Jegou, G. Deniau and S. Palacin, *Langmuir*, 2012, **28**, 11767–11778; F. Mirkhalaf, J. Paprotny and D. J. Schiffrin, *J. Am. Chem. Soc.*, 2006, **128**, 7400–7401; A. T. Overton and A. A. Mohamed, *Inorg. Chem.*, 2012, **51**, 5500–5502; S. A. Neal, S. Orefua, A. T. Overton, R. J. Staples and A. A. Mohamed, *Inorganics*, 2013, **1**, 70–84; S. A. Orefuwa, M. Ravanbakhsh, S. N. Neal, J. B. King and A. A. Mohamed, *Organometallics*, 2014, **33**, 439–442.

15 J. L. Bahr, J. Yang, D. V. Kosynkin, M. J. Bronikowski, R. E. Smalley and J. M. Tour, *J. Am. Chem. Soc.*, 2001, **123**, 6536–6542.

16 R. V. Kumar and K. R. Gopidas, *Chem. – Asian J.*, 2010, **5**, 887–896.

17 A. E. Enciso, F. Ramirez-Crescencio, M. J. Zeiser, R. Redon and E. E. Simanek, *Polym. J.*, 2015, **6**, 5219–5224; A. E. Enciso, Z. M. Abid and E. E. Simanek, *Polym. Chem.*, 2014, **5**, 4635–4640.

18 Lines shift from doublets at 7.1 ppm and 6.5 ppm in the aniline to 8.5 ppm and 7.9 ppm in the diazonium salt.

19 G. Doni, M. D. Nkoua Ngavouka, A. Barducci, P. Parisse, A. De Vita, G. Scoles, L. Casalis and G. M. Pavan, *Nanoscale*, 2013, **5**, 9988–9993.

20 W. L. Jorgensen, J. Chandrasekhar, J. D. Madura, R. W. Impey and M. L. Klein, *J. Chem. Phys.*, 1983, **79**, 926–935.

21 S. Pronk, S. Pail, R. Schulz, P. Larsson, P. Bjelkmar, R. Apostolov, M. R. Shirts, J. C. Smith, P. M. Kasson, D. van der Spoel, B. Hess and E. Lindahl, *Bioinformatics*, 2013, **29**, 845–854.

22 (*a*) M.-C. Daniel, M. E. Grow, H. Pan, M. Bednarek, W. E. Ghann, K. Zabetakis and J. Cornish, *New J. Chem.*, 2011, **35**, 2366–2374; (*b*) T. J. Cho, R. I. MacCuspie, J. Gigault, J. M. Gorham, J. T. Elliott and V. A. Hackley, *Langmuir*, 2014, **30**, 3883–3893.

23 J. Lim, G. M. Pavan, O. Annunziata and E. E. Simanek, *J. Am. Chem. Soc.*, 2012, **134**, 1942–1945.

24 J. Lim, M. Kostiainen, J. Maly, V. C. P. da Costa, O. Annunziata, G. M. Pavan and E. E. Simanek, *J. Am. Chem. Soc.*, 2013, **135**, 4660–4663.

25 D. Tomalia, *New J. Chem.*, 2012, **36**, 264–281.

molecules

MDPI

Article

Nanoparticle Effects on Human Platelets *in Vitro*: A Comparison between PAMAM and Triazine Dendrimers

Alan E. Enciso [1], Barry Neun [2], Jamie Rodriguez [2], Amalendu P. Ranjan [3], Marina A. Dobrovolskaia [2,*] and Eric E. Simanek [1,*]

[1] Department of Chemistry & Biochemistry, Texas Christian University, Fort Worth, TX 76129, USA; a.encisobarros@tcu.edu

[2] Nanotechnology Characterization Lab, Frederick National Laboratory for Cancer Research, Frederick, MD 21702, USA; neunb@mail.nih.gov (B.N.); rodriguezjc@mail.nih.gov (J.R.)

[3] Department of Molecular and Medical Genetics & Institute of Cancer Research, University of North Texas Health Science Center, Fort Worth, TX 76109, USA; amalendu.ranjan@unthsc.edu

* Correspondence: marina@mail.nih.gov (M.A.D.); e.simanek@tcu.edu (E.E.S.); Tel.: +1-301-846-6939 (M.A.D.); +1-817-257-5355 (E.E.S.)

Academic Editor: Ashok Kakkar

Received: 3 February 2016 ; Accepted: 21 March 2016 ; Published: 29 March 2016

Abstract: Triazine and PAMAM dendrimers of similar size and number of cationic surface groups were compared for their ability to promote platelet aggregation. Triazine dendrimers (G3, G5 and G7) varied in molecular weight from 8 kDa–130 kDa and in surface groups 16–256. PAMAM dendrimers selected for comparison included G3 (7 kDa, 32 surface groups) and G6 (58 kDa, 256 surface groups). The treatment of human platelet-rich plasma (PRP) with low generation triazine dendrimers (0.01–1 μM) did not show any significant effect in human platelet aggregation *in vitro*; however, the treatment of PRP with larger generations promotes an effective aggregation. These results are in agreement with studies performed with PAMAM dendrimers, where large generations promote aggregation. Triazine dendrimers promote aggregation less aggressively than PAMAM dendrimers, a factor attributed to differences in cationic charge or the formation of supramolecular assemblies of dendrimers.

Keywords: dendrimer; triazine; PAMAM; platelet; biocompatibility

1. Introduction

Dendrimers are nanosized, hyperbranched polymers with low polydispersity that are amenable to synthetic manipulation [1–4]. While not yet realized, the potential for dendrimers to act as drug delivery vehicles has been long appreciated [5–9]. Our efforts, like others, rely on intravenous administration of such vehicles [10–13]. This strategy promotes interactions of these protein-sized architectures with endogenous proteins, cells, and aggregates such as lipoproteins. A common design strategy for the application of these materials relies on dendrimers to promote sustained systematic distribution by retention in the circulation. Accordingly, dendrimers will experience increased exposure time with components of the blood stream. Assessment of biocompatibility typically commences with studies of dendrimer interactions with specific components of the circulatory system. Interactions with platelets represent a common starting point for such studies. Platelets are abundant in the vasculature and are sensitive to changes in blood microenvironment [14]. Platelet aggregation is a critical step in the clotting cascade [15]. Agents that promote or attenuate this behavior are of clinical interest [16–21]. While nanomaterials have demonstrated these abilities, such effects are "off-target" if the goal is drug delivery [22].

Historically, PAMAM dendrimers have served as a benchmark for other classes of dendrimers. Here, we compare PAMAM standards with triazine dendrimers [23]. Earlier structure activity relationship studies with PAMAM dendrimers revealed that dendrimer size, zeta potential, and density of the surface amines are responsible for the dendrimer interaction with, and activation of, platelets [14,22,23]. The mechanism of activation has been attributed to the disturbance of the cellular membrane integrity [23]. However, the composition of triazine dendrimers is different to PAMAM dendrimers (Chart 1). The branching point for triazine dendrimers is the rigid, aromatic triazine ring. In contrast, PAMAM branch from a tertiary amine. Differences in flexibility, hydrophilicity, size, and basicity are apparent. For the studies described here, the triazine rings are interconnected with a tetraethyleneglycol group to promote water solubility. For simplicity, the molecules will be indicated by class and generation, abbreviated "G."

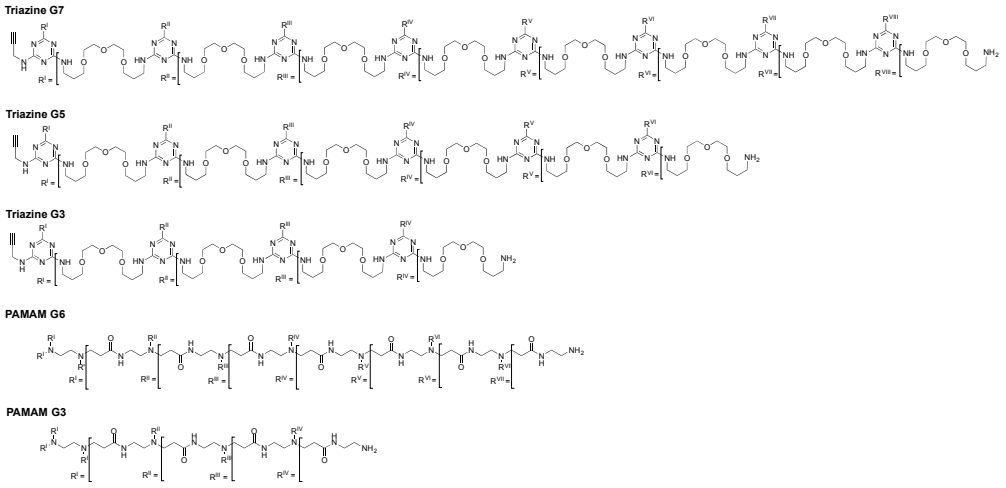

Chart 1. Structures of the triazine and PAMAM dendrimers examined.

2. Results and Discussion

2.1. Zeta Potential

Triazine and PAMAM dendrimers are intrinsically different in composition. However, at large generation both are perceived to exist as globular spheres resembling proteins with biophysical properties that is attributed to their surface chemistry [24–28]. The zeta-potentials measured for these molecules at near neutral pH using 10 mM phosphate buffer (and 136 mM NaCl) show that they are all cationic as expected, but the triazines bear less charge than the corresponding PAMAM, even when surface group numbers are identical. At 10 mM buffer without added salt, the triazines zeta-potentials are 32 mV, 22 mV, and 26 mV, respectively for G3, G5, and G7. This difference could be attributed to the preponderance of interior, tertiary amines of the PAMAM whose pKa are approximately 10 compared with the triazine sites with pKas of approximately 4.5.

Charge density might seem similar given similar charges and monomer size, but these dendrimers aggregate in solution. The triazines monomers of the dimensions shown in Table 1 are in equilibrium with multimeric aggregates measuring hundreds of nanometers. The data presented in Table 1 are summarized from our earlier studies [23,29,30]. Indeed, this behavior underscores the importance of these studies on triazines given their intended uses. While similar in branching architecture and surface chemistry, dendrimers within and across classes of composition can potentially display different behaviors in complex environments like the vasculature.

Table 1. Comparison of triazine and PAMAM dendrimers.

Dendrimer	Z-Potential (mV)	Monomer Size (nm)	Peripheral Amines	Internal Tertiary Amines	MW (Da)
G3-Triazine	23.1	3.7	16	-	7785
G3-PAMAM	43.3	3.1	32	30	6910
G5-Triazine	16.5	8.0	64	-	33 K
G6-PAMAM	46.2	7.5	256	254	58 K
G7-Triazine	19.8	13.7	256	-	130 K

2.2. Platelet Aggregation

Incubating triazine G3, G5, and G7 dendrimers in plate-rich plasma leads to platelet activation, which culminates in platelet aggregation. Using four different concentrations (0.01 μM, 0.10 μM, 1 μM, and 10 μM), we find that activation occurs in a dose-dependent and size-dependent manner. Triazine G5 and G7 dendrimers activate platelets more than triazine G3 dendrimers (Figure 1). Due to the insufficient quantity of material, the triazine G7 dendrimer was not assayed at the highest concentration. These results are in agreement with studies performed with PAMAM dendrimers that show increasing activation with increasing size [23].

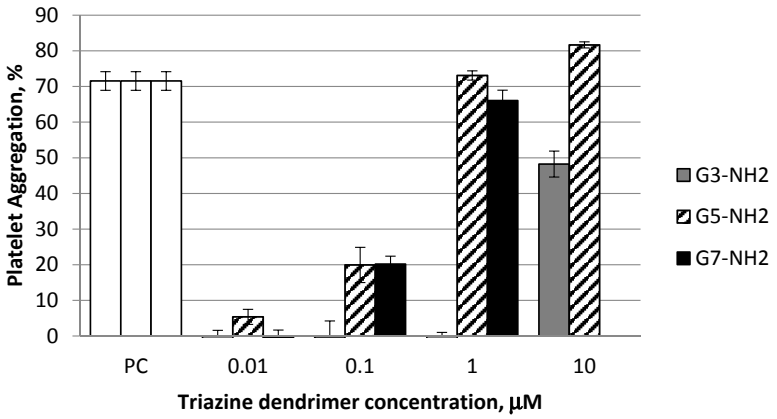

Figure 1. Induction of platelet aggregation by amine terminated triazine dendrimers is size-dependent. Different concentrations of generations 3, 5, and 7 of triazine dendrimers with amine terminal groups that were incubated with human platelet reach plasma for 15 min at 37 °C. After that, platelet count was performed using a Z2 cell and particle counter. Platelet count in the test samples was compared to that in the negative control sample to calculate percent platelet aggregation. Collagen was used as an assay positive control (PC). Shown is mean ± SD (n = 3).

In a comparative test, G3 and G7 triazine dendrimers (1 μM) are seen to be less aggressive at platelet aggregation compared to their PAMAM counterparts of similar generation possessing similar physicochemical properties (G3 and G6) (Figure 2). Due to the absence of well characterized G7 PAMAM dendrimer, we used G6 PAMAM dendrimer in this study. Since platelet aggregation induction by PAMAM dendrimer increases with their size (23), it is reasonable to expect that platelet aggregation by G7 PAMAM dendrimer will be even stronger than that observed with G6. Therefore, the difference between G7 of Triazine and G7 PAMAM dendrimers would be even greater than that reported in this study.

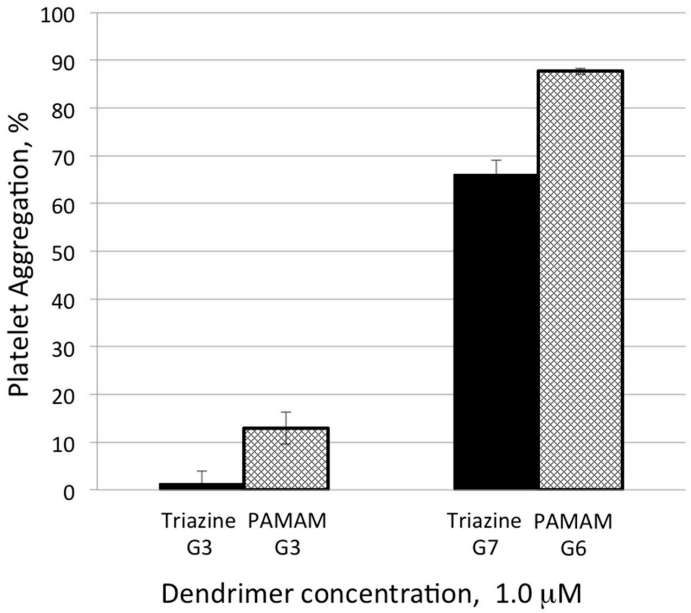

Figure 2. Cationic triazine dendrimers are less reactive with human platelets than cationic PAMAM dendrimers of similar size. G3- and G7-amine-terminated triazine dendrimers and G3- and G6-amine terminated PAMAM dendrimers at equivalent molar concentrations were incubated with human platelet reach plasma for 15 min at 37 °C. After that, platelet count was performed using a Z2 cell and particle counter equipped with a 5-μm aperture tube. Platelet count in the test samples was compared to that in the negative control sample to calculate percent platelet aggregation. Collagen was used as an assay positive control (data not shown). Shown is mean ± SD (n = 3).

3. Materials and Methods

3.1. Reagents

DPBS (Ca^{2+}/Mg^{2+} free), poly-L-lysine hydrobromide, polymyxin B, 2MeSAMP, and 1,10-phenantroline were from Sigma-Aldrich (St. Louis, MO, USA). G3 and G6 PAMAM dendrimers with amine surface were from Dendritic Nanotechnologies Inc. (Mount Pleasant, MI, USA). Collagen was purchased from Helena Laboratories (Beaumont, TX, USA). Triazine dendrimers were synthesized according to procedures previously reported [31,32].

3.2. Research Donor Blood

Healthy volunteer blood specimens were drawn under NCI-Frederick Protocol OH99-C-N046. Blood was collected in BD vacutainer tubes containing sodium citrate as an anticoagulant. To avoid individual variability, specimens from at least three donors were pooled.

3.3. Platelet Aggregation

To study particles effects on platelet aggregation, whole blood was centrifuged 8 min at 200× g in order to obtain platelet rich plasma (PRP). PRP was treated with nanoparticles, PBS (negative control), or collagen (positive control) for 15 min at 37 °C. After that, single platelet count was conducted using a Z2 counter and a size analyzer (Beckman Coulter, Brea, CA, USA). Difference in single platelet count between negative control and test samples was used to calculate percent platelet aggregation. Additional control included incubation of platelet poor plasma and PBS with particles and analyzing these samples on the instrument. These controls were used to monitor potential particle aggregation

in the presence of plasma proteins to avoid false-negative results. Detailed protocol is available [33]. To study potential particle contamination with endotoxin, the test samples were analyzed by turbidity LAL assay according to the protocol published [34]. Endotoxin was not detected in any test samples at concentrations used in the platelet aggregation assay.

3.4. Zeta Potential Measurements

The zeta potential measurement of all the generations of dendrimers were conducted with Zetasizer Nano-ZS (Malvern Instruments, Westborough, MA, USA). Samples were suspended in 1× PBS pH 7.4 (with and without salt) and placed in disposable folded capillary cells DTS1070 (Malvern Instruments, Westborough, MA, USA). The electrophoretic mobility of the samples were measured in an applied electric field. Twelve zeta potential measurements were collected for each run, and the results were averaged. The Zeta potential value was calculated directly from the Smoluchowski model using the Malvern software.

4. Conclusions

Consistent with Tomalia's nanoperiodicity hypothesis [35–37], both triazine and PAMAM dendrimers activate platelets in a size- and charge-dependent manner in that dendrimers of earlier generations (G3) exhibit lower potency in activating platelets than their higher generation (G6 and G7) counterparts. Dendrimers of earlier generation are smaller in hydrodynamic size and have lower number of surface amines. The data obtained for PAMAM dendrimers in our study is similar to the earlier reports [22,23]. Of interest, herein we demonstrated that Triazine dendrimers are less potent than their PAMAM counterparts. The diminished activity displayed by the triazine dendrimers is likely attributed to the lessor density of surface amines. That is, triazine dendrimers due to the lack of interior groups protonated near neutral pH. Systemic administration of cationic PAMAM dendrimers results in consumptive coagulopathy, a thrombogenic disorder halting the use of these particles as drug delivery vehicles [22]. The data presented in our study highlight less thrombogenic properties of cationic triazine dendrimers and warrant further investigation of these particles as potential drug carriers.

Acknowledgments: We thank the Robert A. Welch Foundation (P-0008) and DOD (W81XWH-12-1-0338). The study was supported in part by federal funds from the National Cancer Institute, National Institutes of Health, under contract HHSN261200800001E (M.D., B.N. and J.R.). The content of this publication does not necessarily reflect the views or policies of the Department of Health and Human Services, nor does mention of trade names, commercial products, or organizations imply endorsement by the U.S. Government.

Author Contributions: M.A.D. conceived the biological experiments and led the team comprised of B.N. and J.R. B.N. and J.R. performed endotoxin and platelet aggregation studies, respectively. E.E.S. conceived the synthesis and physicochemical characterization experiments and led the team comprised of A.E.E. and A.P.R. A.E. prepared the samples. A.P.R. performed DLS and Z-potential analysis. All parties contributed to the preparation of the manuscript.

Conflicts of Interest: The authors declare no conflict of interest.

References

1. Sowinska, M.; Urbanczyk-Lipkowska, Z. Advances in the chemistry of dendrimers. *New J. Chem.* **2014**, *38*, 2168–2203. [CrossRef]
2. Deng, X.-X.; Du, F.-S.; Li, Z.-C. Combination of orthogonal ABB and ABC multicomponent reactions toward efficient divergent synthesis of dendrimers with structural diversity. *ACS Macro Lett.* **2014**, *3*, 667–670. [CrossRef]
3. Patra, S.; Kozura, B.; Huang, A.Y.-T.; Enciso, A.E.; Sun, X.; Hsieh, J.-T.; Kao, C.-L.; Chen, H.-T.; Simanek, E.E. Dendrimers terminated with dichlorotriazine groups provide a rout to compositional diversity. *Org. Lett.* **2013**, *15*, 3808–3811. [CrossRef] [PubMed]
4. Simanek, E.E.; Abdou, H.; Lalwani, S.; Lim, J.; Mintzer, M.; Venditto, V.J.; Vittur, B. The 8 year thicket of triazine dendrimers: Strategies, targets and applications. *Proc. R. Soc. A* **2010**, *466*, 1445–1468. [CrossRef]

5. Liu, Y.; Ng, Y.; Toh, M.R.; Chiu, G.N.C. Lipid-dendrimer hybrid nanosystem as a novel delivery system for paclitaxel to treat ovarian cancer. *J. Control. Release* **2015**, *220*, 438–446. [CrossRef] [PubMed]
6. Yu, M.; Jie, X.; Chen, C.; Shen, W.; Cao, Y.; Lian, G.; Qi, R. Recent advances in dendrimer research for cardiovascular diseases. *Biomacromolecules* **2015**, *16*, 2588–2598. [CrossRef] [PubMed]
7. Witte, A.B.; Timmer, C.M.; Gam, J.J.; Choi, S.K.; Banaszak, M.M.; Orr, B.G.; Baker, J.R., Jr.; Sinniah, K. Biophysical characterization of a riboflavin-conjugated dendrimer platform for targeted drug delivery. *Biomacromolecules* **2012**, *13*, 507–516. [CrossRef] [PubMed]
8. Yuan, H.; Luo, K.; Lai, Y.; Pu, Y.; He, B.; Wang, G.; Wu, Y.; Gu, Z. A novel poly(L-glutamic acid) dendrimer based drug delivery system with both pH-sensitive and targeting functions. *Mol. Pharm.* **2010**, *7*, 953–962. [CrossRef] [PubMed]
9. Desai, P.N.; Yuan, Q.; Yang, H. Synthesis and characterization of photocurable polyamidoamine dendrimer hydrogels as a versatile platform for tissue engineering and drug delivery. *Biomacromolecules* **2010**, *11*, 666–673. [CrossRef] [PubMed]
10. Lim, J.; Simanek, E.E. Triazine dendrimers as drug delivery systems: From synthesis to therapy. *Adv. Drug Deliv. Rev.* **2012**, *64*, 826–835. [CrossRef] [PubMed]
11. Lim, J.; Lo, S.-T.; Hill, S.; Pavan, G.M.; Sun, X.; Simanek, E.E. Antitumor activity and molecular dynamics simulations of paclitaxel-laden triazine dendrimers. *Mol. Pharm.* **2012**, *9*, 404–412. [CrossRef] [PubMed]
12. Simanek, E.E.; Enciso, A.E.; Pavan, G.M. Computational design principles for the Discovery of bioactive dendrimers: [s]-triazines and other examples. *Exp. Opin. Drug Disc.* **2013**, *9*, 1057–1069. [CrossRef] [PubMed]
13. Lee, C.; Lo, S.-T.; Lim, J.; da Costa, V.C.; Ramezani, S.; Öz, O.K.; Pavan, G.M.; Annunziata, O.; Sun, X.; Simanek, E.E. Design, synthesis and biological assessment of a triazine dendrimer with approximately 16 paclitaxel groups and 8 PEG groups. *Mol. Pharm.* **2013**, *10*, 4452–4461. [CrossRef] [PubMed]
14. Jones, C.F.; Campbell, R.A.; Franks, Z.; Gibson, C.C.; Thiagarajan, G.; Vieira-de-Abreu, A.; Sukavaneshvar, S.; Mohammad, S.F.; Li, D.Y.; Ghandehari, H.; *et al*. Cationic PAMAM dendrimers disrupt key platelet functions. *Mol. Pharm.* **2012**, *9*, 1599–1611. [CrossRef] [PubMed]
15. Simak, J. Nanotoxicity in Blood: Effects of Engineered Nanomaterials on Platelets. In *Nanotoxicity: From in Vivo and in Vitro Models to Health Risks*, 1st ed.; Sahu, S.C., Casciano, D.A., Eds.; John Wiley and Sons Ltd.: Chichester, UK, 2009; pp. 191–225.
16. Dong, H.-P.; Wu, H.-M.; Chen, S.-J.; Chen, C.-Y. The effect of butanolides from *Cinnamomum tenuifolium* on platelet aggregation. *Molecules* **2013**, *18*, 11836–11841. [CrossRef] [PubMed]
17. Cejas, M.A.; Chen, C.; Kinney, W.A.; Maryanoff, B.E. Nanoparticles that display short collagen-related peptides. Potent stimulation of human platelet aggregation by triple helical motifs. *Bioconjugate Chem.* **2007**, *18*, 1025–1027. [CrossRef] [PubMed]
18. Okamura, Y.; Handa, M.; Suzuki, H.; Ikeda, Y.; Takeoka, S. New strategy of platelet substitutes for enhancing platelet aggregation at high shear rates: Cooperative effects of a mixed system of fibrinogen gamma-chain dodecapeptide- or glycoprotein Ibalpha-conjugated latex beads under flow conditions. *J. Artif. Organs* **2006**, *9*, 251–258. [CrossRef] [PubMed]
19. Zhu, J.; Xue, J.; Guo, Z.; Zhang, L.; Marchant, R.E. Biomimetic glycoliposomes as nanocarriers for targeting P-selectin on activated platelets. *Bioconjugate Chem.* **2007**, *18*, 1366–1369. [CrossRef] [PubMed]
20. Fernandes, E.G.; de Queiroz, A.A.; Abraham, G.A.; San Roman, J. Antithrombogenic properties of bioconjugate streptokinase-polyglycerol dendrimers. *J. Mater. Sci. Mater. Med.* **2006**, *17*, 105–111. [CrossRef] [PubMed]
21. Kim, Y.; Klutz, A.M.; Hechler, B.; Gao, Z.G.; Gachet, C.; Jacobson, K.A. Application of the functionalized congener approach to dendrimer-based signaling agents acting through A(2A) adenosine receptors. *Purinergic Signal.* **2009**, *5*, 39–50. [CrossRef] [PubMed]
22. Jones, C.F.; Campbell, R.A.; Brooks, A.E.; Assemi, S.; Tadjiki, S.; Thiagarajan, G.; Mulcock, C.; Weyrich, A.S.; Brooks, B.D.; Ghandehari, H.; *et al*. Cationic PAMAM dendrimers aggressively initiate blood clot formation. *ACS Nano* **2012**, *6*, 9900–9910. [CrossRef] [PubMed]
23. Dobrovolskaia, M.A.; Patri, A.K.; Simak, J.; Hall, J.B.; Semberova, J.; de Paoli Lacerda, S.H.; McNeil, S.E. Nanoparticle size and surface charge determine effects of PAMAM dendrimers on human platelets *in vitro*. *Mol. Pharm.* **2012**, *9*, 382–393. [CrossRef] [PubMed]
24. Esfand, R.; Tomalia, D.A. Poly(amidoamine) (PAMAM) dendrimers: From biomimicry to drug delivery and biomedical applications. *Drug Discov. Today* **2001**, *6*, 427–436.

25. Svenson, S.; Tomalia, D.A. Dendrimers in biomedical applications—Reflections on the field. *Adv. Drug Deliv. Rev.* **2005**, *57*, 2106–2129. [CrossRef] [PubMed]
26. Tomalia, D.A.; Reyna, L.A.; Svenson, S. Dendrimers as multi-purpose nanodevices for oncology drug delivery and diagnostic imaging. *Biochem. Soc. Trans.* **2007**, *35*, 61–67. [CrossRef] [PubMed]
27. Menjoge, A.R.; Kannan, R.M.; Tomalia, D.A. Dendrimer-based drug and imaging conjugates: Design considerations for nanomedical applications. *Drug Discov. Today* **2010**, *15*, 171–185. [CrossRef] [PubMed]
28. Kannan, R.M.; Nance, E.; Kannan, S.; Tomalia, D.A. Emerging concepts in dendrimer-based nanomedicine: From design principles to clinical applications. *J. Intern. Med.* **2014**, *276*, 579–617. [CrossRef] [PubMed]
29. Dobrovolskaia, M.A.; Patri, A.K.; Potter, T.M.; Rodriguez, J.C.; Hall, J.B.; McNeil, S.E. Dendrimer-induced leukocyte procoagulant activity depends on particle size and surface charge. *Nanomedicine* **2012**, *7*, 245–256. [CrossRef] [PubMed]
30. Lo, S.T.; Stern, S.; Clogston, J.D.; Zheng, J.; Adiseshaiah, P.P.; Dobrovolskaia, M.; Lim, J.; Patri, A.K.; Sun, X.; Simanek, E.E. Biological assessment of triazine dendrimer:toxicological profiles, solution behavior, biodistribution, drug release andefficacy in a PEGylated, paclitaxel construct. *Mol. Pharm.* **2010**, *7*, 993–1006. [CrossRef] [PubMed]
31. Enciso, A.E.; Abid, Z.M.; Simanek, E.E. Rapid, semi-automated convergent synthesis of low generation triazine dendrimers using microwave assisted reactions. *Polym. Chem.* **2014**, *5*, 4635–4640. [CrossRef]
32. Lim, J.; Kostiainen, M.; Maly, J.; da Costa, V.C.; Annunziata, O.; Pavan, G.M.; Simanek, E.E. Synthesis of Large Dendrimers with the Dimensions of Small Viruses. *J. Am. Chem. Soc.* **2013**, *135*, 4660–4663. [CrossRef] [PubMed]
33. Assay Cascade Protocols, Frederick National Lab, Nanotechnology Characterization Laboratory. Available online: http://ncl.cancer.gov/NCL_Method_ITA-2.pdf (accessed on 28 March 2016).
34. Assay Cascade Protocols, Frederick National Lab, Nanotechnology Characterization Laboratory. Available online: http://ncl.cancer.gov/NCL_Method_STE-1.2.pdf (accessed on 28 March 2016).
35. Tomalia, D.A. Dendritic effects: Dependecy of dendritic nano-periodic property patterns on critical nanoscale design parameters (CNDPs). *New J. Chem.* **2012**, *36*, 264–281. [CrossRef]
36. Tomalia, D.A. In quest of a systematic framework for unifying and defining nanoscience. *J. Nanopart. Res.* **2009**, *11*, 1251–1310. [CrossRef] [PubMed]
37. Tomalia, D.A.; Khanna, S.N. A systematic framework and nanoperiodic concept for unifying nanoscience: Hard/Soft nanoelements, superatoms, meta-atoms, new emerging properties, periodic property patterns, and predictive mendeleev-like nanoperiodic tables. *Chem. Rev.* **2016**, *116*, 2705–2774. [CrossRef] [PubMed]

Sample Availability: Samples of the compounds **G1–G9** triazine dendrimers are available from the authors.